The effect of climate change on human bio-meteorological conditions in different climate regions of China

A Dissertation

Submitted in Partial Fulfilment of the Requirements
for the Degree of Doctor rerum naturalium (Dr. rer. nat.)
to the Department of Earth Sciences
of the Freie Universität Berlin

by

Xiaoli Chi

Berlin, November 2017

Supervisor: Prof. Dr. Ulrich Cubasch

Freie Universität Berlin

Second examiner: Prof. Dr. Sahar Sodoudi

Freie Universität Berlin

Date of the viva voce/defense: 11. January 2018

Declaration

I hereby declare that except where specific reference is made to the work of others, the contents of this dissertation are original and have not been submitted in whole or in part for consideration for any other degree or qualification in this, or any other university. This dissertation is my own work and contains nothing which is the outcome of work done in collaboration with others, except as specified in the text and Acknowledgements. This dissertation contains fewer than 50,000 words including appendices, bibliography, footnotes, tables and equations and has fewer than 50 figures.

Xiaoli Chi
November 2017

List of Publications

Chi XL, Li R, Cubasch U, Cao WT. The thermal comfort and its changes in the 31 provincial capital cities of mainland China in the past 30 years. Theoretical and Applied Climatology, 2017, 1-21.

Li R, **Chi XL***. Thermal comfort and tourism climate changes in the Qinghai–Tibet Plateau in the last 50 years. Theorotical and Applied Climatology, 2014, 117(3-4), 621-624.

Cao WT, Li R, **Chi XL**, Chen NH et al. Island urbanization and its ecological consequences: A case study in the Zhoushan Island, East China. Ecological Indicators, 2017 (76): 1-14.

Chi XL, Langer I, Sodoudi S. Influence of building form on human thermal comfort and perception for cold stress in Berlin. International Journal of Biometeorology. (under review)

Chi XL, Cubasch U, Sodoudi S. Assessment of Human Bio-meteorological Environment over the Tibetan Plateau Region based on CORDEX Climate Model Project. Theorotical and Applied Climatology. (under review)

Chi XL, Cubasch U, Sodoudi S. Evaluation of the temperature extremes in Tibetan Plateau regions: WSDI and CSDI in and summer and winter in 2012-2024. (submitted soon)

Sodoudi S, Zhang HW, **Chi XL**, Mueller F et al. The influence of spatial configuration of green areas on microclimate and thermal comfort. Urban forestry & Urban greening. (under review)

Abstract

This thesis investigates the human thermal comfort and its variation in 31 provincial capital cities of mainland China, and Tibetan Plateau (TP) in the light of the anticipated global warming. Physiologically Equivalent Temperature (PET), Universal Thermal Climate Index (UTCI), Warm spell duration index (WSDI) and Cold spell duration index (CSDI) are well united for this research. Besides the data which are observed at the stations, this thesis also evaluates regional climate model data. The HadGEM3-RA and RegCM data from the CORDEX-East Asia project are used to project the human bio-meteorological conditions in TP in the future. The cities in the TP are classified into different types based on their seasonal human thermal comfort distribution. The changes of thermal comfort in recent decades, their regional differences and also the difference between thermal indices are analyzed in this study. Furthermore, the human bio-meteorological conditions of TP in the near future are evaluated with the extreme events included. The aim is to provide guidance for urban planning and management, industrial and agricultural production and people's livelihood, and give some references for related research.

The PET and UTCI values are highly correlated with each other and present similar thermal comfort pattern in mainland China, although their sensitivities differ slightly. The 31 cities cover, 4–8 resp. 6–8 thermal comfort classes of the PET and UTCI scale. On the whole, the annual cumulative number of pleasant days was more than 160 days/year on average in 1981-2010. The 31 provincial capital cities in mainland China can be classified into only 5 types, in terms of seasonal variations in thermal comfort conditions, which are: pleasant summer and severe cold winter (type-I); pleasant spring, autumn, winter, and severe hot summer (type-II); pleasant spring and autumn, slightly pleasant summer, and cold winter (type-III); pleasant spring and autumn, hot stress summer, and slightly cold winter (type-IV); and pleasant spring, summer, autumn, and cool winter (type-V). In the past three decades, the cities in mainland China had experienced increasing pleasant spells in late winter and early spring and an intensification of heat stress in summer. The reduction in annual cumulative number of cold stress days in higher latitude/altitude cities outweighs the increase in duration of heat stress in subtropical cities.

In TP, the UTCI stress category covers four categories: strong cold stress, moderate cold stress, slight cold stress, no thermal stress. The distribution frequency of UTCI

categories varies among regions showing clear altitude/latitude dependency. Cold stresses is prevailing throughout the whole year under present day conditions A small amount of days with the no thermal stress category appears in the summer period. The human bio-meteorological condition is most stable from July to September. According to the climate change projections in 2024-2050, annual cumulative pleasant days will increase significantly while days with cold stress will be reduced. Lhasa, Xining, and Yushu will develop in future to the top three cities in terms of thermal favorability.

More WSDI events are found than CSDI events in TP in 2024-2050. No significant increasing or decreasing trend for both indices in TP over the period of 2024-2050 could be detected. The number of extreme events changes from 0.4 per year to 3.3 per year in whole cities for individual city. Calculated trends of WSDI show an increase of warm-spell events in summertime and cold spells in wintertime. Comparing different cities, the variations in trend are small and very similar.

Zusammenfassung

Die vorliegende Arbeit beschäftigt sich mit dem menschlichen thermischen Komfort und dessen Variation in 31 Provinzhauptstädten Festlandchinas und auf dem Hochland von Tibet vor dem Hintergrund der Globalen Erwärmung. Die Physiologische Äquivalenztemperatur (PET), der thermische Klimaindex (UTCI), der Warmperiodenindex (WSDI) und der Kaltperiodenindex (CSDI) werden für die Auswertung verwendet. Neben den Observationsdaten der meteorologischen Stationen werden in dieser Arbeit ebenfalls Simulationen von regionalen Klimamodellen evaluiert. Daten von HadGEM3-RA und RegCM aus dem CORDEX-East Asia Projekt werden verwendet, um die bio-meteorologischen Konditionen im Hochland von Tibet für die Zukunft zu berechnen. Die Städte im Hochland von Tibet werden bezüglich der saisonalen Verteilung des menschlichen thermischen Komforts klassifiziert. Außerdem werden die Variationen des menschlichen thermischen Komforts in vergangenen Dekaden, die regionalen Unterschiede und die Differenzen zwischen den verschiedenen thermischen Indizes analysiert. Zusätzlich werden die bio-meteorologischen Verhältnisse im Hochland von Tibet unter Einbezug von Extremereignissen ausgewertet. Das Ziel ist es, Empfehlungen für Stadtplanung und -management sowie für industrielle und landwirtschaftliche Produktion zu geben und dabei auch die Lebensbedingungen für den Menschen einzubeziehen. Darüber hinaus werden Referenzen zu ähnlichen Forschungsvorhaben genannt.

Die Werte für die PET und UTCI korrelieren sehr gut miteinander und zeigen ein gleiches Muster des thermischen Komforts auf dem chinesischen Festland mit kleinen Unterschieden bezüglich der Sensitivität. Die 31 Städte umfassen 4-8 beziehungsweise 6-8 Klassen von thermischem Komfort in der PET und UTCI Skala. In der Zeitspanne von 1981-2010 gab es durchschnittlich mehr als 160 schöne Tage pro Jahr. Die 31 Provinzhauptstädte Festlandchinas können bezüglich der saisonalen Variationen der Kondition des thermischen Komforts in 5 Klassen unterteilt werden: Angenehmer Sommer und streng kalter Winter (Typ 1), angenehmer Frühling, Herbst und Winter bei extrem heißem Sommer (Typ 2), angenehmer Frühling und Herbst, erträglicher Sommer und kalter Winter (Typ 3), angenehmer Frühling und Herbst, Sommer mit Hitzestress und erträglich kalter Winter (Typ 4) und angenehmer Frühling, Sommer und Herbst bei kaltem Winter (Typ 5). In den vergangenen drei Dekaden wurde in den Städten des chinesischen Festlandes eine steigende Anzahl von

Wärmperioden im späten Winter und zu Beginn des Frühling sowie eine Intensivierung des Hitzestresses im Sommer beobachtet. Der Rückgang der jährlichen Anzahl der Tage mit Kältestress in höheren Breitengraden beziehungsweise in höher gelegenen Städten überwiegt den Anstieg der Dauer der Hitzestressphasen in subtropischen Städten.

Im Hochland von Tibet gibt es 4 Kategorien für thermischen Stress: starker Kältestress, moderater Kältestress, geringer Kältestress, kein thermischer Stress. Die Verteilung der UTCI Kategorien variiert zwischen den Regionen und zeigt eine klare Breitengrad- und Höhenabhängigkeit. Bei aktuellen Bedingen gibt es das ganze Jahr über Regionen mit Kältestress. Eine kurze Phase von Tagen ohne thermischen Stress ereignet sich im Sommer. Die bio-meteorologischen Konditionen sind in den Monaten Juli bis September am Stabilsten. Entsprechend der Klimawandelprojektionen für 2024-2050 nimmt die jährliche Anzahl der angenehmen Tage signifikant zu, während weniger Tage mit Kältestress zu erwarten sein werden. Die Städte Lhasa, Xining und Yushu werden sich in Zukunft zu den Städten mit den besten thermischen Bedingungen entwickeln.

Im Zeitraum 2024-2050 geschehen im Hochland von Tibet mehr WSDI Ereignisse als CSDI Ereignisse. Allerdings konnte für beide Ereignisse keine Signifikant im ansteigenden beziehungsweise abfallenden Trend gefunden werden. Die Anzahl der Extremereignisse steigt für einzelne Städte von 0,4 pro Jahr auf 3,3 pro Jahr. Berechnete Trends für den WSDI zeigen einen Anstieg der Anzahl von Warmperioden im Sommer und Kaltperioden im Winter. Im Vergleich zwischen verschiedenen Städten sind die Unterschiede in den Trends sehr gering oder gleich.

Table of contents

List of Figures

List of Tables

Chapter 1

1 Introduction

1.1 Climate change and human thermal comfort in mainland China

In the past 132 years (1880–2012), the average global temperature has risen by 0.85 ℃, and each of the past three decades has been successively warmer at the Earth's surface than all the previous decades in the instrumental record (IPCC 2013). Global warming has been exerting obvious influences on human habitat and natural environment (IPCC 2013). In addition, increasing urbanization is resulting in urban heat island (UHI) effects; global warming may overlap with or exacerbate the phenomenon of UHI (Shimoda 2003; Corburn 2009; Zhang et al. 2010; Kim and Kim 2011). The increase of air temperature is reflected Global and Regional Climate Models (GCM and RCM), for example, in the framework of the ENSEMBLES (Linden and Mitchell 2009) or EURO-CORDEX (Jacob et al. 2014) projects.

The study of human bio-meteorological environment can be helpful to understand the effects of the climate change on human beings. The human thermal comfort is defined as the condition of mind which expresses satisfaction with the thermal environment (ASHRAE 1966; Terjung 1966; Parsons 2003). It is a condition in which individuals physically and psychologically prefer neither warmer nor cooler temperature. It is of great implications for people's daily work and life (Anderson 1999; Corburn 2009). An adverse effect of heat and cold stress on mortality due to cardiovascular diseases has been reported in many studies (Cheng and Su 2010, Muthers et al. 2010; Matzarakis et al. 2011; Nastos and Matzarakis 2012). Over the years, a number of studies have been conducted to evaluate the indoor and outdoor thermal comfort of cities all over the world (Shiue and Matzarakis 2011; Chen and Ng 2012), which provided valuable information on understanding the effects of climatic conditions on people's thermal sensation as well as the use of spaces.

China is also a country with the largest population in the world, amounting to 1.34 billion in 2010 according to the sixth national population census of China. In the past three decades, China has been experiencing very rapid urbanization process. Its urbanization rate has increased from 19.4% in 1980 to 52.6% in 2012， and more than half of the population has lived in the cities currently (NBSC 2013). There are 31 administrative provinces, autonomous regions and municipalities (uniformly referred

to as provinces hereafter) in mainland China. The capital cities of these provinces are the largest ones among all cities in China as shown in Fig 1.1, such as Beijing, Shanghai and Guangzhou. 260 million people altogether live in these 31 provincial capital cities in mainland China (Fig 1.1), and more than half of the population lives in the downtown areas (NBSC 2011). In addition, almost all of these provincial capital cities are being popular tourist destinations with long history, splendid culture, and beautiful scenery (Zhao 1994). Thus, the human thermal comfort of these provincial capital cities is of significance not only to the daily work and life of the local residents, but also to the tourism services of vast tourist flow.

Fig 1.1 Location of the 31 provincial capital cities in mainland China and spatial distribution of every climate zone. Numbers represent the different climate zones in Table 1 (from Zhang and Yan 2014)

1.2 Diversity climate zones and human bio-meteorological conditions in mainland China

China is the third largest country in the world, has a total land area of 9.6 million squares kilometres. Differences in latitude, longitude, and altitude give rise to sharp variations in climate, tropical in the south to subarctic in the north, humid in the south-east to arid in the north-west. Monsoon winds dominate the climate. The advance and retreat of the monsoons account in large degree for the timing of season (Zhao 1994). The world or a country, even a province can be divided into various

climate zones on the basis of different climate types. Regions classified under the similar climate type have similar climatic attributes and climate zone is a region with similar climate characteristics. Then, this classification can provide a convenient way to have a better understanding of regional climate variations and regional climate characteristics (Barrett and Barrett 1974; Grigg 1965).

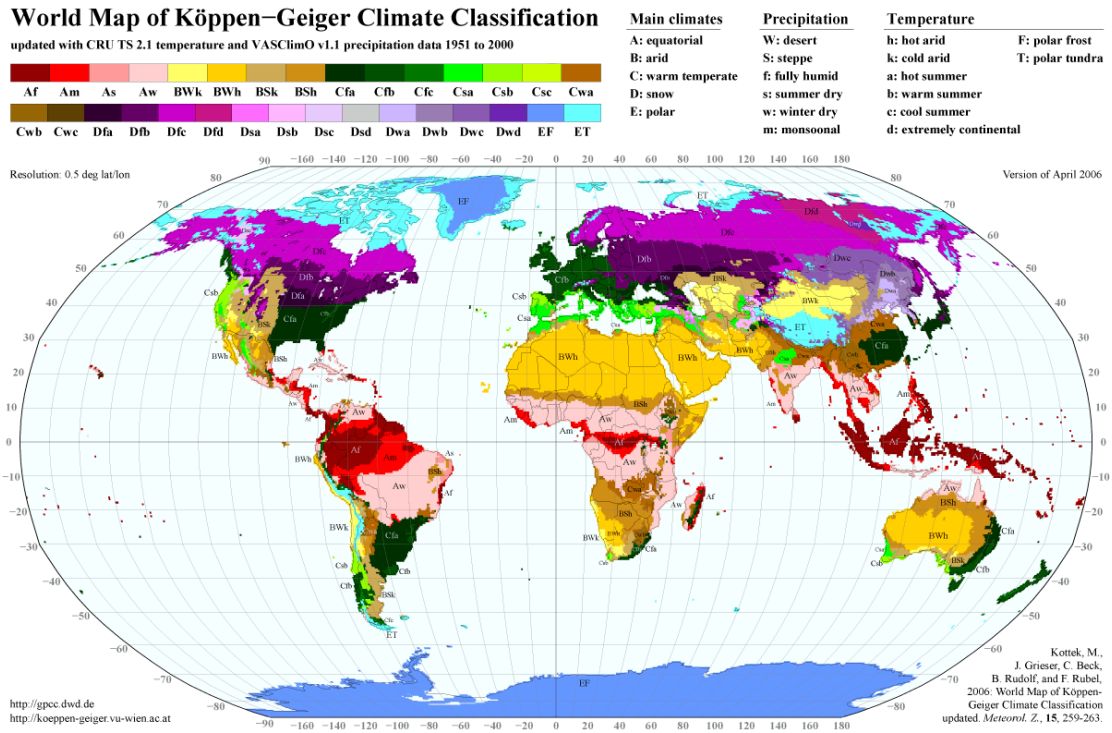

Fig 1.2 Global map of the Köppen-Geiger climate classification in 1951-2000 on a regular 0.5 degree latitude/ longitude grid (Kottek et al. 2006)

Several methods including Köppen-Geiger climate classification (KG climate classification), climate regionalization, and cluster analysis are most commonly used to define climate zones. Köppen-Geiger climate classification and its modified versions (Köppen and Geiger 1923; Thornthwaite 1931, 1948; Geiger and Pohl 1953) have been known to be used widely to define different climate types across the globe (Beck et al. 2005; Kottek et al. 2006; de SA Junior et al. 2011). Fig 1.2 shows the world map of KG climate classification in 1951-2000, based on temperature and precipitation observations for the period 1951-2000. There are seven different climate zones for the whole mainland China and each capital provincial city in mainland China and its corresponding climate zone are shown in Table 1.1. Climate zones are included, cold semi-arid climate (BSk), Cold desert climate (BWk), humid subtropical climate (Cfa), monsoon-influenced humid subtropical (Cwa), subtropical highland

climate or temperate oceanic climate with dry winters (Cwb), monsoon-influenced hot-summer humid continental climate (Dwa) (Fig 1.2, Table 1.2).

Table 1.1 Climate characteristic of every climate zone (Zhang and Yan 2014)

Code	Climate zone	Precipitation (mm)					Temperature (°C)				
		Spring	Summer	Autumn	Winter	Annual	Spring	Summer	Autumn	Winter	Annual
1	Temperate zone	56.5	257.2	68.5	12.1	394.3	2.5	18.7	1.1	-20.1	0.5
2	Sub-humid warm temperate zone	82.7	353.9	93.9	15.5	546.0	6.8	20.9	6.0	-12.4	5.3
3	Humid warm temperate zone	107.1	376.0	134.4	29.8	647.3	12.6	24.0	13.1	-0.5	12.3
4	Arid warm temperate zone	33.8	94.1	36.3	9.7	173.9	10.0	22.0	7.9	-7.7	8.1
5	Northern subtropical zone	242.5	516.0	233.4	75.4	1067.3	16.2	24.6	16.8	6.6	16.0
6	Central subtropical zone	546.6	556.5	230.3	198.8	1532.1	17.4	27.1	19.5	8.3	18.1
7	Southern subtropical zone	377.3	819.6	358.7	100.5	1656.1	22.4	27.1	22.8	15.3	21.9
8	Plateau temperate zone	99.2	316.7	126.8	15.3	558.0	6.6	14.6	6.3	-3.6	6.0
9	Plateau sub-frigid zone	75.7	260.5	92.9	12.0	441.1	0.2	9.8	0.0	-11.1	-0.3
10	Mountain climate type	553.9	776.5	369.3	192.5	1892.1	9.6	18.5	10.8	0.7	9.9

Generally, climate zones in China are classified according to climate regionalization. Similar to the KG climate classification, it has a prior definition of a set of climate rules that are used to classify climate zones. Based on the new investigation by Zhang and Yan 2014, ten climate types were classified using the K-means cluster analysis based on monthly temperature and precipitation data during the period 1966-2005 in China standard. 753 national meteorological stations were included in this research. Table 1.1 indicates ten climate zones and climate characteristic for each climate zone. Nine different types of climate zones in mainland are type2 sub-humid temperate zone, type3 humid warm temperate zone, type4 arid warm temperate zone, type5 Northern subtropical zone, type6 central subtropical zone, type7 southern subtropical zone, type8 plateau temperate zone, type9 plateau sub-frigid zone, type10 mountain climate zone (Fig 1.1, Table 1.1; Zhang and Yan 2014). However, some mountain meteorological stations (11 stations) in southeast China had distinct climate characteristics due to their high elevation, which differentiated them from other meteorological stations, and were classified as one type (type 10), which overlapped with type 6.

Table 1.2 The geographical position and climate zones at the meteorological stations in the 31 provincial capital cities of mainland China

Provincial capital city (Province)	**Köppen-Geiger climate calssification**	**China standards climate calssification**
Beijing (Beijing)	Dwa	3 Humid warm temperate zone
Tianjin (Tianjin)	Dwa	3 Humid warm temperate zone
Shijiazhuang(Hebei)	BSk	3 Humid warm temperate zone
Taiyuan (Shanxi)	BSk	3 Humid warm temperate zone
Hohhot (Inner mongolia)	BSk	4 Arid warm temperate zone
Shenyang (Liaoning)	Dwa	2 Sub-humid warm temperate zone
Changchun (Jilin)	Dwa	2 Sub-humid warm temperate zone
Harbin (Heilongjiang)	Dwa	2 Sub-humid warm temperate zone
Shanghai (Shanghai)	Cfa	5 Northern subtropical zone
Nanjing (Jiangsu)	Cfa	5 Northern subtropical zone
Hangzhou (Zhejiang)	Cfa	5 Northern subtropical zone
Hefei (Anhui)	Cfa	5 Northern subtropical zone
Fuzhou (Fujian)	Cfa	6 Central subtropical zone
Nanchang (Jiangxi)	Cfa	6 Central subtropical zone
Jinan (Shandong)	Cwa	3 Humid warm temperate zone
Zhengzhou (Henan)	Cwa	3 Humid warm temperate zone
Wuhan (Hubei)	Cfa	5 Northern subtropical zone
Changsha (Hunan)	Cfa	6 Central subtropical zone
Guangzhou (Chuangdong)	Cfa	7 Southern subtropical zone
Nanning (Guangxi)	Cfa	7 Southern subtropical zone
Haikou (Hainan)	Cwa	7 Southern subtropical zone
Chongqing (Chongqing)	Cfa	5 Northern subtropical zone
Chengdu (Sichuan)	Cwa	8 Plateau temperate zone
Guiyang (Guizhou)	Cwa	5 Northern subtropical zone
Kunming (Yunnan)	Cwb	5 Northern subtropical zone
Lhasa (Tibet)	Dwb	8 Plateau temperate zone
Hsian (Saanxi)	Cwa/BSk	3 Humid warm temperate zone

Lanzhou (Gansu)	BSk	8 Plateau temperate zone
Xining (Qinghai)	BSk	9 Plateau sub-frigid zone
Yinchuan (Ningxia)	BWk	4 Arid warm temperate zone
Urumqi (Xinjiang)	BSk	4 Arid warm temperate zone

Though, the methods of KG climate classification and China standards of climate classification are different, the types of climate zones are quite similar in mainland China. According to the results of KG climate classification and China standards of climate classification in mainland China, the climate zones of 31 provincial capital cities are shown in Table 1.2. Those various climate zones can also affect a destination by climatic variability which affects the timing of travel and in turn drives the seasonality of tourism demand for the destination (Goh 2012). Based on previous studies in tourism climatology (de Freitas 2003; Matzarakis et al. 2004), regional features, including visual factors, the physical environment and thermal comfort, are important to tourism.

The Tibet Plateau is a remarkable landscape in China, (Mayhew et al. 1999). Furthermore, TP is one of the most sensitive areas for the global climate change. Many studies have showed that in accordance with the global warming, the Qinghai–Tibet Plateau has been experiencing significant warming in the past half century, and its warming rate is generally higher than the global average (Li and Kang 2006). Thus, this work will concentrate more on the effect of climate change on human bio-meteorological conditions in TP.

1.3 The cold climate region-Tibetan Plateau

Tibetan Plateau locates in the central Asia with very high latitude and large scope of geographical area (26°00′～39°47′N, 73°19′～104°47′ E) (Fig 1.3). It is the largest plateau in China and also the highest plateau in the world called as “the roof of the world” and “the third pole”. The climate of TP is typical plateau climate. There are 2500~3200 annual sunshine hours.

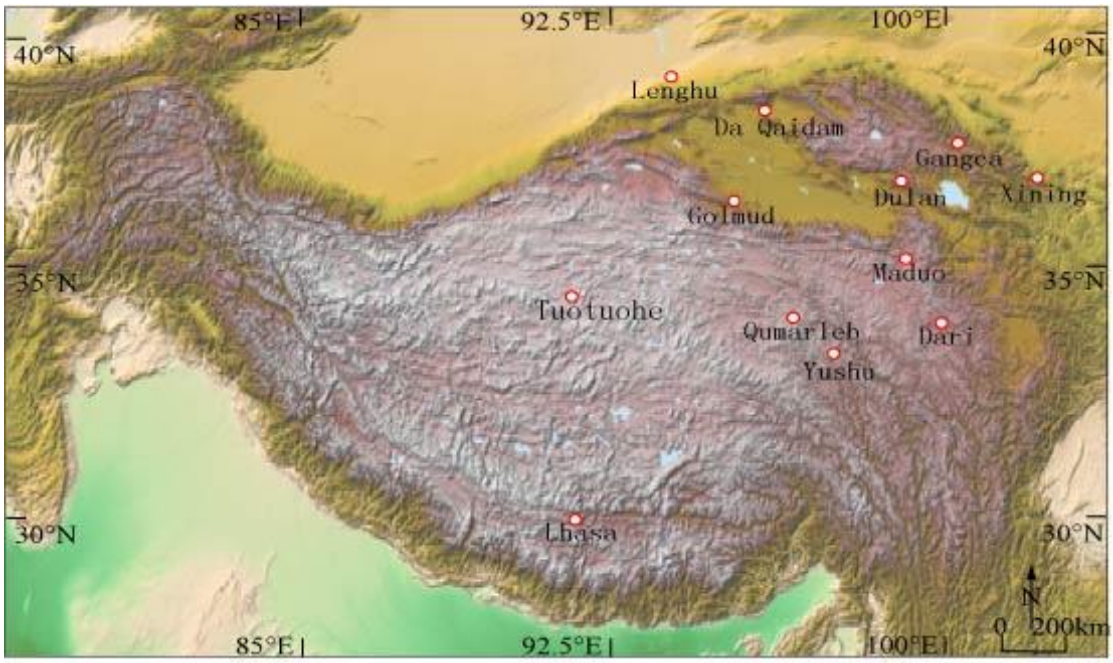

Fig 1.3 Tibetan Plateau and the 12 meteorological stations

Fig 1.4 shows the maximum, minimum and average air temperature (Ta) and average precipitation in TP during 1981-2010. The monthly mean Ta ranges from -9.3 ℃ in December to 13.7 ℃ in July. Summer is more temperate compared to other places in China and the maximum air temperature appears in August and is just 27 ℃, whereas winter is very cold and snowy and the lowest Ta is -36.3 ℃ in January. Summer is warm with high precipitation, especially from June to September. However, winter time (especially from November to March) is cold and dry with very low precipitation. Generally, TP is a very representative region to study the human biomoteorological condition in cold climate zone under the global warming.

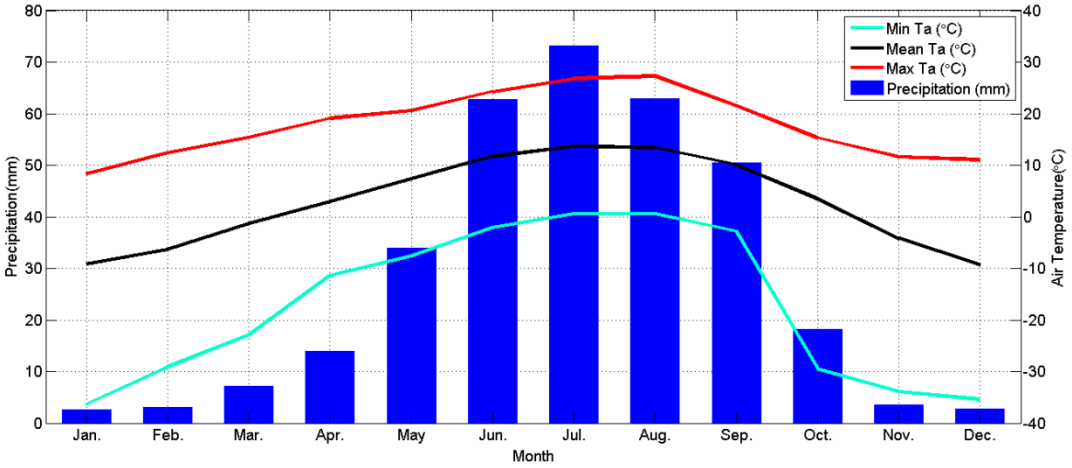

Fig 1.4 Air temperatures and precipitation for TP in1981-2010

Due to this cold climate zone and high elevation, TP boasts of many snow-covered mountains and beautiful lakes. It is the origin of many famous rivers like Yangtze River, Yellow River, Nu River, Lancang River, Yarlung Zangbo River, Ganges River, and Indus River. Its biological diversity is quite unique. It offers fabulous monastery sights, breathtaking high-altitude treks, stunning views of the world's highest mountains and one of the most likeable peoples you will ever meet. Places of interest like Everest, Yarlung Zangbo River, Hoh Xil, Qinghai Lake, Yangbajain Hot Springs, and Potala Palace are captivating attractions to tourists and pilgrims all over the world. Nevertheless, it is the homeland of the Tibetans and other minority groups such as the Hui Muslims and the Qiang people (Mayhew et al. 1999). The Palaeolithic ancestors had left their footprints around the Qinghai Lake as early as 15,000 years ago (Madsen et al. 2006), and the Neolithic ancestors lived there 9,000–5,000 years ago (Rhode et al. 2007). And 4,000 years ago, the ancestors had settled in Lhasa (Kaiser et al. 2009). According to the sixth national census in 2010, the total population size of Tibet and Qinghai provinces has reached 8.629 million, of which 63 % are Tibetans and other ethnic minorities (the Han Chinese account for 37 %). After the construction of Qingzang railway which is a high-elevation railway that connects Xining (Qinghai Province) to Lhasa (Tibet Autonomous Region) of China, more and more tourists visit there.

Most of the present research about the estimation of human bio-meteorological conditions focus on the heat stress related human thermal comfort. Wind chill effects like local cooling of exposed skin, including frostbite risk, should be best regarded as being transient, rather than being a steady state phenomenon (Shitzer 2006; Tikuisis and Osczevski 2002, 2003). People suffer from cold stress in some cold regions like the TP or even in some temperate regions in wintertime. Some researches begin to focus on the human thermal comfort in cold regions recently, i.e. Grigorieva and Matzarakis 2011 calculated the human-bio-meteorological climatic conditions throughout the southern part of the Russian Far East by using the PET and identified areas with extreme and uncomfortable thermal conditions for all seasons and throughout a year. Li and Chi 2014 chose 12 stations of the TP and showed the special and temporal variations of human bio-meteorological environment in the TP during the past 50 years.

1.4 Research background and motivation

More than half of world's population live in urban areas now, and this number is projected to be 66% by 2050 (United Nations 2014). The urbanized and urbanizing landscapes have exerted significant impacts on the local and global ecosystems (Masek et al. 2000). Among severe environmental issues associated with human activities, the urban heat island (UHI) effect has become increasingly important. UHI has received much attention in climatic research (Mitchell 1961). A warming climate will likely result in an increase in the frequency and intensity of heat waves (McMichael et al. 1996; Meehl et al. 2001; Patz and Khaliq 2002).This results in additional hot days in urban locales, which can directly influence the health and welfare of city residents. It can affect human health and well-beings like an increase in morbidity, mortality, and risk of violence (Gong et al. 2012; O'Loughlin et al. 2012; Patz et al. 2005). These impacts were expected to be more serious when interacting with global climate changes (IPCC 2007; McCarthy et al. 2010; Patz et al. 2005). The UHI has become one of the largest problems associated with the urbanization and industrialization of human civilization, as the increased temperatures associated with the UHI tend to exacerbate the threats to human health posed by thermal stress.

In mainland China, with the rapid urbanization and fast development of tourism sectors, the thermal condition has gained growing concern in recent years. In the Yangtze River Valley and South China, the UHI effect enhances the warming trends by about 0.011 ℃/decade (Lin et al. 2004). The spatial variation of urban human thermal comfort in Hangzhou was analyzed based on discomfort index and Landsat TM images (Wang et al. 2004). The indoor thermal comfort in Shanghai's non-air-conditioned buildings was explored, and results showed that the actual mean thermal sensation of a tested group of local Shanghai people was lower than the Predicted Mean Vote (PMV), and the upper operative temperature bound for comfort was as high as 29°C (Ji et al. 2006). The outdoor thermal comfort in Guangzhou was surveyed using the method of thermal sensation vote, and it was found that the neutral temperature and upper acceptable temperature were 25.4°C and 31.6°C respectively (Zhai et al. 2009). Lin and Matzarakis (2011) determined the tourist thermal perceptions in 20 destination cities in eastern China based on PET, and modified the thermal comfort classifications for subtropical regions like eastern China and Taiwan. Lai et al. (2014) revealed that the UTCI satisfactorily predicted the outdoor thermal comfort in Tianjin, North China, and the PMV overestimated it, while the neutral PET range in Tianjin was lower than the ranges in Europe and Taiwan. Yang and Matzarakis (2016) described the human thermal comfort (HTC) and air humidity (AH) information by frequencies of PET and frequencies of vapor pressure (VP) in 12

representative Chinese cities of 11 Köppen-Geiger climate classification types. In spite of these, the knowledge on the spatial and temporal patterns of the human thermal comfort in the major cities across the country is still insufficient.

TP exerts a huge influence on regional and global climate through thermal forcing mechanisms (Duan and Wu 2005; Yanai et al. 1992; Yeh and Gao 1979). The warming trend of this region has been widely studied in the last decades (Chen et al. 2003; Duan et al. 2006; Frauenfeld et al. 2005; Liu and Chen 2000; Liu et al. 2006; Meehl et al. 2007; Niu et al. 2004; Wang et al. 2008; Xu et al. 2003; You et al. 2008a; Kang et al. 2010). It has been also described that the warming trend will be more serious in the next century (Hu et al. 2015; Zhang et al. 2015; Zhou et al. 2014). However, research on the human bio-meteorological conditions for TP just begins. Li and Chi (2014) studied the human thermal environment of TP by using PET and found that the human bio-meteorological conditions had been improved in the past 50 years under the effect of the global warming. In line with global warming, cold stress in TP may be expected to be mitigated, and the thermal comfort conditions become more favourable. Nevertheless, few detailed bioclimatic studies have been conducted in this region. The tourism potential and habitat improvement cannot be achieved unless applied bioclimatic research is carried out.

This study aims to comprehensively study the human thermal comfort features of the 31 provincial capital cities in mainland China, to explore their spatial variations across the country, to research their changes in the past 30 years, and to discuss the implications of the spatiotemporal variations in human thermal comfort of these cities. The comparisons of the performance of different thermal indices in mainland China are also considered in this study. Additionally, this study is also designed to evaluate the effect of reproducing the present climate by climate simulations (ERA-Interim, HadGEM3-RA and RegCM), to project the human thermal comfort in TP in the near future through HadGEM3-RA and RegCM under the scenarios of RCP4.5 and RCP8.5 and evaluate them in terms of UTCI. The cold spell duration and warm spell duration in Tibetan Plateau in the near future will also be presented. The present work extends the application of the UTCI to the cold and high altitude regions. In addition, efforts are made to improve the human thermal environment in mainland China and also TP and potentially guide the government to make policies for population migration, urban and tourism planning, energy consumption, social economy .etc.

The following main research questions will be explored in this study:

Question 1: How different is the Human bio-meteorological condition in different regions in China?

Question 2: How do the different human thermal indices like PET and UTCI compare with each other?

Question 3: How will the anticipated climate change affect the human bio-meteorological condition in the future?

This thesis is arranged into seven chapters. Chapter 2 explains the description of the data and methods which are applied in this research. Chapter 3 deals with question 1 and 2. It investigates the human bio-meteorological conditions and the variations in the 31 provincial capital cities of mainland China in the past 30 years. In this chapter, the comparison between PET and UTCI is also presented. Chapter 4 explores the assessment of human-bio-meteorological environment over the Tibetan Plateau region based on CORDEX climate model projections. Chapter 5 is designed for the analysing of cold spell duration and warm spell duration in Tibetan plateau to evaluate the human bio-meteorological conditions in the near future. Question 3 will be discussed in Chapter 4 and 5. Chapter 6 and Chapter 7 are dedicated to discussions, conclusions and outlook, respectively.

Chapter 2

2 Data and Methods

2.1 Data sources

2.1.1 Observation data

For different countries and regions, the Urban Heat Island (UHI) effect will be different due to the situation of meteorological observations in different countries (Li et al. 2004). Peterson (2003) used different methods on the air temperature data and tried to eliminate the biases which caused by changes in elevation, latitude, time of observation, and instrumentation. No statistically significant impact between urban and rural stations' surface temperature was found after the application of methods. Wang et al. (1990) chose 42 pairs of China urban and rural stations to study UHI effects on urban and rural regions.

The stations, which we use are the national stations and the data are reliable. Furthermore, we study the period 1981-2010. All of the stations are the new stations, established after 1951, when, because of the urbanization, all of the national urban stations moved to suburban areas. All the stations are located in the suburban areas and can be compared with each other. 31 provincial capital cities in China have been considered in this study, namely, Beijing, Tianjin, Harbin, Changchun, Shenyang, Hohhot, Taiyuan, Shijiazhuang, Hsian, Lanzhou, Yinchuan, Xining, Urumqi, Zhengzhou, Wuhan, Changsha, Shanghai, Jinan, Nanjing, Hefei, Hangzhou, Nanchang, Fuzhou, Guangzhou, Nanning, Haikou, Chengdu, Chongqing, Guiyang, Kunming, and Lhasa (Fig 1.1, Table 2.1). Table 2.1 presents the geographical position and seasonal climate condition in every capital provincial city.

Table 2.1 The geographical position and seasonal climate condition (1981-2010) at the meteorological stations in the 31 provincial capital cities of mainland China

Provincial capital city/ Province	Latitude (°N)	Longitude (°E)	Altitude (m)	Season	Air temperature (℃)	Vapor pressure (hpa)	Relative humidity (%)	Wind speed (m/s)
				Winter	-1.4	2.4	44.0	2.5
Beijing	39 °48'	116 °28'	31.3	Spring	14.0	7.7	45.7	3.0
(Beijing)				Summer	25.5	21.8	69.7	2.0
				Autumn	12.8	9.8	61.0	2.1
				Winter	-1.6	3.1	56.7	2.2
Tianjin	39 °05'	117 °04'	2.5	Spring	13.9	8.6	52.0	2.9

Provincial capital city/ Province	Latitude (°N)	Longitude (°E)	Altitude (m)	Season	Air temperature (℃)	Vapor pressure (hpa)	Relative humidity (%)	Wind speed (m/s)
(Tianjin)				Summer	25.8	23.5	71.7	2.0
				Autumn	13.5	11.0	64.7	2.0
				Winter	-0.7	3.2	58.0	2.0
Shijiazhuang	38 °02'	114 °25'	81	Spring	14.3	9.3	58.0	2.7
(Hebei)				Summer	26.1	22.9	71.3	2.1
				Autumn	13.7	11.2	67.7	1.9
				Winter	-3.2	2.4	50.7	1.8
Taiyuan	37 °47'	112 °33'	778.3	Spring	12.0	6.8	47.3	2.4
(Shanxi)				Summer	22.8	18.4	68.3	1.7
				Autumn	10.0	8.8	66.7	1.5
Hohhot				Winter	-8.4	1.8	55.0	1.3
(Inner	40 °49'	111 °41'	1063	Spring	9.3	4.6	39.7	2.1
Mongolia)				Summer	22.0	13.8	56.7	1.5
				Autumn	7.6	6.4	56.7	1.4
				Winter	-8.5	2.1	60.0	2.6
Shenyang	41 °44'	123 °31'	49	Spring	9.8	6.8	52.7	3.5
(Liaoning)				Summer	23.5	21.4	74.0	2.6
				Autumn	9.3	8.8	65.7	2.8
				Winter	-12.0	1.7	63.3	3.3
Changchun	43 °54'	125 °13'	236.8	Spring	7.6	5.5	49.3	4.3
(Jilin)				Summer	22.1	19.0	72.3	3.0
				Autumn	6.8	7.3	62.7	3.4
				Winter	-14.8	1.5	68.7	2.5
Harbin	45 °45'	126 °46'	142.3	Spring	6.8	5.4	51.3	3.5
(Heilongjiang)				Summer	21.9	18.7	72.0	2.7
				Autumn	5.5	6.9	64.3	2.9
				Winter	6.1	7.2	72.0	2.1
Shanghai	31 °24'	121 °27'	5.5	Spring	15.2	13.1	72.7	2.4
(Shanghai)				Summer	27.1	27.9	78.7	2.4
				Autumn	19.2	17.3	73.7	2.1
				Winter	4.2	6.1	73.3	2.2
Nanjing	32 °00'	118 °48'	7.1	Spring	15.3	12.8	71.3	2.6
(Jiangsu)				Summer	26.8	27.6	78.7	2.4
				Autumn	17.3	15.8	76.3	2.1
				Winter	6.0	7.0	74.0	2.1
Hangzhou	30 °14'	120 °10'	41.7	Spring	16.0	13.8	74.3	2.2
(Zhejiang)				Summer	27.3	27.7	78.0	2.2
				Autumn	18.6	17.0	76.3	2.0
				Winter	4.4	6.2	74.0	2.6
Hefei	31 °52'	117 °14'	27.9	Spring	16.0	13.4	71.3	3.1
(Anhui)				Summer	27.1	28.1	79.0	2.8
				Autumn	17.3	15.6	75.0	2.5
				Winter	11.9	10.5	73.3	2.4

Provincial capital city/ Province	Latitude (°N)	Longitude (°E)	Altitude (m)	Season	Air temperature (℃)	Vapor pressure (hpa)	Relative humidity (%)	Wind speed (m/s)
Fuzhou	26 °05'	119 °17'	84	Spring	18.3	17.0	78.7	2.3
(Fujian)				Summer	28.0	28.7	77.0	2.9
				Autumn	22.2	19.5	71.5	2.7
				Winter	7.0	7.6	74.7	2.1
Nanchang	28 °36'	115 °55'	46.7	Spring	17.3	16.2	78.7	2.0
(Jiangxi)				Summer	28.1	29.2	78.0	2.0
				Autumn	19.6	17.2	72.3	2.2
				Winter	1.4	3.6	52.5	2.9
Jinan	36 °36'	117 °03'	170.3	Spring	15.7	8.9	48.3	3.7
(Shandong)				Summer	26.6	23.1	67.5	2.8
				Autumn	15.5	11.2	59.8	2.8
				Winter	2.2	4.1	59.3	2.4
Zhengzhou	34 °43'	113 °39'	110.4	Spring	15.4	10.7	59.7	2.7
(Henan)				Summer	26.3	24.4	72.7	2.1
				Autumn	15.0	12.3	69.0	1.9
				Winter	5.6	6.8	74.7	1.4
Wuhan	30 °37'	114 °08'	23.1	Spring	17.0	15.0	74.7	1.6
(Hubei)				Summer	27.9	28.6	77.0	1.7
				Autumn	18.1	16.2	75.3	1.3
				Winter	6.5	7.9	79.7	2.3
Changsha	28 °13'	112 °55'	68	Spring	17.0	15.9	80.0	2.3
(Hunan)				Summer	27.8	28.4	78.0	2.2
				Autumn	18.4	17.2	79.0	2.2
				Winter	14.0	12.7	77.0	1.2
Nanning	22 °38'	108 °13'	121.6	Spring	22.0	21.7	80.3	1.4
(Guangxi)				Summer	28.2	30.6	81.7	1.4
				Autumn	23.1	21.7	75.7	1.1
				Winter	18.8	18.6	84.8	2.2
Haikou	20 °00'	110 °15'	63.5	Spring	24.9	26.3	83.8	2.4
(Hainan)				Summer	28.7	31.5	82.2	2.2
				Autumn	25.3	26.3	81.7	2.1
				Winter	9.0	9.5	83.0	1.2
Chongqing	29 °31'	106 °29'	351.1	Spring	18.3	16.3	77.0	1.5
(Chongqing)				Summer	27.2	27.1	77.0	1.5
				Autumn	19.0	18.3	82.7	1.2
				Winter	6.0	7.5	79.2	2.4
Guiyang	26 °35'	106 °44'	1223.8	Spring	15.2	13.3	75.5	2.6
(Guizhou)				Summer	22.8	21.3	77.5	2.3
				Autumn	16.0	14.3	77.2	2.2
				Winter	9.6	7.5	66.0	2.2
Kunming	25 °01'	102 °41'	1892.4	Spring	16.9	11.0	59.3	2.7
(Yunnan)				Summer	20.1	18.4	79.3	1.8
				Autumn	15.5	13.6	77.7	1.7

Provincial capital city/ Province	Latitude (°N)	Longitude (°E)	Altitude (m)	Season	Air temperature (℃)	Vapor pressure (hpa)	Relative humidity (%)	Wind speed (m/s)
				Winter	-2.1	1.6	29.7	1.0
Lhasa	29 °40'	91 °08'	3648.7	Spring	6.8	3.8	40.7	1.8
(Tibet)				Summer	13.8	9.8	64.3	1.0
				Autumn	6.6	5.5	51.3	1.3
				Winter	-6.4	2.1	52.7	2.3
Lanzhou	36 °03'	103 °53'	1517.2	Spring	9.2	5.0	46.7	2.7
(Gansu)				Summer	19.4	12.8	63.0	2.2
				Autumn	7.3	7.4	65.3	2.0
				Winter	-5.6	1.8	47.0	1.1
Xining	36 °43'	101 °45'	2295.2	Spring	7.5	5.0	49.3	1.6
(Qinghai)				Summer	16.4	11.5	64.7	1.2
				Autumn	6.1	6.3	63.3	1.0
				Winter	-5.1	2.3	54.7	2.0
Yinchuan	38 °29'	106 °13'	1111.4	Spring	11.2	5.9	43.7	2.7
(Ningxia)				Summer	22.6	15.9	60.0	2.2
				Autumn	9.4	7.8	62.7	2.0
				Winter	-9.0	2.3	50.3	1.1
Urumqi	43 °47'	87 °39'	935	Spring	1.2	5.7	57.3	2.0
(Xinjiang)				Summer	11.5	10.8	66.3	1.8
				Autumn	1.4	5.9	55.3	1.5
				Winter	14.9	12.2	70.3	1.5
Guangzhou	23 °10'	113 °20'	41	Spring	22.2	22.0	80.3	1.5
(Guangdong)				Summer	28.6	30.7	79.0	1.6
				Autumn	24.1	21.4	69.3	1.5
				Winter	6.9	2.9	84.3	1.0
Chengdu	30 °40'	104 °01'	506.1	Spring	16.5	6.1	79.3	1.3
(Sichuan)				Summer	24.7	12.8	84.7	1.5
				Autumn	17.1	8.5	84.7	1.2
				Winter	1.3	4.4	67.3	1.2
Hsian	34 °18'	108 °56'	397.5	Spring	14.7	10.8	66.0	1.5
(Shaanxi)				Summer	25.7	21.6	72.3	1.2
				Autumn	13.6	12.4	78.7	1.0

Meteorological data of the 31 meteorological stations, including the air temperature, wind velocity, vapour pressure, and cloud cover at 2 am, 8 am, 2 pm, 8 pm (GMT +8) per day during the period of January 1st, 1981 to December 31th, 2010 were downloaded from the China Meteorological Data Sharing Service System (China Meteorological Administration National Meteorological Information Center 2013). 12 Meteorological stations in Qinghai Province and Tibet Autonomous Region of China are selected in the study as shown in Fig 1.3. The corresponding geography

information can be found in Table 2.2. These stations are representative for analysing the human bio-meteorological conditions since they contain different administrative division levels: city, county and town. The daily data of air temperature, relative humidity, vapour pressure, cloud cover, precipitation and wind velocity for the period of 1979–2005 are downloaded from the China Meteorological Data Sharing Service System (China Meteorological Administration National Meteorological Information Center 2013) for the 12 meteorological stations Dari, Da Qaidam, Dulan, Gangca, Golmud, Lhasa, Lenghu, Maduo, Qumarleb, Tuotuohe, Xining, and Yushu (Fig 1.3, Table 2.2).

Table 2.2 Selected Meteorological stations in Tibetan Plateau in this study

Station	Latitude (°E)	Longitude (°N)	Altitude (m)	Population	Administration division level
Dari	35.95	99.69	4,547	30,000	County
Da Qaidam	38.06	95.33	3,173	10,127	County
Dulan	36.39	98.07	2,677	53,000	County
Gangca	37.32	100.13	3,300	42,000	County
Golmud	36.26	94.55	2,800	300,000	City
Lhasa	29.66	91.14	3,650	559,400	City
Lenghu	38.91	93.33	2,783	24,000	Town
Maduo	35.08	98.25	4,200	14,400	County
Qumarleb	34.34	95.79	4,500	20,000	County
Tuotuohe (Tanggula Town)	34.29	91.69	4,547	1,900	Town
Xining	36.66	101.78	2,261	2,310,800	City
Yushu	33.03	97.00	4,200	100,000	City

In order to explore the influence of seasonal thermal comfort variation on tourist flow, monthly tourist flow data of five representative cities including Hohhot, Shanghai, Chengdu, Haikou, and Kunming in 2010 were extracted from the tourism e-government network of these cities.

2.1.2 Model data

The Coordinated Regional climate Downscaling Experiment (CORDEX), one of the international inter-comparison projects, aims at improving coordination of international efforts in regional climate modelling research (Giorgi et al. 2009). CORDEX-East Asia is the East Asian branch of the CORDEX initiative and produces ensemble climate simulations based on multiple dynamical and statistical downscaling models forced by multiple global climate models (https://cordex-ea.climate.go.kr/main/mainPage.do).

The data sets of CORDEX-East Asia include data archived from the Hadley Centre Global Environment Model (HadGEM3-RA) (Martin et al. 2006) and regional climate model version 4 (RegCM4) (Giorgi et al. 2012) respectively. The daily data such as air temperature (mean, maximum, and minimum), wind speed (10m height), global radiation and water vapour pressure during 1979-2005 are analysed with the spatial resolution of 0.44°×0.44° (48.84 km) per grid. To evaluate the simulations, results for observation data are compared with the selected 12 stations (Table 2.2). The data of HadGEM3-RA and RegCM4 are used to calculate the future climate (2024-2050) under two different emission scenarios (RCP 4.5 and RCP 8.5).

2.2 Methods

A climate comfort index is an indicator of how the human body feels in response to the atmospheric environment, considering the combined effects of meteorological factors such as temperature, humidity, wind velocity, cloud cover and vapour pressure. To measure the degree of human comfort in relation to weather, some meteorological parameters should be applied. Besides air temperature, wind speed, humidity, radiation should be also considered to describe the human bio-meteorological conditions (Robinson 2001). A large number of thermal models have been developed in the last decades, such as the pioneering Predicted Mean Vote (PMV) by Fanger (1970), the Standard Effective Temperature (SET) by Gagge et al. (1986), the Apparent Temperature (AT) by Steadman (1984, 1994), the Physiologically Equivalent Temperature (PET) by Höppe (1999) and Matzarakis et al. (1999, 2007), the Perceived Temperature (PT) by Jendritzky et al. (2000) and Staiger et al. (2012), and the Universal Thermal Climate Index (UTCI) by Jendritzky et al. (2012). Of these, the PET and UTCI are preferable to other thermal indices for their widely known unit (℃), as the indicators of thermal stress and/or comfort. These indices are of particular importance for common users such as residents, tourists, planners, and policy makers, who most likely are unfamiliar with human bio-meteorological terminology (Matzarakis et al. 2007; Matzarakis and Amelung 2008; Pappenberger et al. 2015). Therefore, in this work focusses on both, PET and UTCI.

Both PET and UTCI were respectively applied to describe the human thermal comfort and its changes in the 31 provincial capital cities of mainland China. Based on the PET and UTCI values with 6-h resolution in every day, the daily average PET and UTCI values were calculated for each city, then their monthly and annual cumulative

day-number of every PET and UTCI classes, and that in mainland China as a whole, were respectively compiled for the period of 1981-2010 according to climatological convention. The similarity and difference in the results between PET and UTCI were compared. The hierarchical cluster method was used to classify the 31 provincial capital cities according to their frequencies of PET and UTCI classes during 1981–2010 (Kendrick 2005). The correlation coefficient was applied to test whether the monthly tourists flow in representative cities follows the rhythm of seasonal variation in thermal comfort.

2.2.1 Physiologically Equivalent Temperature (PET)

Physiologically equivalent temperature (PET), a thermal index is defined as "the air temperature at which, in a typical indoor setting (without wind and solar radiation), the heat balance of human body is maintained with core and skin temperatures equal to those under the conditions being assessed (indoors/ outdoors)" (Mayer and Höppe 1987; Höppe 1993, 1999; Matzarakis et al. 1999). It is based on a human energy balance model "Munich Energy Balance Model for individuals" (MEMI, Höppe 1984) and the equation (Eq 2.1, Höppe 1999) is as following:

$$M + W_o + R + C + E_{sk} + E_{res} + E_{sw} + S = 0 \qquad (2.1)$$

In this equation, M stands for the metabolic heat production, W_o is the mechanical work, R are the fluxes of radiation, C stands for the sensible heat, and E means the latent heat. E is divided into fluxes from or to the $skin_{sk}$, through $sweating_{sw}$ and via the $respiratory\ system_{res}$. All of these parameters are in the unit W . The heat storage S is assumed to equal 0 W at any time (assuming a steady state). Additionally, all parameters mentioned above are closely related to meteorological factors. C and E are related to the air temperature; E_{res} and E_{sw} are corresponding to the humidity; C and E_{sw} are related to wind speed and R is depending on mean radiant temperature.

The mean radiant temperature Tmrt (°C) is one of the most important input parameters for calculation of PET (Herrmann and Matzarakis 2012; Charalampopoulos et al. 2013; Chen and Matzarakis 2014). It is an equivalent surface temperature, which summarizes the effect of all the different short- and longwave radiation fluxes (Fanger 1972; Jendritzky et al. 1990; Kántor and Unger 2011; Chen et al. 2014). It is defined as the surface temperature of a perfect black equal environment, which leads to the same energy balance as the current environment (VDI-Kommission Reinhaltung der Luft 1988, Helbig et al. 1999; VDI 2008; Fanger

1972). Tmrt can be estimated from the amount of clouds covering the sky can be included due to their impact on the radiation fluxes (Matzarakis and Rutz 2005).

Clothes and activity are two individual factors that have significant correlation with human thermal comfort. The amount of thermal insulation worn by a person has a substantial impact on thermal comfort, because it influences the heat loss and consequently the thermal balance (Havenith 1999; McCullough et al. 2009). The index clo describes the clothing insulation (Toftum 2005). Fig 2.1 shows the different wearing and the related clo values.

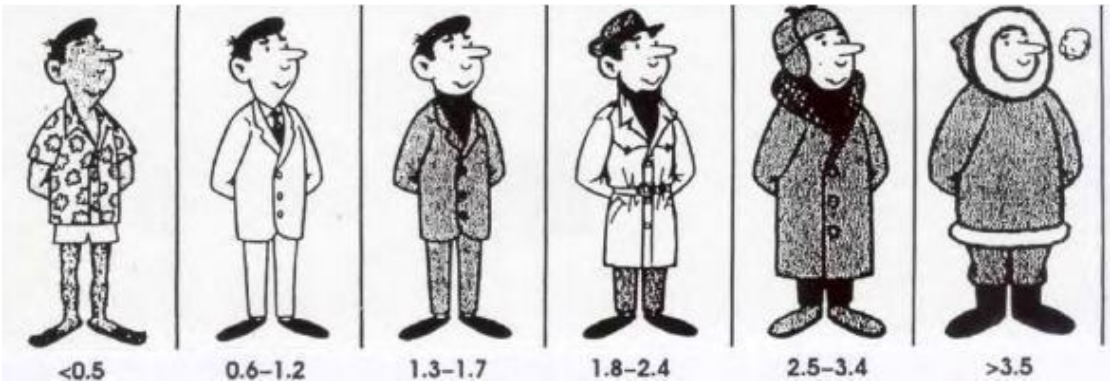

Fig 2.1 Insulation of clothing in clo index (Andris and Steven, 1997)

People have different metabolic rates that can fluctuate due to activity level and environmental conditions (Toftum 2005). Table 2.3 shows the metabolic rates of usual activities. Food and drink habits may have an influence on metabolic rates, which indirectly influences human thermal preferences (Szokolay, 2010).

Table 2.3 Metabolic rates for typical task (ASHRAE 2010)

Activity	**met**	**W/m^2**	**W(av)**
Sleeping	0.7	40	70
Reclining, lying in bed	0.8	46	80
Seated, at rest	1.0	58	100
Standing, sedentary work	1.2	70	120
Very light work (shopping, cooking, light industry)	1.6	93	160
Medium light work (house, machine tool)	2.0	116	200
Steady medium work (jackhammer, social dancing)	3.0	175	300
Heavy work (sawing, planning by hand, tennis)	6.0	350	600
Very heavy work (squash, furnace work)	7.0	410	700

The RayMan model (Matzarakis et al. 2007, 2010) is used to calculate PET and UTCI (in the part 2.2.2). The following variables were input in the model: air temperature,

vapour pressure, wind velocity, and cloud cover. Specifically, the wind velocity values at 1.1 m and 10 m height were used for the calculation of PET and UTCI respectively, and the former was converted from the latter in terms of the wind velocity-height empirical formula as follows (Gandemer and Guyot 1976; NEAC 2012):

$$V_n = V_1 \left[\frac{Z_n}{Z_1}\right]^{\alpha} \qquad (2.2)$$

Of which, V_n denotes the wind velocity at heightZ_n, V_1 represents the observed wind velocity at heightZ_1, αis a surface roughness coefficient, being 0.22 for urban area (NEAC 2012).

People from different regions have different thermal sensations because of different physiology, physics and culture. Each country has unique lifestyle and regulation; therefore, the standards of perception are disimilar in different countries (Eisler et al. 2003). Table 2.4 shows the different thermal sensation classifications in different climate zones; PET range Western/ Middle European is based on the study of Matzarakis and Mayer 1996 in Western/ Middle European. Lin and Matzarakis 2008 explored the human thermal perception in Taiwan which is in tropical climate zone and found that the thermal sensation varied compared to Western/ Middle European standards. However, according to the results of Lai et al. 2014, in Tianjin (city in northern China) larger difference are in the thermal sensation among the three types of standards. PET is well suited to the evaluation of the thermal component of different climates. PET uses a 9-class thermal sensation scale (Table 2.3).

Table 2.4 Thermal sensation scale of PET (Lai et al. 2014; Lin and Matzarakis 2008; Matzarakis and Mayer 1996)

PET range (°C) Western/middle European	PET range (°C) Taiwan	PET range (°C) Tianjin	Thermal sensation	Physiologically thermal stress
<4	<14	<-16	Very cold	Extreme cold stress
4~8	14~18	-16~-11	Cold	Strong cold stress
8~13	18~22	-11~-6	Cool	Moderate cold stress
13~18	22~26	-6~11	Slightly cool	Slightly cold stress
18~23	26~30	11~24	Neutral/comfortable	No thermal stress
23~29	30~34	24~31	Slightly warm	Slightly heat stress
29~35	34~38	31~36	Warm	Moderate heat stress
35~41	38~42	36~46	Hot	Strong heat stress
>41	>42	>46	Very hot	Extreme heat stress

2.2.2 Universal Thermal Climate Index (UTCI)

A decade ago, the International Society on Biometeorology (ISB) recognised these shortcomings in thermal indices and established Commission 6: "On the development of a Universal Thermal Climate Index (UTCI)" (Jendritzky et al. 2002). Since 2005, these efforts have been reinforced by the COST Action 730 (Cooperation in Science and Technology, supported by the EU RTD Framework Programme), which has provided the basis for European scientists from 19 countries plus experts from Australia, Canada, Israel and New Zealand to collaborate on the development of such an index (COST UTCI 2004). The aim was an international standard based on the latest scientific progress in human-response-related thermo-physiological modelling over the last four decades. The term "universal" must be understood in terms of being appropriate for all assessments of the outdoor thermal conditions in the major human bio-meteorological applications such as daily forecasts and warnings of extreme weather, to bioclimatic mapping, urban and regional planning, environmental epidemiology and climate impact research (Jendritzky et al. 2012). This covers the fields of public weather service, the public health system, precautionary planning, and climate impact research in the health sector.

Universal Thermal Climate Index (UTCI) is defined as the isothermal air temperature of the reference conditions that would elicit the same dynamic response (strain) of the physiological model than the actual environment (Jendritzky 2012). The reference conditions are defined as follows: walking at a speed of 4 km/h (which is equivalent to a metabolic rate of 2.3 MET or 135W/m2), Tmrt equal to UTCI, a 10-m wind speed of 0.5 m/s and relative humidity of 50 % that is capped at a water vapour pressure of 20 hPa for Ta > 29 ℃. The thermal stress assessment scale (Table 2.5) has been derived from the modelled physiological and psychological response (Bröde et al. 2012).

Table 2.5 UTCI equivalent temperatures categorized in terms of thermal stress (Bröde et al. 2012)

UTCI (°C) range	Stress Category
above +46	extreme heat stress
+38 to +46	very strong heat stress
+32 to +38	strong heat stress
+26 to +32	moderate heat stress
+9 to +26	no thermal stress
+9 to 0	slight cold stress
0 to -13	moderate cold stress
-13 to -27	strong cold stress
-27 to -40	very strong cold stress
below -40	extreme cold stress

UTCI is based on a multi-node model (Fiala et al. 1999, 2001, 2012) of thermo-regulation which simulates the exchange of the energy between the surroundings and human body and also the responses of the human body and environment. Thermo-regulation is the ability of an organism to keep its body temperature within certain boundaries, even when the surrounding temperature is very different (Eq 2.3).

$$\mathrm{UTCI} \sim \mathrm{f}(T_a, T_{mrt}, \mathrm{v}, \mathrm{e}) \qquad (2.3)$$

Fiala's model is coupled with a state-of-the-art clothing model (Havenith et al. 2012) that takes into consideration Ta-driven behavioural adaptation of clothing insulation by the general urban population in response to actual environmental temperature (Jendritzky 2012) (Fig 2.2).

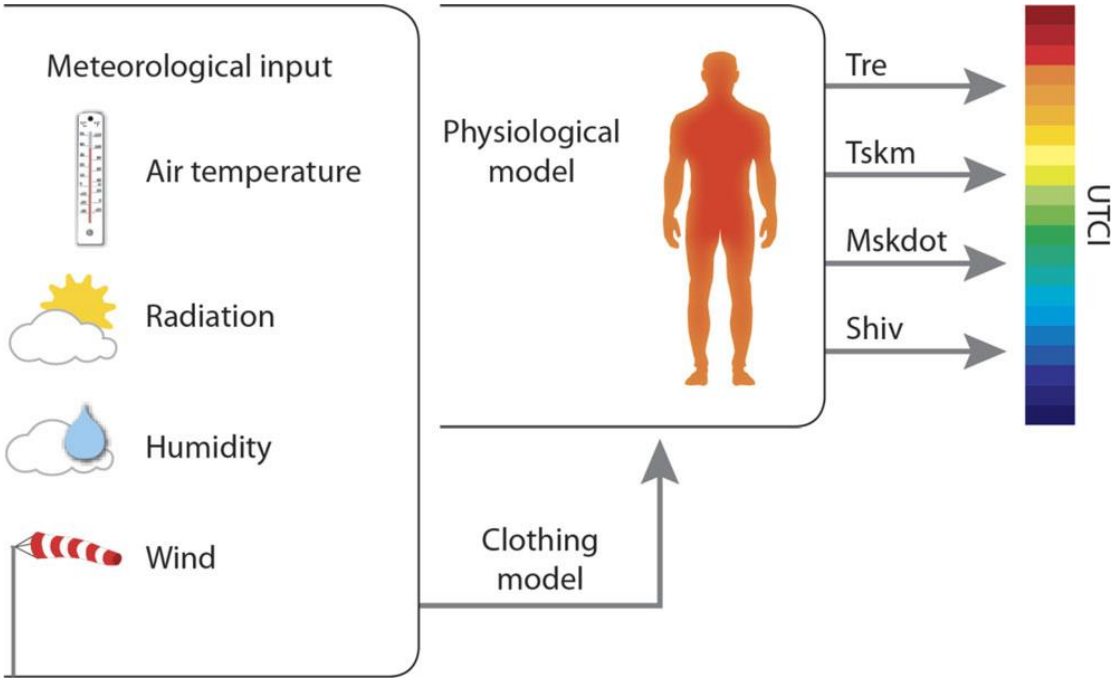

Fig 2.2 Concept of the UTCI derived from the dynamic multivariate response of the thermo physical UTCI-Fiala model (Fiala et al. 2012), which was coupled with a clothing model (Havenith et al. 2012). Tre rectal temperature, Tskm mean skin temperature, Mskdot sweat production, Shiv heat generated by shivering. Figure after Błażejczyk et al. 2013, Pappenberger et al. 2015.

Compared to PET, the physiological parameters cannot be set in UTCI. The walking speed of 4 km/h (1.1m/s), an internal heat production of 135W/m^2 and a self-adapting clothing insulation are assumed (Jendritzky 2012). Different meteorological variables are required for calculation of UTCI: air temperature, relative humidity, wind speed at 10m height, mean radiant temperature (an indicator of the global radiation). As PET, Tmrt also strongly influences UTCI (Chen and Matzarakis 2014; Fröhlich and Matzarakis 2016). Besides, UTCI is very sensitive to wind speed (Chen and Matzarakis 2014; Fröhlich and Matzarakis 2016). The RayMan model (Matzarakis et al. 2007, 2010) is also used to calculate the UTCI values in this study.

Chapter 3

3 The thermal comfort and its changes in the 31 provincial capital cities of mainland China in the past 30 years

In this chapter, the thermal comfort and its changes in the 31 provincial capital cities of mainland China in the past 30 years are comprehensively evaluated using the Physiologically Equivalent Temperature (PET) and Universal Thermal Climate Index (UTCI) indicators.

3.1 The thermal comfort spectrum of PET and UTCI

Fig 3.1 shows the calculated UTCI and PET for the studied 31 cities. In terms of the PET, in 21 temperate and subtropical provincial capital cities, their thermal comfort class covered 8 classes, there detected no extreme heat stress. These cities included Beijing, Tianjin, Taiyuan, Shijiazhuang, Lanzhou, Hohhot, Nanning, Guangzhou, Zhengzhou, Wuhan, Changsha, Shanghai, Jinan, Nanjing, Hefei, Hangzhou, Nanchang, Hsian, Fuzhou, Chengdu and Chongqing (Fig 3.1 (a), Table 2.1). While, in Guiyang and Kunming in the Yunnan-Guizhou Plateau in Southwest China, in Xining, Yinchuan and Urumqi in Northwest China, in Harbin, Changchun and Shenyang in Northeast China, include 7 thermal sensation classes, *extreme cold stress, strong cold stress, slight cold stress, no thermal stress, slight heat stress and moderate heat stress*. In tropical Haikou, it covered another 7 classes, *strong cold stress, moderate cold stress, slight cold stress, no thermal stress, slight heat stress, moderate heat stress, and strong heat stress* (Fig 3.1 (a)). In Lhasa, the city located at the highest elevation, only 6 classes appeared, various degrees of cold stress was predominant, there experienced dozens of neutral and slight heat stress days, yet sensed no moderate to extreme heat stress.

In terms of the UTCI, 4–8 classes of the 10 categories sensation scale appear in the 31 provincial capital cities of mainland China, depending on their locations (Fig 3.1 (b), Table 2.1). In high-latitude or high-altitude cities, such as Harbin, Changchun, Shenyang, Urumqi, Hohhot, Yinchuan, and Lhasa, Xining, etc. cold stress classes dominated, lasting even for more than half a year (Fig 3.1 (b), Table 2.1). On the contrary, in low-latitude cities, i.e. Haikou, Guangzhou, and Nanning, heat stress

classes prevailed (Fig 3.1 (b), Table 2.1). Most of the other cities suffered from both heat and cold stress (Fig 3.1 (b)). There experienced no extreme heat stress in all of these cities, and there occurred only a few extreme cold stress days in a few high-latitude/altitude cities (Fig 3.1 (b), Table 2.1), i.e. Harbin, Shenyang, Changchun and Lhasa.

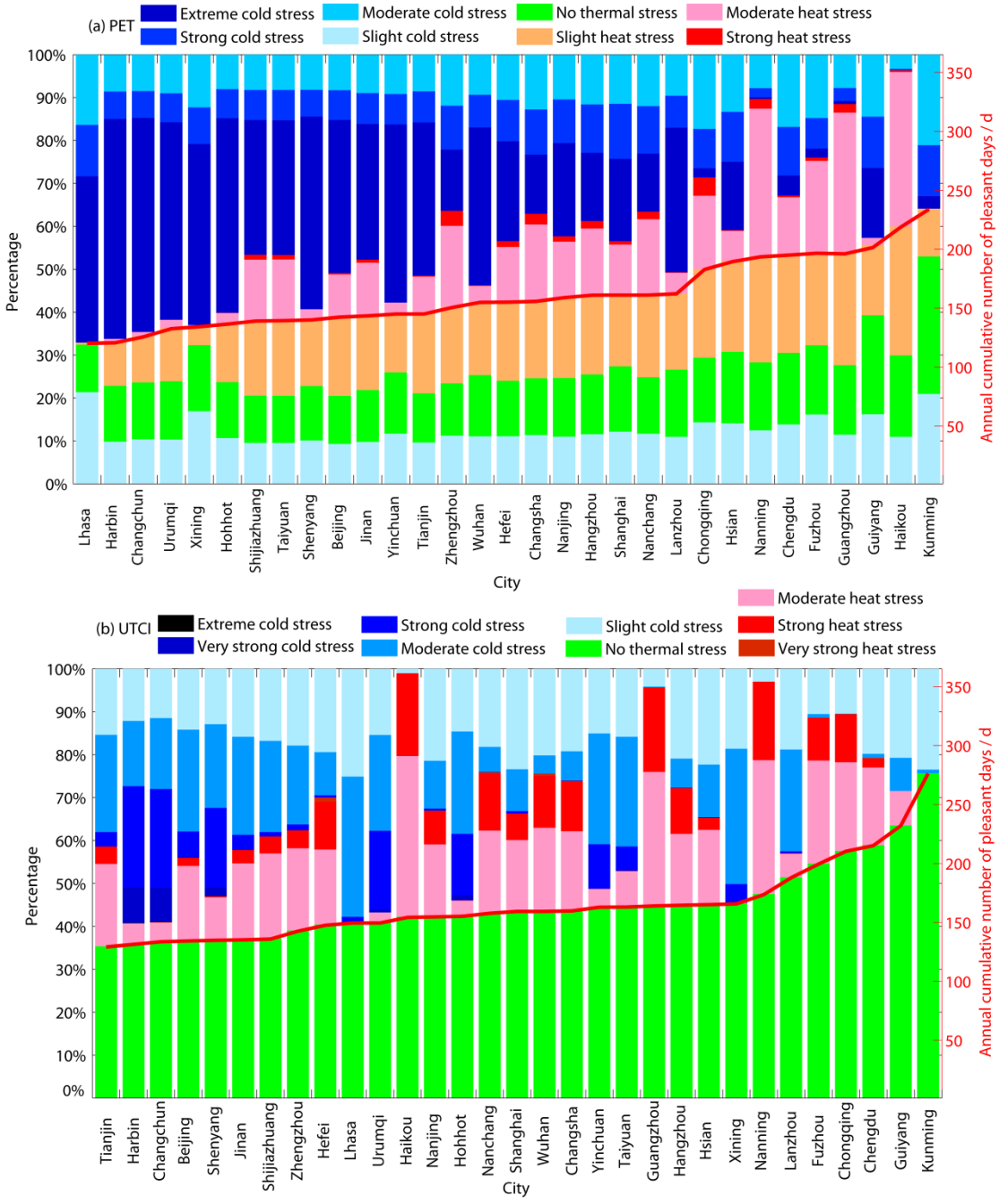

Fig 3.1 Annual cumulative number of days at each thermal sensation class of PET (a) and UTCI (b) and their mean fractions during 1981–2010 in the 31 provincial capital cities of mainland China. The red line separates the annual cumulative number of pleasant ($PET_{13\text{-}29°C}$) days and that of heat plus cold stress days in Fig. 2a, and it separates the annual cumulative number of no thermal stress ($UTCI_{9\text{-}26°C}$) days and that of heat plus cold stress days in Fig.

3.1(b). The PET and UTCI threshold of each thermal sensation category was shown in Table 2.4 and Table 2.5.

Generally, both PET an UTCI showed similar results (Fig 3.1). Kunming and Guiyang, two cities in Yunnan-Guizhou Plateau, experienced the maximum annual cumulative number of *no thermal stress* days. In high latitude/altitude cities, such as Lhasa and Harbin, etc. cold stress prevailed throughout the year. While, in low latitude/altitude cities, such as Haikou, Guangzhou, and Nanning, heat stress was the dominated thermal sensation. *No extreme heat stress* occurred in all cities.

On average, the annual cumulative day-number of $PET_{13\text{-}29°C}$, including no thermal stress and slightly cold/heat stress, amounted to 161.0 days/year, accounting for 44% of the total number of days over the year. While, the annual cumulative day-number of $UTCI_{9\text{-}26°C}$, i.e. *no thermal stress* amounted to 164.7 days/year, accounting for 45% days over the year. Their durations were close to each other, and they can be regarded as pleasant days in terms of both PET and UTCI.

3.2 Variation in monthly cumulative number of pleasant days during 1981–2010

In terms of both PET and UTCI scale, the monthly cumulative number of pleasant days presented a similar quasi-M shaped trajectory throughout the year (Fig 3.2). Spring and autumn were more pleasant, compared with summer and winter.

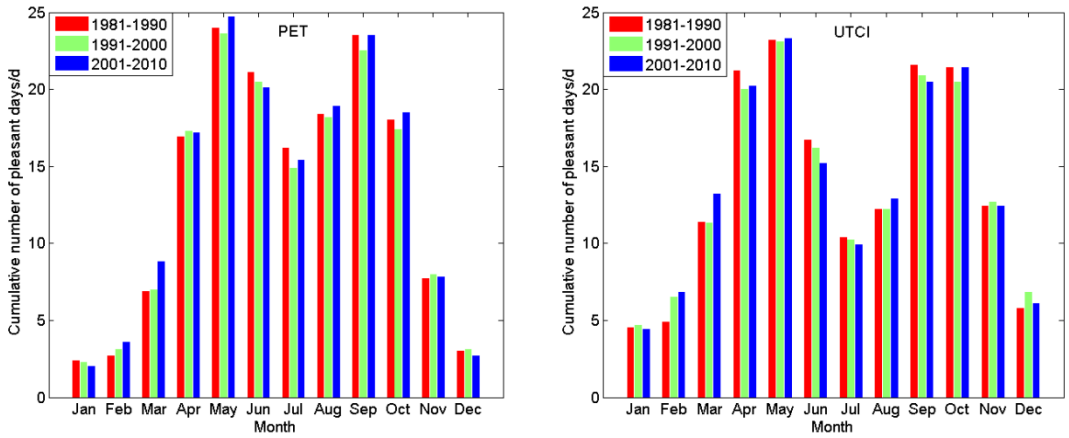

Fig 3.2 The monthly cumulative number of pleasant ($PET_{13\text{-}29°C}$, $UTCI_{9\text{-}26°C}$) days in the provincial capital cities in mainland China during 1981–1990, 1991–2000 and 2001–2010.

According to the PET, the cumulative number of pleasant days mainly concentrated in the period from April to October (Fig 3.2). In spring, summer and autumn, almost

more than half time sensed pleasant, particularly in May, June and September, the cumulative number of pleasant days exceeded 20.0 days/month (Fig 3.2). In winter, early spring and late autumn, i.e. January, February, March, November and December, the cumulative number of pleasant days was less than 9.0 days/month, particularly, in January, February, and December, it was less than 4.0 days/month (Fig 3.2) and the minimum was only 2.0 days/month in January during 2001–2010.

According to the UTCI, the pleasant days mainly concentrated in the period from April to June and September to October (Fig 3.2), particularly in April, May, September and October, the cumulative number of pleasant days exceeded 20.0 days/month (Fig 3.2). In winter, from December, January, to February, the cumulative number of no thermal stress days was less than 7.0 days/month, particularly; in January, it was less than 5.0 days/month (Fig 3.2).

The PET results showed more pleasant days in the summer months and less pleasant days during the winter time, in comparison with that of the UTCI. In terms of PET and UTCI, the average cumulative number of pleasant days in summer (June, July and August) was 18.2 days/month and 13.0 days/month respectively (Fig 3.2); May was the most pleasant month in the whole year. Winter was under cold stress and the monthly cumulative number of pleasant days in January was the least over the year, being only 2.0 days/month and 4.4 days/month respectively.

According to both PET and UTCI, over the last three decades in mainland China，the monthly cumulative number of pleasant days had been increasing in late winter and early spring, during December, February and March, while decreasing in early and middle summer and early autumn, during June, July, and September (Fig 3.2). This was consistent with the warming winter and increasing summer heat extremes of global climate change. The changes in the other months were relatively less.

3.3 General comparison between PET and UTCI

The average values of annual PET and UTCI all over the country were 13.7°C and 13.2°C respectively (Fig 3.3), being very close to each other. The maximum daily PET (48.8°C) occurred in July in Changsha, while the maximum daily UTCI (42.8°C) occurred in Hefei (Fig 3.3). Both cities are located in the subtropical climate zone, and controlled by the subtropical anticyclone in summer. On the other hand, the minimum daily PET (-39.4°C) and UTCI (-47.1°C) appeared in Changchun and

Harbin (Fig 3.3), two northernmost provincial capital cities in mainland China, they experienced severe cold stress in winter due to the winter monsoon. The PET pleasant period began in the early April and ended at the end of October, amounting to 200 days/year totally (Fig 3.3). The UTCI pleasant period was longer than PET, ranging from the end of March to the early November, and amounting to 223 days/year.

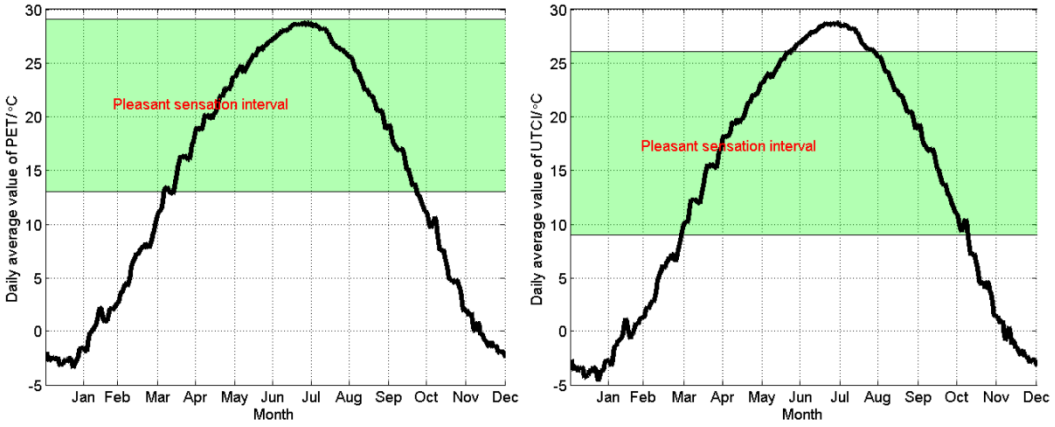

	Maximum value/ City		Minimum value/ City		Maximum value for average	Minimum value for average	Annually average value
PET	48.8°C	Changsha	-39.4°C	Changchun	28.6°C	-3.2°C	13.7°C
UTCI	42.8°C	Hefei	-47.1°C	Harbin	28.7°C	-4.6°C	13.2°C

Fig 3.3 Variation of daily average PET and UTCI in mainland China during 1981–2010 (Green area: pleasant sensation interval, left: PET, right: UTCI)

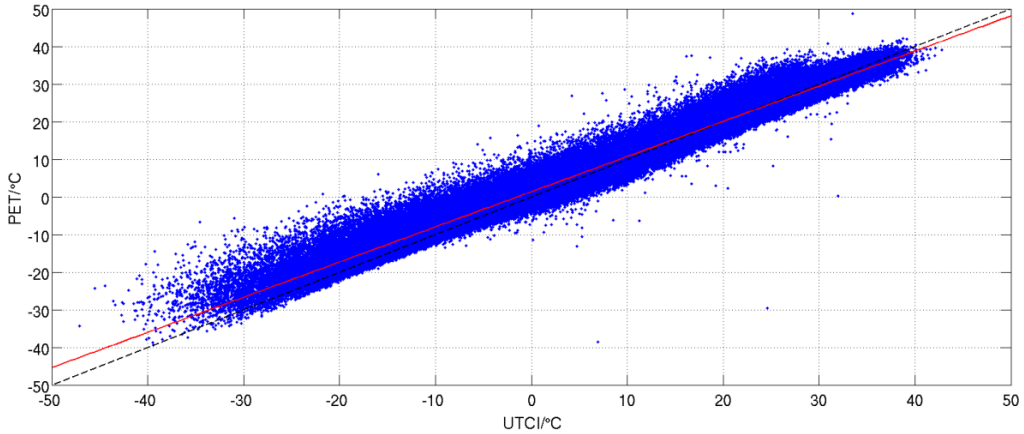

Fig 3.4 Linear regression between the daily PET and UTCI of the 31 capital provincial cities in mainland China during 1981–2010 (The red line denotes the regression and the black dashed line shows the identity)

The result of the linear regression analysis showed that the daily PET and UTCI were highly correlated (Fig 3.4). R^2 coefficient was 0.9855 and the coefficient of the slope of regression line was 0.93495. The regression line (red line) was very close to the identity line (dashed line) (Fig 3.4). This suggested that both PET and UTCI can

consistently indicate the thermal comfort in mainland China. However, their sensitivity may differ to some extent. The UTCI showed lower values under very strong to *extreme cold stress*, and the UTCI-50°C ~ -30°C was roughly correspondent to PET-40°C ~ -20°C (Fig 3.4). This may be attributed to the difference in sensitivities to the meteorological variables used for the calculation of the two indices. The UTCI was more sensitive to wind velocity, vapor pressure, and cloud coverage, while the PET was more closely related to air temperature (Blazejczyk et al. 2012; Fröhlich and Matzarakis 2016). In addition, the wind velocity at 10 m height for the UTCI model usually was larger than that at 1.1 m height for the PET calculation, particularly in windy winter. Under strong to *extreme heat stress*, the UTCI and PET values presented similar range from 30°C to 40°C (Fig 3.4). In addition, when the UTCI values were above 40°C, the PET values were below 40°C. The UTCI range stretched wider than that of the PET (Fig 3.4).

3.4 Classification of the 31 provincial capital cities based on seasonal thermal comfort

According to the results of hierarchical clustering, the 31 provincial capital cities in mainland China can be classified into five types based on their differences in seasonal UTCI and PET thermal sensation patterns (Fig 3.5), though the categories of a few cities may differ.

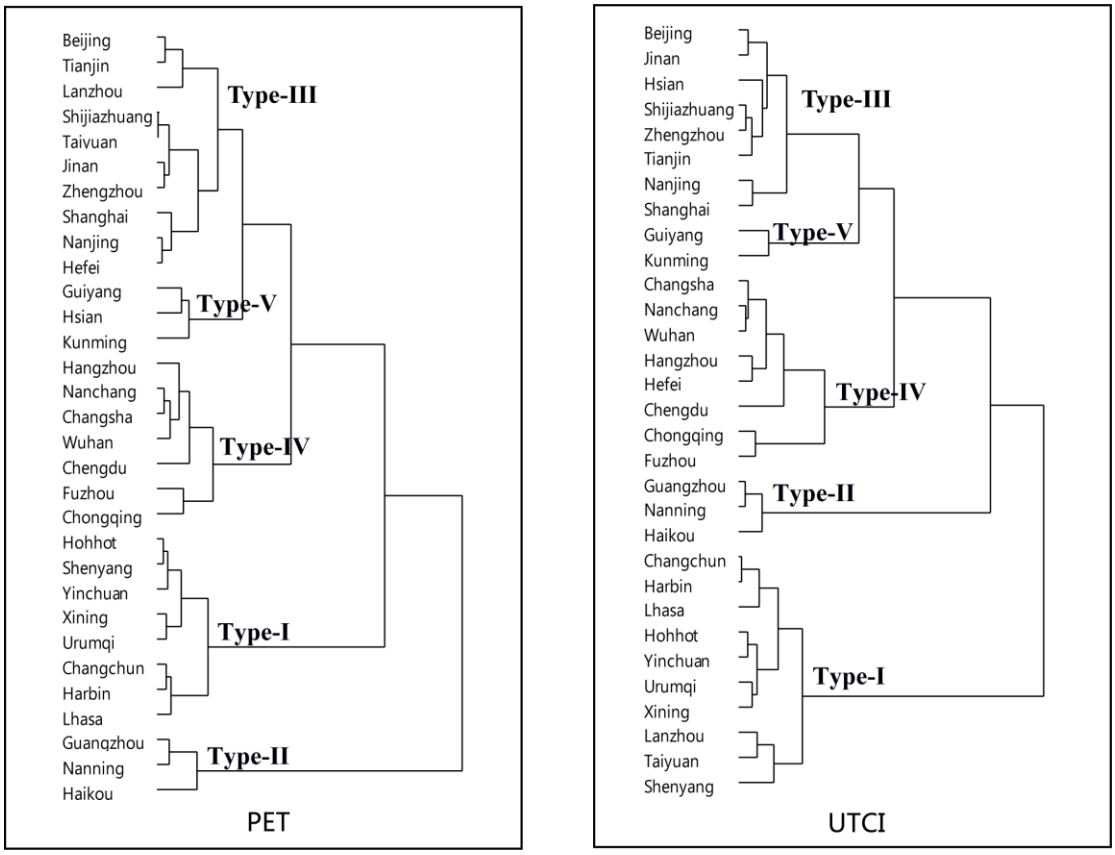

Fig 3.5 Clustering pedigree charts of the 31 provincial capital cities in mainland China based on their monthly cumulative number of pleasant days on average during 1981–2010

The first type of (hereinafter referred to as Type-I) cities were characterized by pleasant summer and severe cold winter (Fig 3.6). According to both PET and UTCI, eight high-latitude or high-altitude cities fell into this type, including Changchun, Harbin, Shenyang, Hohhot, Yinchuan, Xining, Urumqi, and Lhasa (Fig 3.5, Fig 3.6). Besides, Taiyuan and Lanzhou were also classified into this type in terms of the UTCI. Of these, Lhasa and Xining are located in the TP, the altitudes of Hohhot, Yinchuan, and Lanzhou are all higher than 1000 m a.s.l.; The latitudes of Changchun, Harbin, Shenyang, and Urumqi are all located at the north of latitude 40 ℃N. In these cities, the most pleasant days were mainly concentrated in the period from May to September, in May, June, and September in particular, only a few days of heat stress occurred in July and August in a few cities such as Shenyang, Lanzhou, and Taiyuan (Fig 3.6).

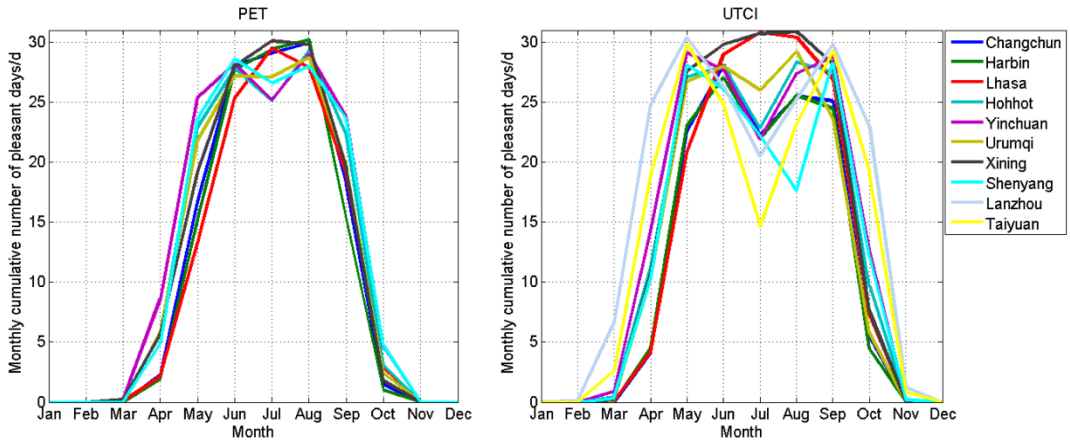

/days	spring	summer	autumn	winter
monthly PET $_{13\text{-}29℃}$	0.0~25.4	25.3~30.2	0.0~23.8	0.0
monthly UTCI $_{9\text{-}26℃}$	0.0~30.4	12.2~30.9	0.0~29.8	0.0~0.1
monthly PET$_{<13℃}$				28.2~31.0
monthly UTCI $_{<9℃}$				27.7~31.0

Fig 3.6 The monthly cumulative number of pleasant days on average during 1981–2010 in 10 provincial capital cities in high-altitude plateaus or high-latitude provinces in China (Type-I cities)

In summer (June, July and August), the monthly pleasant days can be up to 30.2 days (PET) and 30.9 days (UTCI) in Type-I cities. They are all ideal summer resorts in mainland China. Especially in Lhasa, Xining, and Harbin, the monthly cumulative numbers of pleasant days were more than 29.0 days during summer, in terms of both PET and UTCI. However, in winter, the cold stress was quite serious in these cities, amounting to 27.7–31.0 days/month (Fig 3.6).

The second type of (Type-II) cities were characterized by pleasant spring, autumn, winter, and severe hot summer. They included Guangzhou, Haikou, and Nanning, three tropical cities in South China (Fig 3.5, and Fig 3.7). The curves of the monthly cumulative number of pleasant days in these cities were U-shaped (Fig 3.7). Higher values occurred in spring and autumn, amounting to more than 20.0 days/month in March, April, October, and November in particular (Fig 3.7). It is worth mentioning that in these three cities the thermal conditions in winter (December, January, and February) were the most pleasant, $PET_{13\text{-}29°C}$ = 17.0–28.4 days/month and $UTCI_{9\text{-}26°C}$ = 24.3–29.7 days/month (Fig 3.7), allowing them to act as the rare natural winter resorts in mainland China.

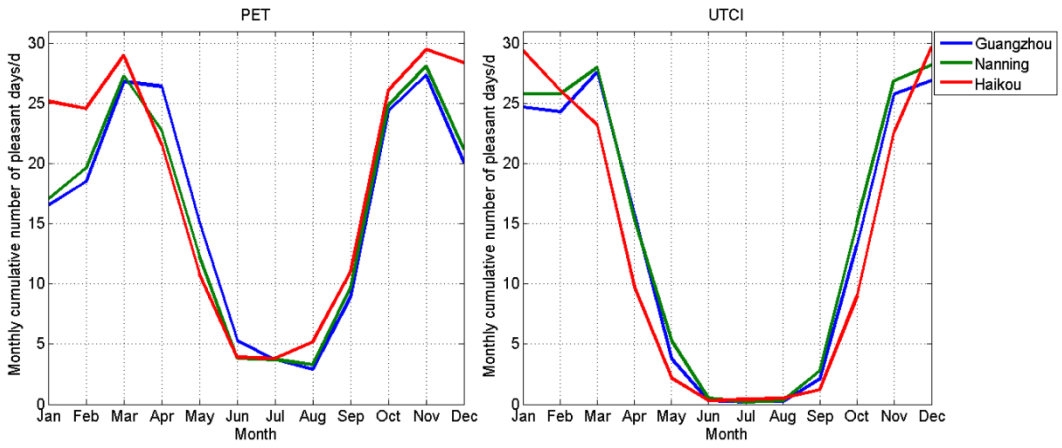

/days	spring	summer	autumn	winter
monthly PET $_{13\text{-}29℃}$	10.8~29.0	2.9~5.3	8.9~29.5	17.0~28.4
monthly UTCI $_{9\text{-}26℃}$	2.2~28.0	0.2~0.5	1.2~26.9	24.3~29.7
monthly PET $_{>29℃}$		24.7~28.1		
monthly UTCI $_{>26℃}$		29.0~31.0		

Fig 3.7 The monthly cumulative number of pleasant days in Guangzhou, Haikou, and Nanning in South China on average during 1981–2010 (Type-II cities)

Especially, Haikou, the southernmost provincial capital city, was the most pleasant city in winter among all of the 31 cities under study (Fig 3.7). On the contrary, in summer (June, July, and August), under the control of hot and humid weather, their monthly cumulative number of pleasant days was less than 6.0 days and 1.0 days in terms of PET and UTCI respectively (Fig 3.7). The severe hot summer can be reflected by $PET_{>29°C}$ = 24.7–28.1 days/month and $UTCI_{>26°C}$ = 29.0–31.0 days/month (Fig 3.7). In these type–II cities, their annual cumulative number of PET and UTCI pleasant days ranged 193.6–218.9 days/year and 154.3–173.6 days/year respectively.

The third type of (Type-III) cities were characterized by pleasant spring and autumn, slightly pleasant summer, and cold winter ($PET_{<13°C}$ = 27.6–31.0 days/month, $UTCI_{<9°C}$ = 25.0–31.0 days/month). According to both PET and UTCI, seven middle-high-latitude cities fell into this type, *i.e.* Shijiazhuang, Beijing, Tianjin, Jinan, Zhengzhou, Shanghai, and Nanjing (Fig 3.5, and Fig 3.8). Besides, Taiyuan, Hefei, and Lanzhou were also Type-III cities in terms of PET, and Hsian was also Type-III city in terms of UTCI. Of these, Shijiazhuang, Beijing, Tianjin, Jinan are temperate coastal cities around Bohai Sea, Zhengzhou and Taiyuan are two cities in the plains of Central China, Shanghai and Nanjing are two cities in the lower reaches of the Yangtze River. The curves of the monthly cumulative numbers of both PET and UTCI pleasant days over the year presented M-shaped (Fig 3.8). Peak values occurred

in May-June, and August-October, reaching the maximum values in May and October. The cold stress in winter was very severe in these cities and there were few pleasant days ($PET_{13\text{-}29℃}$ = 0.0–0.6 days/month, $UTCI_{9\text{-}26℃}$ = 0.0–4.5 days/month) in January, February and December (Fig 3.8). Relatively higher latitude or location near the sea made them slightly pleasant in summer (Fig 3.8).

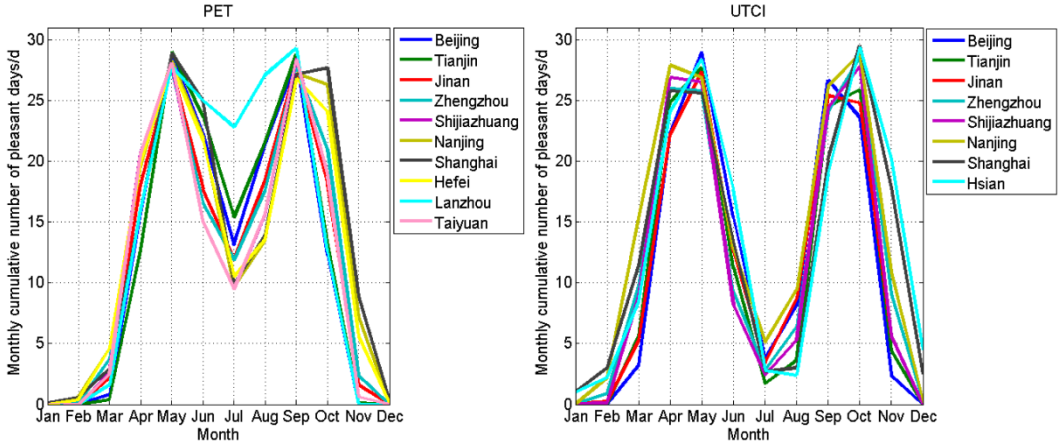

/days	spring	summer	autumn	winter
monthly $PET_{13\text{-}29℃}$	0.4~29.0	9.5~27.1	0.0~29.3	0.0~0.6
monthly $UTCI_{9\text{-}26℃}$	3.2~29.0	2.4~17.7	2.4~29.5	0.0~4.5
monthly $PET_{<13℃}$				27.6~31.0
monthly $UTCI_{<9℃}$				25.0~31.0

Fig 3.8 The monthly cumulative number of pleasant days on average during 1981–2010 in several temperate or subtropical provincial capital cities in mainland China (Type-III cities)

The fourth type of (Type-IV) cities were characterized by pleasant spring and autumn, hot stress summer and slightly cold winter (Fig 3.9). In terms of both PET and UTCI, seven subtropical provincial capital cities, including Changsha, Wuhan, Nanchang, Chengdu, Chongqing, Fuzhou, and Hangzhou, were classified into this type. In terms of UTCI, Hefei, another subtropical city, was also in this type. Of these, Changsha, Wuhan, Nanchang, Hefei and Hangzhou are situated in the middle-lower reaches of the Yangtze River, Chongqing and Chengdu are located in Sichuan Basin (Fig 3.5, Fig 3.9). The curves of their monthly cumulative number of pleasant days presented quasi-M-shaped, nearly more than two-thirds of the time were pleasant in April, May, October, and November (Fig 3.9).

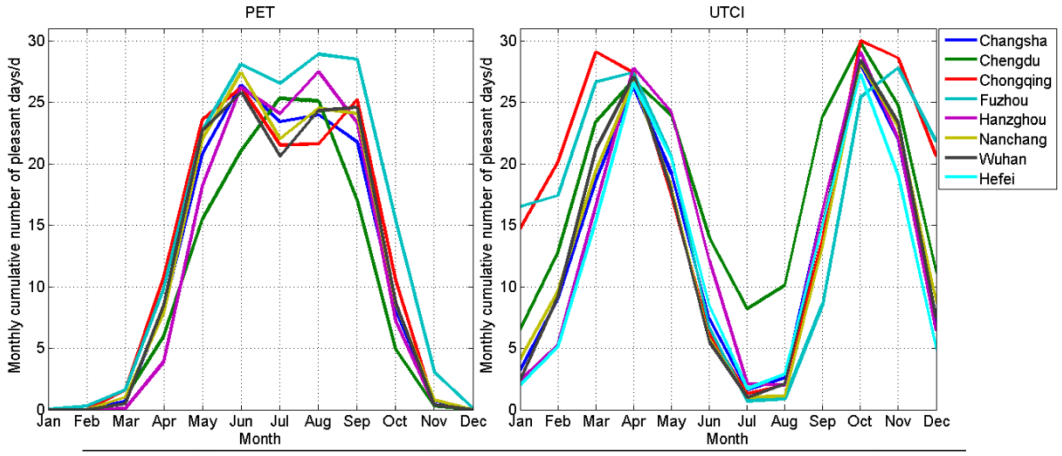

/days	spring	summer	autumn	winter
monthly PET $_{13\text{-}29℃}$	7.4~28.5	4.2~21.4	11.1~30.0	0.2~10.7
monthly UTCI $_{9\text{-}26℃}$	15.3~29.1	0.7~14.0	8.6~30.0	2.0~21.8
monthly PET $_{>29℃}$		8.5~26.8		
monthly UTCI $_{>26℃}$		15.4~30.7		
monthly PET $_{<13℃}$				19.7~30.8
monthly UTCI $_{<9℃}$				9.4~28.6

Fig 3.9 The monthly cumulative number of pleasant days on average during 1981–2010 in subtropical provincial capital cities in mainland China (Type-IV cities)

Nevertheless, these cities are often controlled by the subtropical anti-cyclone in summer, resulting severe heat stress. Thus, they have been described as "stove cities" in mainland China. Furthermore, these cities suffer from winter cold stress resulting from cold wave from the north is also quite obvious. Their monthly cumulative number of UTCI pleasant days in winter months (December, January, and February) was less than 10.1 d/mon, and only 4.0 d in January in Wuhan, Hangzhou, and Hefei (Fig 3.9). There were few PET pleasant days in these cities in winter (Fig 3.9). Nevertheless, the duration of cold stress in Type-IV cities was relatively shorter than that in the above-mentioned Type-I and Type-III cities in higher latitude/altitude regions (Fig 3.6, Fig 3.7).

The fifth type of (Type-V) cities were characterized by pleasant spring, summer, autumn and cool winter. They included Guiyang, Kunming and Hsian. Of these, Guiyang and Kunming are two subtropical plateau cities, while Hsian is a temperate city in Northwest China. Their weather conditions were quite neutral for most of the year, and the annual cumulative number of pleasant days amounted to the most among all cities in mainland China (Fig 3.10). These cities are also the very good summer resorts ($PET_{13\text{-}29°C}$ = 20.2–31.0 days/month, $UTCI_{9\text{-}26°C}$ = 20.4–31.0 days/month).

Because of its year-round balmy conditions, Kunming is known as the “spring city” in China.

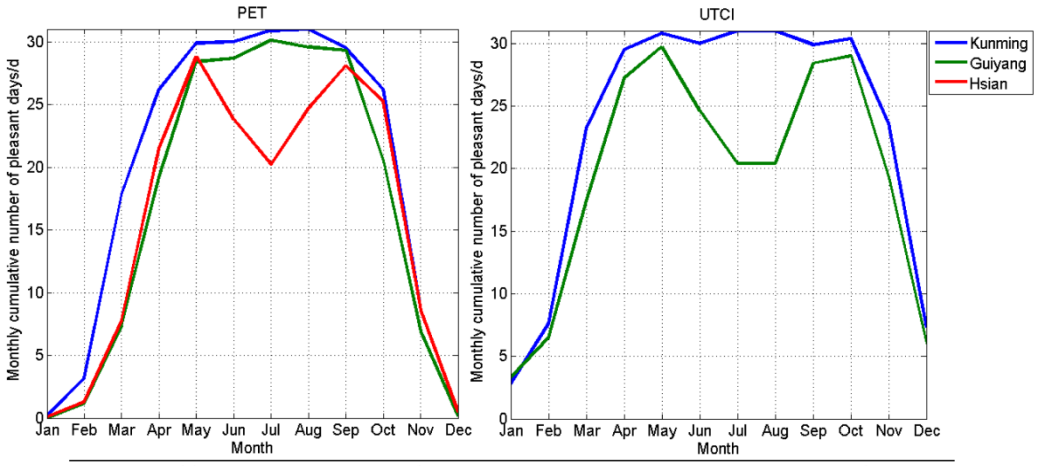

/days	spring	summer	autumn	winter
monthly PET $_{13\text{-}29℃}$	7.8~29.9	20.2~31.0	8.6~29.5	0.1~3.2
monthly UTCI $_{9\text{-}26℃}$	17.4~30.8	20.4~31.0	19.3~30.4	3.3~7.6
monthly PET $_{<13℃}$				25.0~30.9
monthly UTCI $_{<9℃}$				24.1~28.1

Fig 3.10 The monthly cumulative number of pleasant days on average during 1981–2010 in Kunming, Guiyang and Hsian in mainland China (Type-V cities)

3.5 Changes in urban thermal comfort in the past 30 years

With the combination of global climate change and UHI, the urban thermal comfort has been changing in the past decades. The differences in annual cumulative number of pleasant ($PET_{13\text{-}29°C,}$ $UTCI_{9\text{-}26°C}$), cold stress ($PET_{<13°C,}$ $UTCI_{<9°C}$) and heat stress ($PET_{>29°C,}$ $UTCI_{>26°C}$) days between the period of 1981–1990 and 2001–2010 were compared as follows:

3.5.1 Changes in annual cumulative number of pleasant days

The difference in the number of PET and UTCI pleasant days between the period of 1981-1990 and 2001-2010 varied among cities (Fig 3.11). In terms of the PET, in 16 of the 31 cities, the annual cumulative number of pleasant days in 2000s increased in comparison with that in 1980s (Fig 3.11). The first four cities where the thermal comfort increased the most were Harbin (10.8 days/year), Changchun (10.3 days/year) in Northeast China, Kunming (11.8 days/year) in the Yunnan-Guizhou Plateau, Lhasa (9.8 days/year) in the Qinghai-Tibet Plateau. The annual cumulative number of the pleasant days increased 2.3 days/year on average in all of the 31 cities. In terms of the UTCI, the annual cumulative number of pleasant days increased in 17 cities (Fig 3.11), amounting to the most in Kunming (23.8 days/year) and Lhasa (14.2 days/year) also.

The thermal comfort has improved more in higher-latitude/altitude cities than in lower-latitude/altitude cities (Fig 1.1, Fig 3.11 and Table 1.2). Overall, the increases in thermal comfort outweighed the decreases.

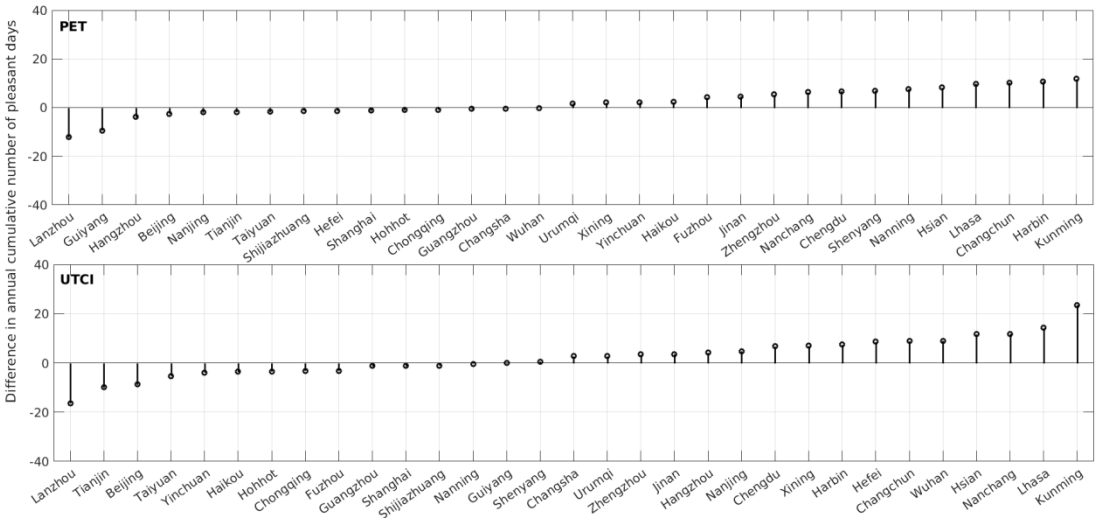

Fig 3.11 The difference in annual cumulative number of pleasant days between the period of 1981–1990 and 2001–2010 in the 31 provincial capital cities of mainland China

3.5.2 Changes in cold stress

The annual cumulative number of cold stress days reduced in most cities (Fig 3.12). Most of them were located in temperate and subtropical zone. In terms of the PET, the cold stress reduced the most in Hsian, Lanzhou, and Wuhan, decreasing 24.7 days/year, 16.2 days/year and 16.0 days/year respectively. While, in terms of the UTCI, the cold stress reduced the most in Wuhan (26.6 days/year), Hsian (25.9 days/year), Hefei (24.0 days/year), Kunming (23.6 days/year), Nanchang (22.5 days/year), Harbin (20.7 days/year), and Hangzhou (20.1 days/year) respectively.

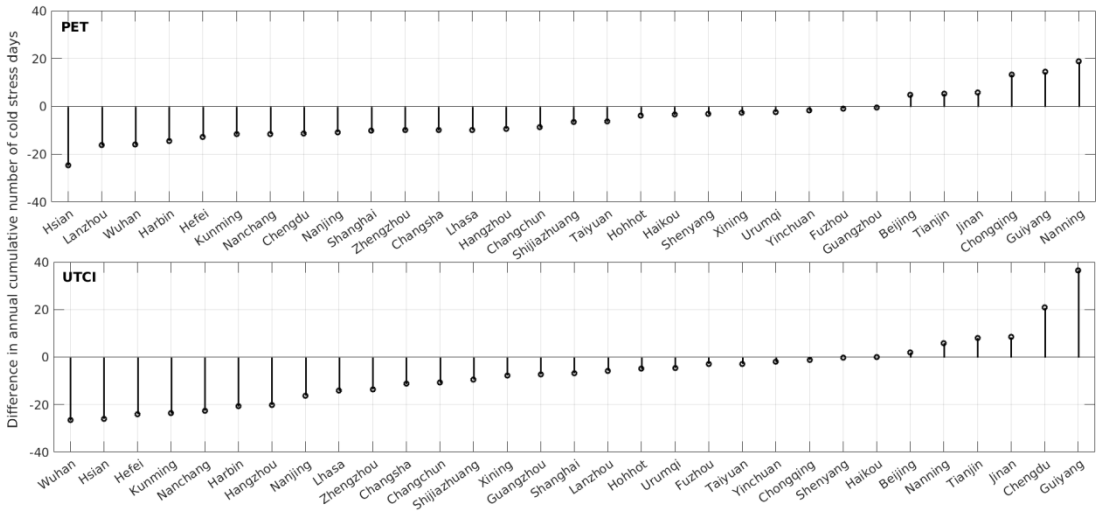

Fig 3.12 The difference in annual cumulative number of cold stress days between the period of 1981–1990 and 2001–2010 in the 31 provincial capital cities of mainland China

On the other hand, according to both PET and UTCI, in another five cities (Fig 3.12), *i.e.* Nanning, Guiyang, Jinan, Tianjin and Beijing, the cold stress was intensified. Besides, it was also intensified in Chongqing in terms of the PET, and in Jinan and Chengdu in terms of UTCI. Particularly, in Guiyang and Chengdu, two cities in Southwest China, the cold stress increased the most (Fig 3.12). Overall, the PET and UTCI indicate in all 31 cities a reduction of the annual cumulative number of the cold stress days by 5.1 days/year resp.6.5 days/year on average in 2000s in comparison with that in 1980s.

3.5.3 Changes in heat stress

We observe an increase of heat stress in 18 resp. 24 out of the 31 provincial capital cities in terms of PET resp. UTCI (Fig 3.13). The top 6 cities in which the heat stress aggravated the most were Hsian, Wuhan, Hefei, Hangzhou, Shanghai and Nanjing. Hsian is the most populous city in Northwest China, which is among the regions with most significant warming over the last decades (Li et al. 2004). The other 5 cities were located in the middle and lower reaches of the Yangtze River, where the rapid urbanization and global warming significantly increased the air temperature in the past decades (Xie et al. 2010). Besides, in summer they were often controlled by the heat wave of subtropical anti-cyclone (Chen 2001; Rodwell and Hoskins 2001). the annual cumulative number of heat stress days increased also in Shijiazhuang, Harbin, Zhengzhou, Nanchang, Hohhot, Changsha, Xining, Urumqi, Chengdu, Taiyuan, Guangzhou and Haikou (Fig 3.13).

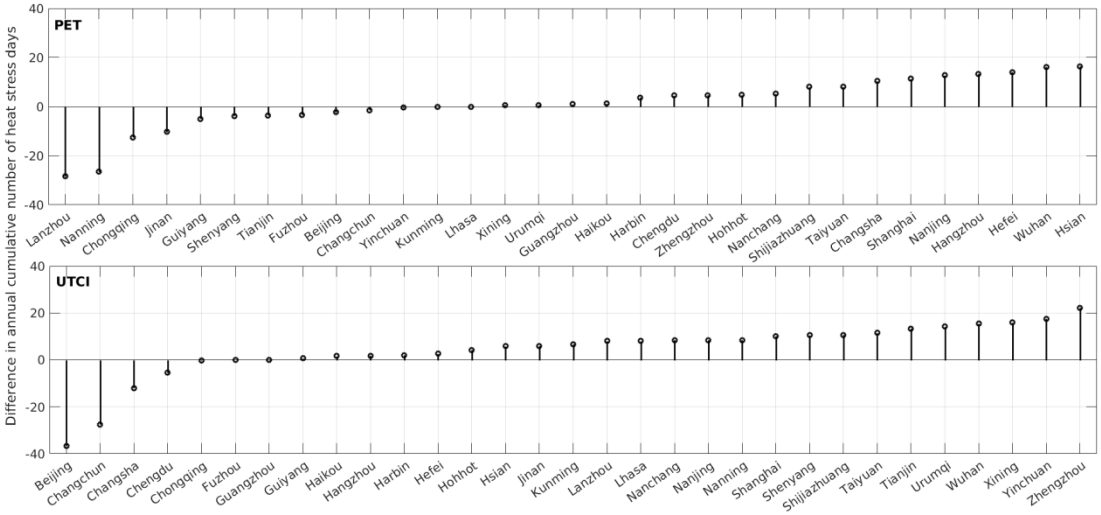

Fig 3.13 The difference in annual cumulative number of heat stress days between the period of 1981–1990 and 2001–2010 in the 31 provincial capital cities of mainland China

On the other hand, the heat stress decreased in Nanning, Guiyang, Kunming, Chongqing, Beijing, Tianjin, Shenyang, Changchun, Jinan, Fuzhou, Lanzhou, and Yinchuan in terms of the PET (Fig 3.12), and in Nanning, Jinan, Chengdu and Guiyang in terms of the UTCI. While, in Lhasa and Kunming there found almost no changes in heat stress in the past decades in terms of both PET and UTCI. Overall, the increase surpassed the decrease, and in all of the 31 cities, the annual cumulative number of the PET and UTCI heat stress days increased 2.3 days/year and 4.3 days/year respectively on average in 2000s in comparison with that in 1980s.

3.6 Correlation between monthly favorable duration and tourist flow

Correlation analyses were conducted to explore the relationship between the monthly cumulative number of thermally favourable days, including the value intervals of $PET_{13\text{-}29°C}$, $PET_{13\text{-}18°C}$, $PET_{13\text{-}23°C}$, $PET_{18\text{-}23°C}$, $PET_{18\text{-}29°C}$, $UTCI_{9\text{-}26°C}$, $UTCI_{9\text{-}14°C}$, $UTCI_{9\text{-}19°C}$, $UTCI_{14\text{-}19°C}$, $UTCI_{14\text{-}26°C}$, and the monthly tourist flows (which mean the monthly reception number of tourist in individual city) in 2010 (Fig 3.14, Table 3.1), respectively. The monthly tourist flows of Haikou and Hohhot were positively correlated with the cumulative day-number of $PET_{13\text{-}29°C}$, $PET_{13\text{-}23°C}$, $PET_{18\text{-}23°C}$, $UTCI_{9\text{-}26°C}$, and $UTCI_{14\text{-}26°C}$. The monthly tourist flow of Chengdu was positively correlated with the cumulative day-number of $PET_{13\text{-}23°C}$ and $UTCI_{9\text{-}26°C}$. The monthly tourist flow of Shanghai was positively correlated with the monthly cumulative day-number of $PET_{13\text{-}18°C}$, $UTCI_{9\text{-}14°C}$, $UTCI_{9\text{-}19°C}$, and $UTCI_{14\text{-}19°C}$. The monthly tourist flow of Kunming was significantly correlated with the monthly cumulative day-number of $PET_{13\text{-}18°C}$ and $UTCI_{9\text{-}19°C}$. Thus, the tourist flows of these cities were largely influenced by their durations of pleasant days.

Table 3.1 The correlation coefficient between the monthly cumulative number of thermally favourable days and monthly tourist flows in 2010 in Haikou, Hohhot, Chengdu, Shanghai and Kunming

		$PET_{13\text{-}29°C}$	**$PET_{13\text{-}18°C}$**	**$PET_{13\text{-}23°C}$**	**$PET_{18\text{-}23°C}$**	**$PET_{18\text{-}29°C}$**	**$UTCI_{9\text{-}26°C}$**	**$UTCI_{9\text{-}14°C}$**	**$UTCI_{9\text{-}19°C}$**	**$UTCI_{14\text{-}19°C}$**	**$UTCI_{14\text{-}26°C}$**
Monthly reception number of tourists	Haikou	0.625	0.930	0.909	0.841	0.280	0.719	0.848	0.842	0.758	0.611
	Hohhot	0.874	0.451	0.733	0.825	0.833	0.837	0.054	0.355	0.427	0.847
	Chengdu	0.451	0.592	0.600	0.428	0.180	0.643	-0.447	0.097	0.442	0.735
	Shanghai	0.068	0.721	0.448	0.102	-0.266	0.541	0.661	0.742	0.685	0.257
	Kunming	0.255	0.664	0.405	0.102	-0.062	0.341	0.420	0.690	0.580	0.068

PET or UTCI values were the average during 1981–2010; n=12, P<0.05.

Besides, more and more aged people in mainland China are living out their retirement in a seasonal migrationary way in search for pleasant cities, *i.e.* migrating to Type-II cities in winter and to Type-I, Type-V and some Type-III cities in summer, only staying at their home in spring and autumn. For instance, every year in winter, a large number of people migrated from northern China to Haikou and nearby cities such as Sanya to seek warmth and sunshine. But the rush of visitors during winter causes a shortage of accommodation, which results in a steep increase in prices (Zheng and Huang 2013). The seasonal population flow brings new problems to urban planning and administration.

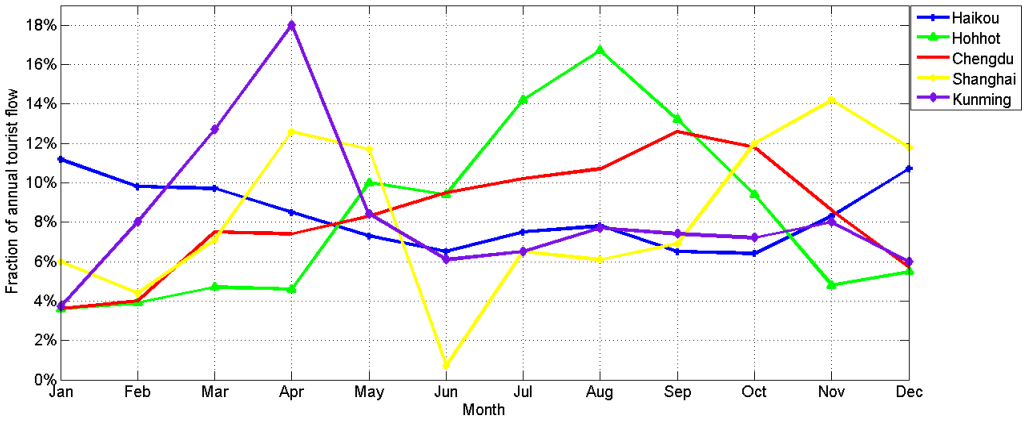

Fig 3.14 Monthly variations in tourist flows in five cities with different thermal comfort conditions in 2010 in mainland China

This chapter shows that PET and UTCI values are highly correlated with each other and presented similar thermal comfort pattern, although their sensitivities might differ slightly. The results show that these cities cover 4–8 resp. 6–8 thermal comfort classes of the PET and UTCI scale. On the whole, the annual cumulative number of pleasant days is more than 160 days/year. In terms of seasonal variations in thermal comfort conditions, the 31 provincial capital cities in mainland China can be classified into 5 types, which are shown in Table 3.2.

Table 3.2 Thermal comfort types and characteristics for 31 cities in mainland China in 1981-2010

Types	Characteristics
Type-I	pleasant summer and severe cold winter
Type-II	pleasant spring, autumn, winter, and severe hot summer

Type-III	pleasant spring and autumn, slightly pleasant summer, and cold winter
Type-IV	pleasant spring and autumn, hot stress summer, and slightly cold winter
Type-V	pleasant spring, summer, autumn, and cool winter

During the recent three decades, the cities in mainland China have experienced increasing pleasant conditions in late winter and early spring and an intensifying heat stress in summer. The reduction in annual cumulative number of cold stress days in higher latitude/altitude cities is outweighed by the increase in the duration of heat stress in subtropical cities.

Chapter 4

4 Assessment of Human-Bio-meteorological Environment over the Tibetan Plateau Region based on CORDEX Climate Model Projections

This chapter mainly evaluates the human bio-meteorological conditions and its changes in the Tibetan Plateau over the past 27 years under the simulation of regional climate models of HadGEM3-RA and RegCM from the CORDEX-East Asia experiments by using the Universal Thermal Climate Index.

4.1 Model evaluation

A comparison of the model data and the observation data has been made. The closest grids of model data to the station points are applied. Through the comparisons, it has been observed that the model data have some bias for several cities. According to Table 4.1, the elevation differences are also very large between simulation data grid and observational station data. The elevation correction can reduce the elevation difference bias difference significantly. There are different methods to adjust the height differences, like barometric height correction and statistical methods. The lapse rate can represent the empirical relationship between the air temperature and elevation and it can be also used to scale the model data of Ta with respect to altitude (Gao et al. 2016). Different lapse rate values are calculated by various approaches. The most common value is -6.0°C /km e. g. Dodson and Marks 1997, which is also applied to this research. Another universal value is -6.5°C/km (e.g. Stahl et al. 2006; Gerlitz et al. 2014). Gerlitz et al. (2014) using a polynomial function based on temperature and geopotential values corrected ERA-Interim temperature data over the TP. According to the approach of them, we also used the polynomial fitting curve to reduce the model bias in this study.

Table 4.1 The elevation for different data sets and the difference between observation station data and ERA-Interim, RCM data (HadGEM3-RA and RegCM data) grid point data (unit m)

Station	Observation	Reanalysis	Difference (R-O)	RCM	Difference (M-O)
Dari	4547	3621	-926	4512	-35
Da Qaidam	3173	3813	640	4055	882
Dulan	2677	3485	808	4539	1862
Gangca	3300	3639	339	3091	-209
Golmud	2800	3941	1141	4887	2087
Lhasa	3650	4722	1072	4502	852
Lenghu	2783	2800	17	4134	1351
Maduo	4200	4335	135	3902	-298
Qumarleb	4500	4622	122	4893	393
Tuotuohe	4547	4934	387	5005	458
Xining	2261	3335	1074	4183	1922
Yushu	4200	4446	246	4816	616

To get the UTCI analysis more precise and trustable, we did model data correction first before calculating the UTCI, which can be separated into the following steps:

1. Correct the elevation in ERA-Interim, HadGEM3-RA and RegCM, which is based on the elevation difference between observation station data and the models`grids. Then take the corrected elevation and related Ta, according to the following equation:

$$T_{a_\Delta} = Elevation_\Delta \times \mathrm{r} \qquad (4.1)$$

$$T_{a_{new}} = T_a + T_{a_\Delta} \qquad (4.2)$$

$Elevation_\Delta$ is the elevation difference between observation stations and simulation grid data, r is the lapse rate, T_{a_Δ} is the Ta difference related to the elevation data, T_a is the original data for each simulation and $T_{a_{new}}$ is the Ta for simulation data after correcting the elevation. $T_{a_{new}}$ will be used in the next step to get the difference between the observation data and simulation data.

2. Get the difference between the observation data and simulation data and derive the polynominal fitting curve to match the difference to the observation data;

3. Apply the fitting curve to the simulation data and add the fitted result to the simulation data to get the corrected simulation data. Fig 4.1 shows the results of year 1990 before and after correction compared to the observation data for Lhasa.

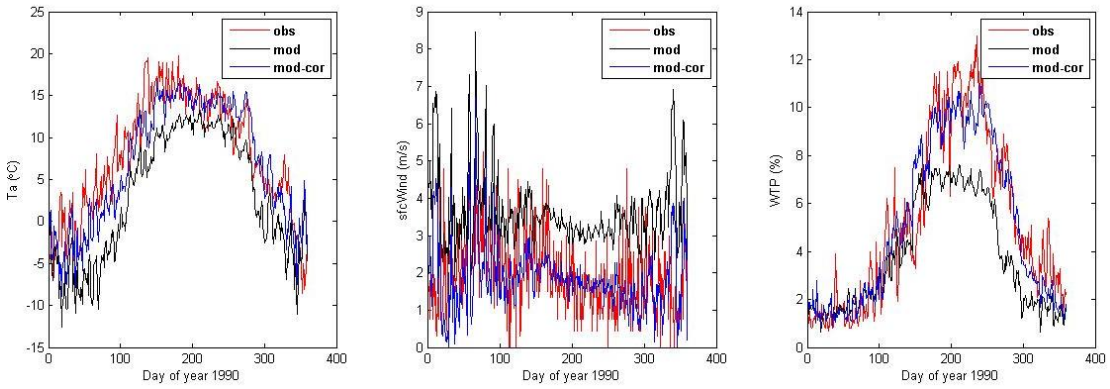

Fig 4.1 Comparisons among observation, simulation and corrected simulation data

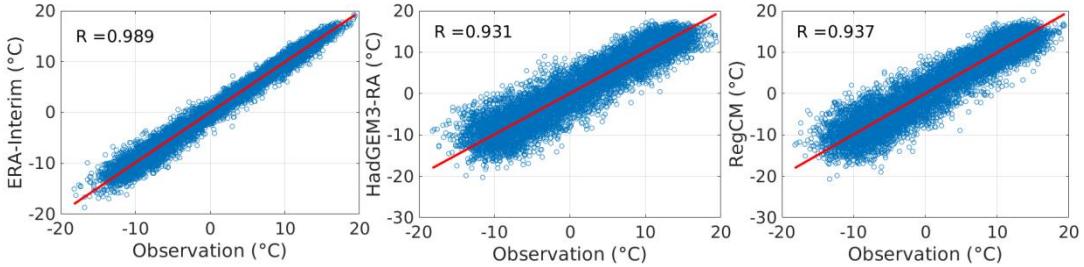

Fig 4.2 Air temperature comparison between ERA-Interim, HadGEM3-RA RegCM and the observation data separately during 1979-2005. *R* is the correlation coefficient for each pair of data

Fig 4.2 shows the results of the correlation analysis of air temperature between ERA-Interim, HadGEM3-RA, RegCM and the observation data respectively. Each result shows high agreement level with the observation data after correction. The correlation coefficients are from 0.931 to 0.989 with the ERA-Interim data giving the best correlation result, as shown in Table 4.2. Other variables, like wind speed, and vapour pressure have also been corrected and the results are presented in the Table 4.2. In all of the variables, Ta showed the best results and has the highest correlation between observation and other data sets. As shown in Fig 4.2, RegCM displays better correlation than HadGEM3-RA in the range of Ta higher than 10°C. According to the correlation analysis, these three corrected data sets can be used to make further analysis of the human thermal comfort of the TP and for the projection of the future human bio-meteorological environment in the TP.

Table 4.2 The correlation coefficient and RMSE for Ta, Wind speed and VP between observation data and the corrected ERA-Interim, HadGEM3-RA and RegCM data

Data set	Variable name	Correlation coefficient	RMSE
ERA_Interim	Ta	0.989	1.2
	Wind	0.661	0.5
	Vp	0.500	3.4
HadGEM3-RA	Ta	0.931	3.2
	Wind	0.668	0.8
	Vp	0.900	3.4
RegCM	Ta	0.937	3.0
	Wind	0.327	1.1
	Vp	0.254	4.0

4.2 The intra-annual variation of UTCI in 1979-2005

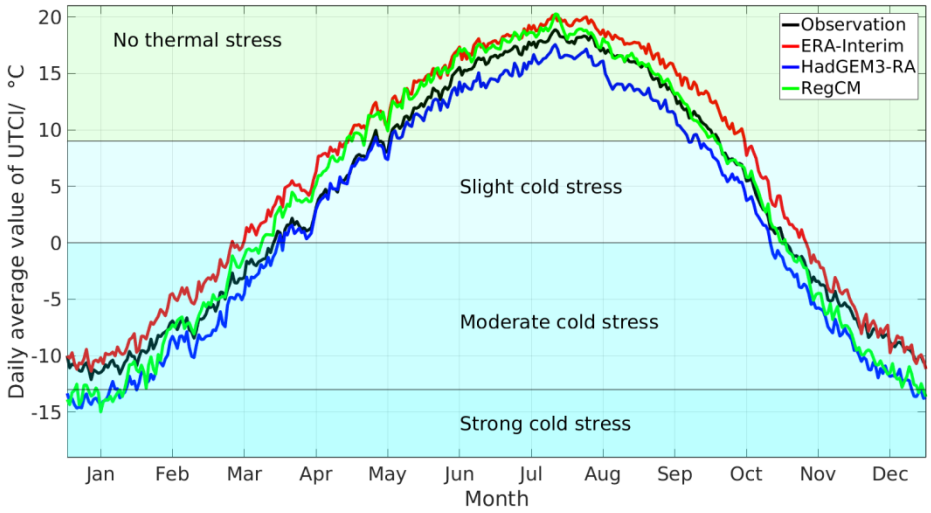

Fig 4.3 Intra-annual temporal diagram of UTCI of Observation, ERA-Interim, HadGEM3-RA, and RegCM in TP in1979-2005

Fig 4.3 shows temporal distribution of the observed and simulated UTCI results during the past period (1979-2005). All of the data sets show a similar changing trend throughout the whole year and the annual human thermal comfort period of TP can be divided into two main periods: warm period and cold period. The cold stress is dominant through almost the whole year and no thermal stress appears only very shortly in the warm period of the year. The warm period of the TP concentrates from late spring to early autumn (specifically from the second half of May to the first half

of September). From the second half of September to the first half of May in the next year is the cold period. The general trend of human thermal comfort is cold based on the cold climate.

ERA-Interim, HadGEM3-RA and RegCM indicate a very similar trend and the duration of warm period and cold period. While for the HadGEM3-RA and RegCM show, lower values in wintertime (November to February) compared to the observation data (Fig 4.3). HadGEM-RA simulates better in spring (March to May) and RegCM shows better in autumn (August to October). ERA-Interim shows the most similar values to observation in wintertime (November to January) compared to the two models. However, ERA-Interim shows the higher values than observation almost the whole year. In summer time, ERA-Interim and RegCM shows the higher value and HadGEM3-RA is lower than the observation. Generally, all of the data sets capture the human thermal comfort in TP (Fig 4.3).

4.3 The thermal spectrum of TP during 1979-2005

Fig 4.4 shows the UTCI stress category spectrum of the TP based on the observation station data and simulation corrected data. Four different sensation categories were classified in the TP during 1979-2005: *no thermal stress, slight cold stress, moderate cold stress and strong cold stress*. *No thermal stress* and *moderate cold stress* are the dominant stress categories in the TP. The fraction of *no thermal stress* is also very large: observation, 39.1%; ERA-Interim, 46.3%; HadGEM3-RA, 35.9%; RegCM, 42.3%. The percentage of *moderate cold stress* is also very high for each data set (minimum percentage: 31%, average percentage: 33.4%). Compared to observation and ERA-Interim, the main categories of two models are the same and show somehow extension for the lower values. The cold stress fractions of HadGEM3-RA and RegCM are larger (Fig 4.4). However, the cold stress shows very high percentages (54%-64%) for all data sets. Generally, the cold stresses are the main stress categories in the TP at present.

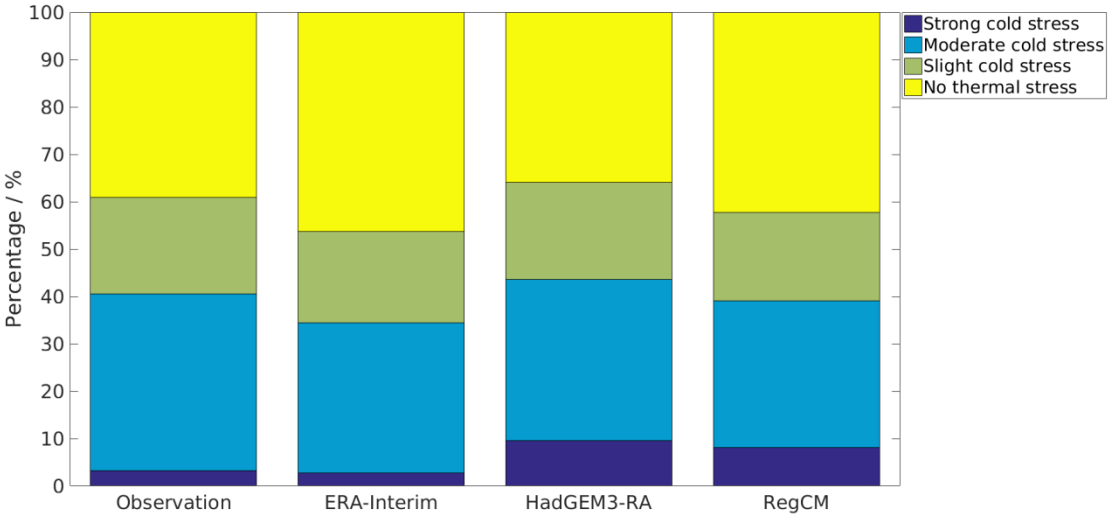

Fig 4.4 The annual frequency diagram of UTCI in TP in 1979-2005

4.4 Monthly changing rate of Ta and UTCI

Climate information is important for the tourist to choose its destination (Hamilton and Lau 2005; Lin et al. 2006). People would like to travel to countries with more stable weather conditions. In this research, we will present the use of the changing rate to evaluate the stability of the human bio-meteorological conditions. The calculation of monthly changing rate *CR* is shown as following

$$\mathrm{CR}(yr, mt) = \frac{1}{n-1}\sum_{i=1}^{n-1}\left|d_{yr_{mt}}(i+1) - d_{yr_{mt}}(i)\right| \qquad (4.3)$$

$$\mathrm{CR}(mt) = \frac{1}{m}\sum_{yr=2024}^{2050} CR(yr, mt) \qquad (4.4)$$

In the equations, $d_{yr_{mt}}(i)$ is the daily UTCI data for day i, month mt and year yr while n is the days for month mt. , is the years and is 27 here.

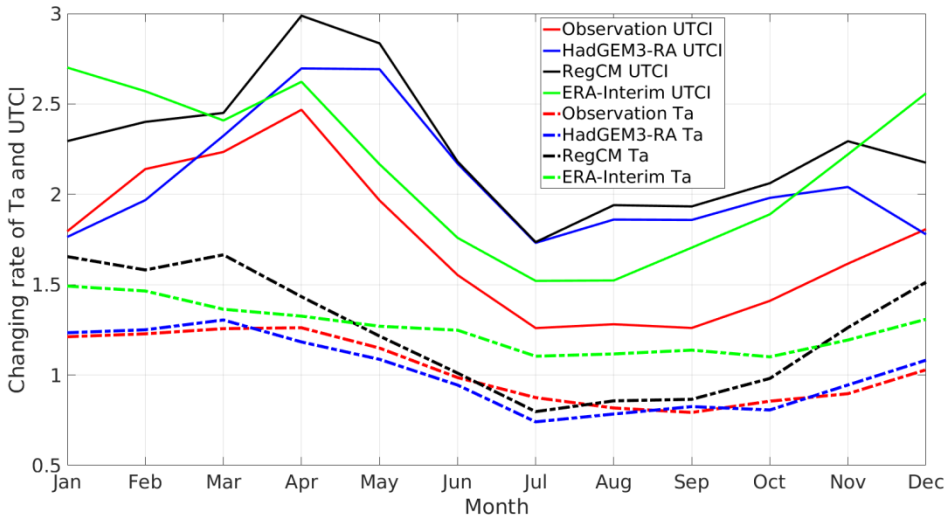

Fig 4.5 Monthly average changing rate of Ta and UTCI in TP during 1979-2005

Fig 4.5 shows the changing rate of Ta and UTCI for both the simulation and observation data in TP in 1979-2005. Overall, they indicated similar trends from month to month. The changing rate of UTCI (monthly average value is 2.1) is generally higher than that of Ta (monthly average value is 1.1) (Fig 4.5). Since UTCI is calculated by using Ta and additional parameters like wind speed and relative humidity; it is more sensitive to the ambient environment than just Ta. However, the changing rate of UTCI and Ta are similar. The most stable period is from July to October for both UTCI and Ta with the smallest value and fluctuation. The average values from July to October for UTCI and Ta are 1.7 and 0.9 respectively (Fig 4.5). The highest values concentrate from December to next May and the mean monthly values of UTCI and Ta are 2.3 and 1.3 (Fig 4.4). Compared to other seasons, spring shows the highest changing rate and March, April and May are the most unstable months along the whole year. The maximum changing rate for Ta appears in March. However, the maximum changing rate for UTCI shows one or two months delay which was in April or May.

The average difference between UTCI and Ta for each data set is 0.7 °C (observation), 0.8 °C (ERA-Interim), 1.1 °C (RegCM) and 1.1 °C (HadGEM3-RA) (Fig 4.5). The ERA-Interim data show the most similar change trend compared to the observation. The trend in change of RegCM and HadGEM3-RA is quite similar in both, UTCI and Ta. HadGEM3-RA shows more stable for both UTCI (2.1 °C) and Ta (1.0 °C) than ERA-Interim and RegCM. In general, summer is the most stable time in the whole

year in the TP, followed by autumn. The largest changing rate is in spring for both Ta and UTCI.

4.5 Prediction of the human bio-meteorological conditions in the TP by the simulation of HadGEM3-RA and RegCM during 2024-2050 under the scenarios of RCP4.5 and RCP8.5

The Representative Concentration Pathways (RCPs) describe four different 21st century pathways of greenhouse gas (GHG) emissions and atmospheric concentrations, air pollutant emissions and land use (IPCC 2014). The RCPs have been developed using Integrated Assessment Models (IAMs) as input to a wide range of climate model simulations to project their consequences for the climate system (IPCC 2014). They include a stringent mitigation scenario (RCP2.6), two intermediate scenarios (RCP4.5 and RCP6.0) and one scenario with very high GHG emissions (RCP8.5) (IPCC 2014). A climate prediction or climate forecast is a statement about the future evolution of some aspect of the climate system encompassing both forced and internally generated components. In this research, in order to reflect the variation of the human bio-meteorological conditions of the TP in the future, nonetheless, limitation of the data availability, RCP4.5 and RCP8.5 are applied to project the variation by the simulation of HadGEM3-RA and RegCM during 2024-2050.

4.5.1 Evaluation of the distribution and variation of thermal spectrum of TP in 2024-2050 compared to the present

Fig 4.6 shows the annual frequency of the UTCI stress categories in present (1979-2005) and in the near future (2024-2050) by the simulation of HadGEM3-RA and RegCM under the scenarios of RCP4.5 and RCP8.5. There will still be four different stress categories by the simulation of two models in 2024-2050: *strong cold stress, moderate cold stress, slight cold stress and no thermal stress*. Compared to the present time, *no thermal stress* will increase and cold stresses will be stable or decrease. For HadGEM3-RA, the changing range of *no thermal stress* is the largest (from 35.9% in the present to 42.8% under the RCP4.5 and 43.1% under the RCP8.5) (Fig 4.6). On the contrary, *strong cold stress, moderate cold stress* and *slight cold stress* will decrease. Evenly, *strong cold stress* will decrease from 9.5% currently to 3.9% after 30 years under the RCP8.5 (Fig 4.6). For *moderate cold stress* and *slight cold stress*, the changing trends vary between RCP4.5 and RCP8.5. For RCP4.5, two

stress categories will decrease 2.0% and 0.5% separately; for RCP8.5, *moderate cold stress* and *slight cold stress* will decrease 1.8% and 0.1% respectively (Fig 4.6). The decreasing trends of those two stress categories for RCP8.5 are less than RCP4.5. By the simulation of HadGEM3-RA, the percentage of cold stresses will decrease and *no thermal stress* will have a considerable increase in the near future.

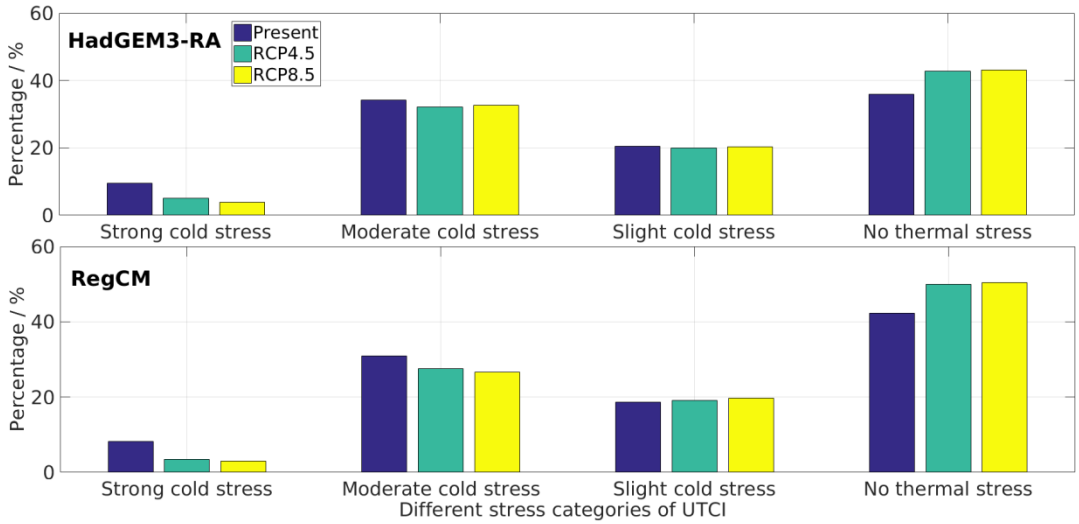

Fig 4.6 Annual frequency of UTCI sensation classes in present (1979-2005) & RCP4.5, RCP8.5 (2024-2050) under the simulation of HadGEM3-RA and RegCM in TP

For RegCM, the general variation trend will turn to be warm in the near future. The clearest increased stress category will be also *no thermal stress* and the annual frequency is from 42.3% currently to 50.0% (RCP4.5) and 50.5% (RCP8.5). The increasing trend for RegCM is larger than HadGEM3-RA for the same stress category and indicates a considerable warming trend (Fig 4.6). The warm period can last a half year. However, we note that the *slight cold stress* shows a only small increase from 18.6% (present) to 19.1% (RCP4.5) and 19.8% (RCP8.5) (Fig 4.6). For the other two cold stress categories, the annual frequency shows the decreasing trend and *moderate cold stress* decreases 3.4% (RCP4.5) and 4.2% (RCP8.5) respectively compared to the present. Equally, *strong cold stress*, the annual frequency is from 8.1% (present) to 3.4% (RCP4.5) and 3.0% (RCP8.5) (Fig 4.6) and this stress category shows more decrease than that of HadGEM3-RA.

The annual frequency of the *no thermal stress* increases in both simulations of HadGEM3-RA and RegCM in the near future (Fig 4.6). The percentage of cold stresses decreases for HadGEM3-RA under both of RCP4.5 and RCP8.5 conditions. In the RegCM, *no thermal stress* will increase and *slight cold stress* also increases marginally (Fig 4.6). In general, the percentage of *no thermal stress* will increase and

cold stresses decreases. The human bio-meteorological conditions improve and tend to be warm in the near future.

4.5.2 The variation of the thermal spectrum of TP under the scenarios of RCP4.5 and RCP8.5

Fig 4.7 shows the relative variation ratio of the UTCI stress categories under RCP4.5 and RCP8.5 during 2024-2050 compared to the present. The relative variation ratio is shown as follows:

$$\text{relative variation ratio} = \frac{percentage_{future} - percentage_{present}}{percentage_{present}} \qquad (4.5)$$

The warmest stress category will increase and the coldest ones will decrease considerably. The largest variation for both models will appear in *strong cold stress*. For HadGEM3-RA, the *strong cold stress* will have a considerable decrease (46.3% for RCP4.5 and 59.2% for RCP8.5) (Fig 4.7). Other two cold stress categories *moderate cold stress* and *slight cold stress* also show a small decrease. The smallest variation appears in *slight cold stress* and will decrease 2.1% (RCP4.5) and 0.4% (RCP8.5). The increasing variation of *no thermal stress* of HadGEM3-RA will be up to 19.2% (RCP4.5) and 20.1% (RCP8.5) (Fig 4.7).

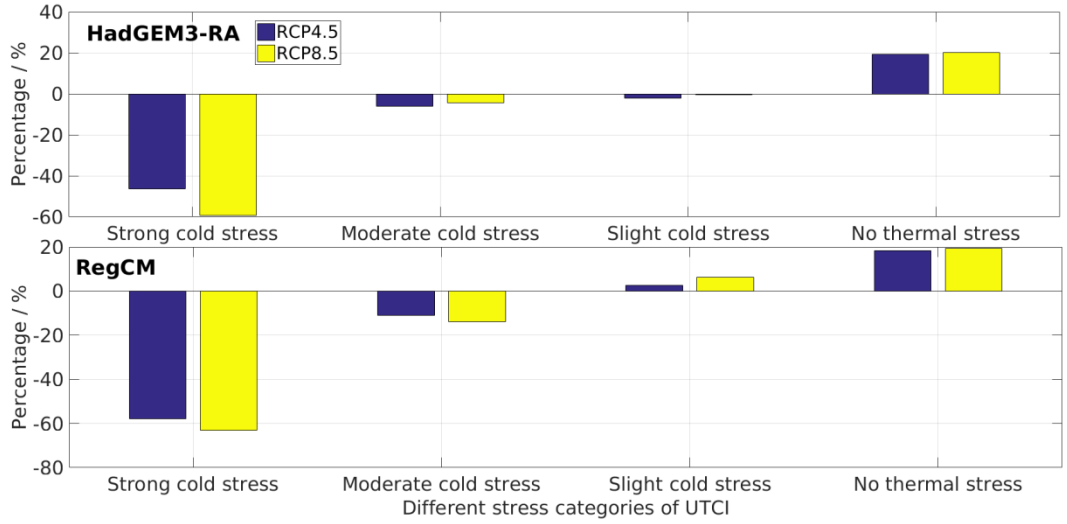

Fig 4.7 Fraction of UTCI stress categories change under RCP4.5 and RCP8.5 conditions during 2024-2050 compared with the present (1979-2005) climate in TP

The variation of RegCM simulation shows a very similar trend to HadGEM3-RA (Fig 4.7). *Strong cold stress* will be the one which changes the most (-58.0% for RCP4.5 and -63.1% for RCP8.5). *Moderate cold stress* also indicates the decreasing change (11.1% for RCP4.5 and 13.9% for RCP8.5). *No thermal stress* will show an increasing trend, 18.2% (RCP4.5) and 19.4% (RCP8.5) (Fig 4.7). The increasing

percentage is not as high as that of HadGEM3-RA. Except that, *slight cold stress* will increase slightly. Compared to the HadGEM3-RA, the simulation of RegCM shows a smaller variation for *no thermal stress* and a larger decrease for *strong cold stress* and *moderate cold stress*. Generally, the most considerable change occurs in *no thermal stress* and *strong cold stress* for both models.

4.5.3 Intra-annual distribution of UTCI under the scenarios of RCP4.5 and RCP8.5 in 2024-2050 for TP

The distribution of daily UTCI value and the average of daily UTCI value by the simulations of the HadGEM3-RA and RegCM under RCP4.5 and RCP8.5 in 2024-2050 are shown in Fig 4.8. The UTCI range of RegCM is larger than that of HadGEM3-RA. For both simulations, UTCI values are lower under RCP4.5 than that under RCP8.5 (Fig 4.8). The distribution of the UTCI values is almost in line with that for the present.

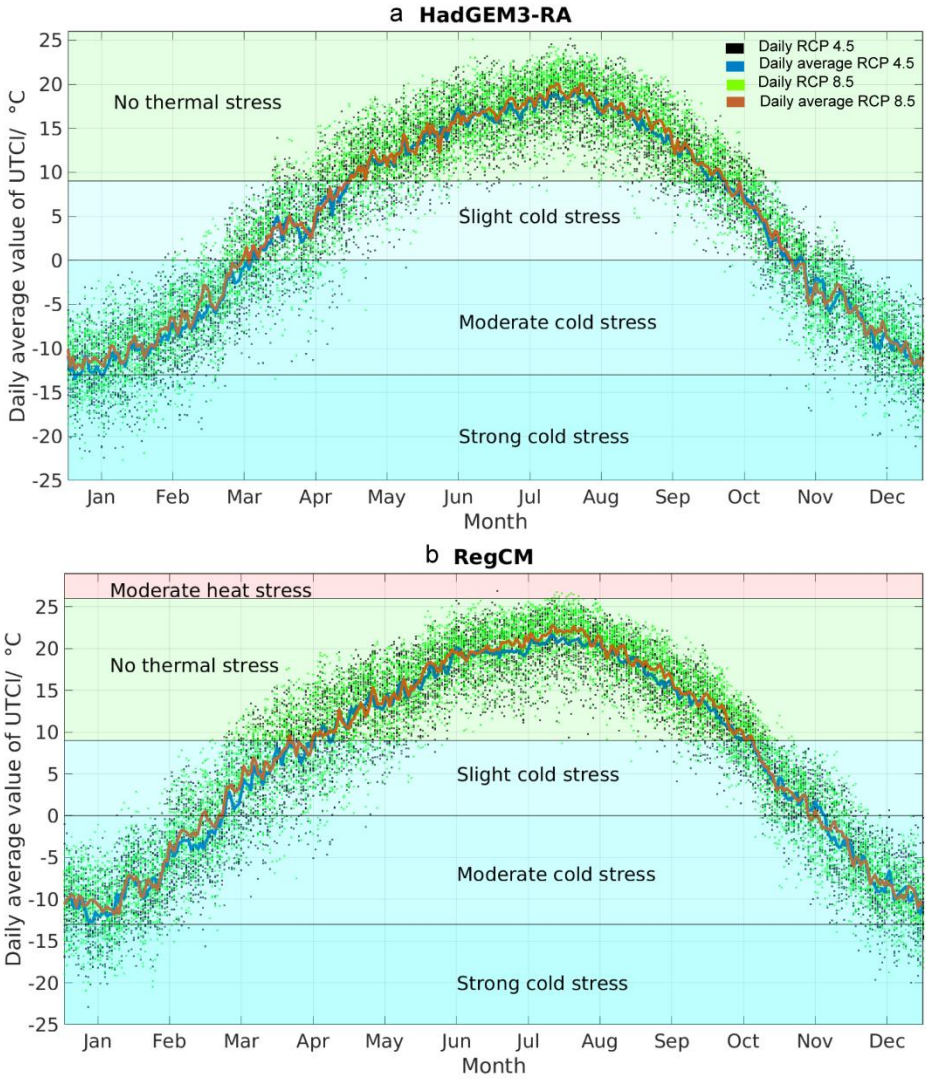

Model name	Scenario	UTCI maximum (°C)	UTCI minimum (°C)	Range of average values (°C)
HadGEM3-RA	RCP4.5	25.2	-25.0	-13.5~19.3
	RCP8.5	25.1	-22.7	-12.4~20.0
RegCM	RCP4.5	26.9	-22.9	-12.7~21.7
	RCP8.5	26.7	-21.0	-11.9~22.8

Fig 4.8 Intra-annual distribution of UTCI by the simulation of HadGEM3-RA (a) and RegCM (b) in 2024-2050 under the scenarios RCP4.5 and RCP8.5 for TP

Compared to HadGEM3-RA, RegCM shows higher values for both maximum (26.9°C, RCP4.5 and 26.7°C, RCP8.5) and minimum values (-22.9°C, RCP4.5 and -21.0°C, RCP8.5). The UTCI values under RCP4.5 are smaller than that of RCP8.5 for minimum values for RegCM. However, the average range of RCP8.5 shows more extension in the higher values, compared with RCP4.5. This situation is also applicable for HadGEM3-RA. The range of average value for HadGEM3-RA is -13.5~19.3°C (RCP4.5) and -12.4~20.0°C (RCP8.5) (Fig 4.8). Generally, for both models maximum values (minimum values) are larger (smaller) under RCP4.5 than

under RCP8.5. For the range of average values, UTCI values under RCP4.5 are lower than that under RCP8.5. For both models, the human bio-meteorological conditions will be warmer under RCP8.5 than under RCP4.5 in TP.

4.5.4 Human bio-meteorological conditions among regions under the scenarios of RCP4.5 and RCP8.5

According to the UTCI stress categories, annual spectrum percentages of stress categories by the simulation of HadGEM3-RA and RegCM under the scenarios of RCP4.5 and RCP8.5 during 2024-2050 in the 12 regions are presented in Fig 4.9. Six different UTCI stress categories will appear and the actual human bio-meteorological conditions will vary among regions under RCP4.5 and RCP8.5 for HadGEM3-RA. Five UTCI stress categories will show for RegCM. The two simulations show very similar distribution of the stress categories in every city (Fig 4.9). However, HadGEM3-RA shows lower values than RegCM.

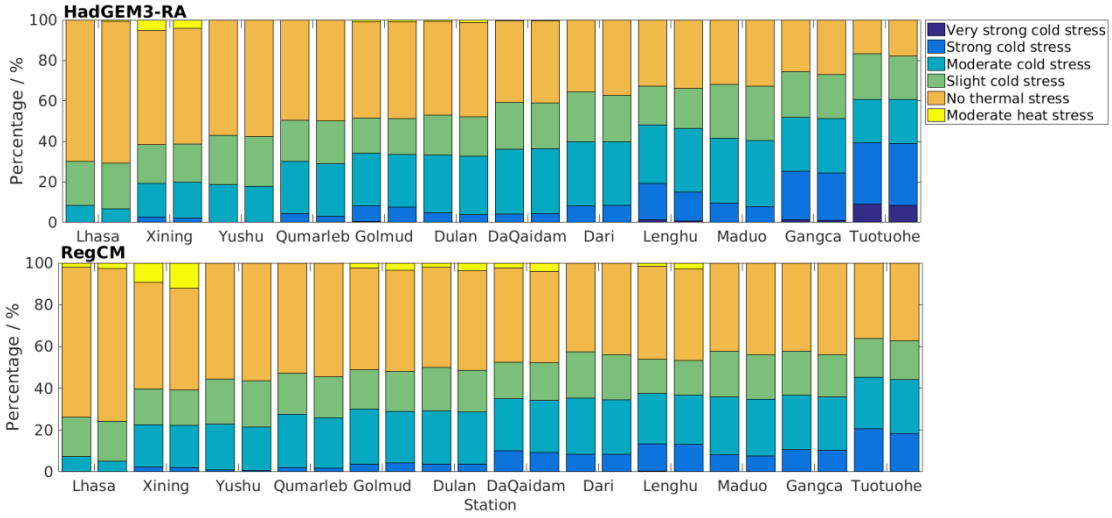

Fig 4.9 Frequency diagram of UTCI stress categories by the simulation of HadGEM3-RA (a) and RegCM (b) under the scenarios of RCP4.5 (left) and RCP8.5 (right) for 12 stations in TP

For HadGEM3-RA, six different UTCI stress categories: *very strong cold stress, strong cold stress, moderate cold stress, slight cold stress, no thermal stress and moderate heat stress*. The percentage of the *very strong cold stress* is very small (Fig 4.9). Tuotuohe, Gangca and Lenghu are the only three cities, in which this stress category appears. The percentage of *very strong cold stress* in Tuotuohe for HadGEM3-RA, which is the most for this stress category, is 9.1% (RCP4.5) and 8.4% (RCP8.5) (Fig 4.9). The warmest regions are Lhasa, Xining and Yushu, according to the percentages of *no thermal stress* and *moderate heat stress*. Lhasa is the most

pleasant city and the sum percentages of *no thermal stress* and *moderate heat stress* can be up to be 70.0% (RCP4.5) and 70.7% (RCP8.5). The percentage of *moderate heat stress* in Xining is the highest (5.3%, RCP4.5; 4.3%, RCP8.5) in the whole of the TP (Fig 4.9).

For RegCM, five UTCI stress categories emerge: *strong cold stress, moderate cold stress, slight cold stress, no thermal stress and moderate heat stress* (Fig 4.8). Compared to HadGEM3-RA, RegCM shows warmer UTCI stresses. There is no *very strong cold stress*. The numbers of cities, which show *moderate heat stress*, has increased, and their share in every city is larger than that of HadGEM3-RA. Xining also shows the largest proportion for *moderate heat stress* among the whole region (9.2%, RCP4.5; 12.0%, RCP8.5). Additionally, some cities under RCP8.5 also show a very high percentage, like Da Qaidam (4.0%), Dulan (3.9%), and Golmud (3.5%).

Generally, Lhasa, Xining and Yushu are the most pleasant cities in the whole regions according to the simulations. Lhasa lies on the Lhasa River's north bank in a valley of the Himalayas and is affected by the river and valley, which shows very warm and pleasant human bio-meteorological conditions in TP. Xining, located nearby the Qinghai Lake (which is the largest inland lake in China) is moderated by the lake. On the other hand, Tuotuohe, Gangca, Maduo and Lenghu are the coldest cities, especially Tuotuohe, which is the coldest city with the highest air sounding station in the whole world, experiences a cold climate almost throughout the whole year. Based on the simulation of HadGEM3-RA, Tuotuohe shows a *very strong cold stress* under RCP4.5. Other cities like Qumarleb, Golmud, Dulan, DaQaidam and Dari have an about average climate.

This chapter shows that both models are able to reproduce the present climate realistically. As an extension, the human thermal comfort information about TP in the next 27 years is projected under the scenarios of RCP4.5 and RCP8.5. The results show that the UTCI stress index in Tibetan Plateau covers mainly four categories—*strong cold stress, moderate cold stress, slight cold stress, no thermal stress*. Cold stresses are prevailing throughout the whole year. A small amount of no thermal stress category appears in the summer period. The human bio-meteorological condition is most stable from July to September. According to the projections in the near future, with climate change taken into account, annual cumulative pleasant days will increase significantly while the cold stresses days will be reduced. The distribution frequency

of UTCI categories shows a clear altitude/latitude dependency. Lhasa, Xining, and Yushu will be the top three cities in terms of thermal favourable conditions.

Chapter 5

5 Evaluation of the temperature extremes in Tibetan Plateau regions: WSDI and CSDI in summer and winter in 2024-2050

In this chapter, the warm spell duration index (WSDI) and cold spell duration index (CSDI) have been selected to analyse the extreme events analysis in TP in summer and winter. Based on the CORDEX-East Asia (HadGEM3-RA and RegCM) daily maximum and minimum data, we analysed the temporal and spatial variation of WSDI and CSDI in the selected 12 cities in TP in 2024-2050 under RCP4.5 and RCP8.5 scenario conditions in relation to the present day climate (1979-2005).

5.1 Evaluation of the WSDI and CSDI in TP regions in 2024-2050

The warm spell duration index (WSDI) and cold spell duration index (CSDI) are calculated. Both two climate extreme indices are defined by the Expert Team on Climate Change Detection and Indices (ETCCDI, http://etccdi.pacificclimate.org/list_27_indices.shtml).

WSDI in a specific season is defined as the sum over the consecutive days where the daily maximum temperature exceeds TX90, with the different time periods, which is called as warm spell event (the minimum duration is 6 consecutive days). TX90 means the 90th percentile calculated from a five-day window running mean of the daily maximum temperature of the reference period. CSDI in a specific season is defined as the sum over the number of consecutive days where the daily minimum temperature is below TX10, also with different time periods (called as cold spell event and at least 6 consecutive days). TX10 is the 10th percentile calculated from a five-day running average of the daily minimum temperature of the reference period.

$$WSDI{\sim}T_{max} > 90th\ percentile \quad (5.1)$$

$$CSDI{\sim}T_{min} < 10th\ percentile \quad (5.2)$$

The entire cold/warm spell events are divided into 3 types: 6-10 days (short term event), 11-15 days (medium term event), >15 days (long term event). The WSDI and CSDI are calculated in all of the grids in which the 12 stations (Fig 1.4, Table 2.2) are located. The units of WSDI and CSDI are days (Table 5.1).

Table 5.1 shows the partial extreme temperature indices recommended by ETCCDI (Zhang et al. 2011). In this study, we focus on the summer (June, July and August) and winter (December, January and February) season. To explore the climate extreme in TP in the future (2024-2050), the present period 1979-2005 is considered as the reference period.

Table 5.1 The extreme temperature indices recommended by the ETCCDI (from Zhang et al. 2011)

ID	Indicator name	Indicator definitions	Unit
TXx	Max Tmax	Monthly maximum value of daily max temperature	°C
TNx	Max Tmin	Monthly maximum value of daily min temperature	°C
TXn	Min Tmax	Monthly minimum value of daily max temperature	°C
TNn	Min Tmin	Monthly minimum value of daily min temperature	°C
TN10p	Cool nights	Percentage of time when daily min temperature < 10th percentile	%
TX10p	Cool days	Percentage of time when daily max temperature < 10th percentile	%
TN90p	Warm nights	Percentage of time when daily min temperature > 90th percentile	%
TX90p	Warm days	Percentage of time when daily max temperature > 90th percentile	%
DTR	Diurnal temperature range	Monthly mean difference between daily max and min temperature	°C
GSL	Growing season length	Annual (1^{st} Jan to 31^{st} Dec in NH, 1^{st} July to 30^{th} June in SH) count between first span of at least 6 days with TG>5°C and first span after July 1 (January 1 in SH) of 6 days with TG < 5°C	days
FD0	Frost days	Annual count when daily minimum temperature < 0°C	days
SU25	Summer days	Annual count when daily max temperature > 25°C	days
TR20	Tropical nights	Annual count when daily min temperature >	days

		20°C
WSDI	**Warm spell duration indicator**	**Annual count when at least six consecutive days days of max temperature > 90th percentile**
CSDI	**Cold spell duration indicator**	**Annual count when at least six consecutive days days of min temperature < 10th percentile**

5.1.1 The temporal variation of WSDI and CSDI

Two scenarios RCP4.5 and RCP8.5 are considered in this study to discuss the WSDI and CSDI distribution and variation. For CSDI, more events happen under RCP4.5 than RCP8.5. To the opposite, the WSDI shows more events under RCP8.5 than RCP4.5, especially for the long term events (> 15 days). The specific analysis is in the following parts.

5.1.1.1 The temporal variation of CSDI

Fig 5.1 indicates the CSDI events distribution during 2024-2050 in summertime (colour-filled) and in wintertime (black circle) under RCP4.5 and RCP8.5 by the simulation of HadGEM3-RA and RegCM in TP regions. For both simulations, it appears more events under RCP4.5 than under RCP8.5 and more events show in wintertime than in summertime (Fig 5.1).

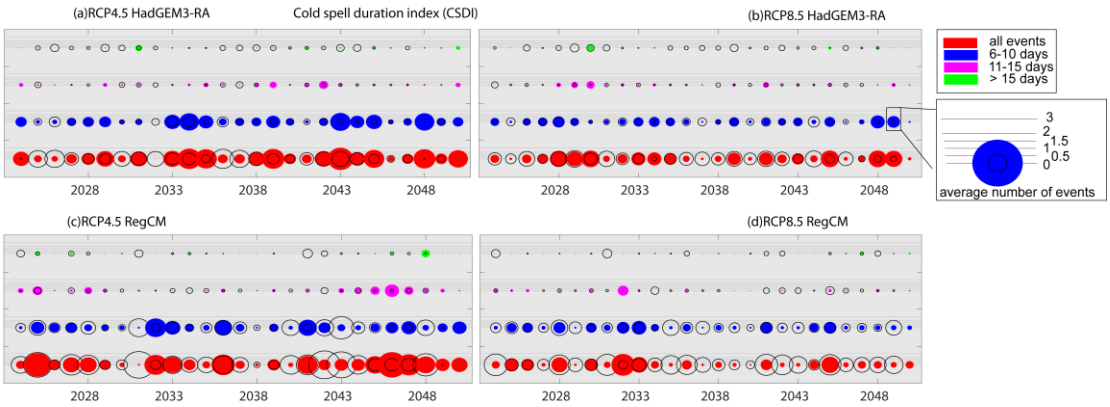

Fig 5.1 Time series of future CSDI events in TP. Events are categorised and presented in the figure, all events (red), 6-10 days (blue), 11-15 days (pink) and >15 days (green) in summertime. The same categories are depicted by black circle for wintertime. The radii of the circles represent the average number of events per year in 2024-2050; horizontal lines refer to 0, 0.5, 1, 1.5, 2 and 3 average numbers of events

Under RCP4.5, in summertime, by HadGEM3-RA, as shown in Fig 5.1 (a) the CSDI events are from 0.08 to 2.42 for 6-10 days events (blue), from 0 to 1.08 for 11-15 days events (pink), from 0 to 0.83 for >15 days events (green), respectively. Additionally, the average CSDI events in TP in 2024-2050 are 1.2 (6-10 days), 0.3 (11-15 days),

and 0.1 (>15 days), respectively (Table 5.2). For RegCM, in summertime, the CSDI events are from 0.25 to 2.50 for 6-10 days events (Fig 5.1 (c), blue), from 0 to 1.67 for 11-15 days events (Fig 5.1 (c), pink), from 0 to 1.00 for >15 days events (Fig 5.1 (c), green), respectively. Based on Table 5.3, the average CSDI events in TP for RegCM are 1.2 (6-10 days), 0.4 (11-15 days) and 0.1 (>15 days), separately. The range of average CSDI for all events in all of cities are from 0.8 (Lhasa) to 2.3 (Maduo) for HadGEM3-RA (Table 5.2) and from 1.3 (Lhasa) to 2.1 (Qumarleb) for RegCM (Table 5.3) in summer time in 2024-2050. Lhasa shows least CSDI events in both simulations in summer time under RCP4.5.

In wintertime, RegCM shows more CSDI events than HadGEM3-RA, especially for 6-10 days and 11-15 days events (Fig 5.1 (a, c), black circle). The average events in 27-years in TP are 0.7 (6-10 days), 0.3 (11-15 days), and 0.5 (>15 days) for HadGEM3-RA and 1.4 (6-10 days), 0.4 (11-15 days) and 0.3 (>15 days) for RegCM (Table 5.2, Table 5.2). As shown in Fig 5.1 (c), For RegCM, more CSDI events appears in wintertime, especially for 6-10 days (0~3.00) and >15 days (0~1.17). However, the number of 11-15 days events (0~0.83) decrease than in summertime. For HadGEM3-RA, the numbers of events are less in wintertime. According to Fig 5.1 (a), the CSDI events are from 0 to 1.33 (6-10 days), 0 to 0.83 (11-15 days), and 0 to 1 (>15 days), respectively. The range of average CSDI for all events in all of cities are from 0.8 (Maduo) to 2.3 (Golmud) for HadGEM3-RA (Table 5.2) and from 1.7 (Lhasa) to 2.4 (Maduo, Xining) for RegCM (Table 5.3) in wintertime in 2024-2050.

Table 5.2 The CSDI average number of the events by the simulation of HadGEM3-RA in TP in 2024-2050

Cold spell duration index events— HadGEM3-RA									
		Winter				Summer			
		All events	6-10 days	11-15 days	>15 days	All events	6-10 days	11-15 days	>15 days
Dari	RCP4.5	1.9	0.9	0.3	0.6	1.4	1.0	0.3	0.1
	RCP8.5	1.8	0.7	0.7	0.4	1.2	0.9	0.3	0.1
Da	RCP4.5	1.0	0.3	0.3	0.4	1.7	1.2	0.3	0.1
Qaidam	RCP8.5	1.1	0.6	0.1	0.4	1.3	0.7	0.4	0.1
Dulan	RCP4.5	2.0	1.1	0.3	0.5	1.3	1.0	0.3	0.1

Gangca	RCP8.5	1.4	0.5	0.5	0.4	1.1	0.9	0.2	0.1
	RCP4.5	1.4	0.3	0.5	0.6	1.7	1.1	0.4	0.2
	RCP8.5	1.4	0.8	0.2	0.4	1.1	0.7	0.3	0.1
Golmud	RCP4.5	2.3	1.5	0.3	0.5	1.6	1.1	0.3	0.2
	RCP8.5	1.3	0.5	0.4	0.4	1.3	0.8	0.3	0.1
Lhasa	RCP4.5	2.0	1.3	0.4	0.4	0.8	0.6	0.2	0
	RCP8.5	2.0	1.3	0.4	0.3	0.4	0.2	0.1	0
Lenghu	RCP4.5	1.6	0.7	0.3	0.6	1.4	0.9	0.4	0.1
	RCP8.5	1.8	0.9	0.3	0.6	1.0	0.9	0.1	0
Maduo	RCP4.5	0.8	0.4	0.1	0.3	2.3	1.7	0.4	0.1
	RCP8.5	1.0	0.7	0.1	0.3	1.9	1.4	0.4	0.1
Qumarleb	RCP4.5	1.1	0.6	0.3	0.2	2.2	1.7	0.3	0.2
	RCP8.5	1.2	0.5	0.1	0.6	1.7	1.3	0.3	0.2
Tuotuohe	RCP4.5	1.9	1.1	0.3	0.5	2.0	1.4	0.3	0.3
	RCP8.5	2.4	1.1	0.6	0.7	1.6	1.1	0.4	0.1
Xining	RCP4.5	1.3	0.6	0.2	0.5	1.9	1.3	0.4	0.2
	RCP8.5	1.3	0.5	0.3	0.4	1.4	0.9	0.4	0.1
Yushu	RCP4.5	1.6	0.9	0.3	0.4	2.1	1.7	0.3	0.1
	RCP8.5	1.3	0.8	0.2	0.3	1.6	1.2	0.2	0.1
All TP	RCP4.5	1.5	0.7	0.3	0.5	1.7	1.2	0.3	0.1
	RCP8.5	1.5	0.7	0.3	0.5	1.3	0.9	0.3	0.1

Under RCP8.5, less CSDI events appear in both simulations and both seasons (summer and winter) (Fig 5.1 (b, d), Table 5.2, and Table 5.3). In summertime, for HadGEM3-RA, the CSDI events are from 0.25 to 1.75 (6-10 days, Fig 5.1 (b), blue), 0 to 1.0 (11-15 days, Fig 5.1(b), pink), and 0 to 0.75 (>15 days, Fig 5.1(b), green). For RegCM, 6-10 days events are from 0.25 to 1.83 (Fig 5.1 (d), blue); 11-15 days events are from 0 to 1.33 (Fig 5.1 (d), pink) and 0 to 0.33 for >15 days events (Fig 5.1 (d), green). The >15 days events appear less than other two events categories. For the average CSDI events in TP in 2014-2050 under RCP8.5, it shows the similar results by two simulations (Table 5.2, Table 5.3). The average CSDI events are 0.9 (6-10 days), 0.3 (11-15 days) and 0.1 (>15 days) by HadGEM3-RA (Table 5.2) and 0.8 (6-10 days), 0.2 (11-15 days) and 0.1 (>15 days) by RegCM (Table 5.3). In all cities,

Lhasa shows the least number of average CSDI events (all events, 0.4) and Maduo shows the most (all events, 1.9) in summertime (Table 5.2) for HadGEM3-RA; for RegCM, the range is from 0.8 (Dari) to 1.3 (Golmud) (Table 5.3).

Table 5.3 The CSDI average number of the events by the simulation of RegCM in TP in 2024-2050 (unit: days)

Cold spell duration index events— RegCM									
		Winter				Summer			
		All events	6-10 days	11-15 days	>15 days	All events	6-10 days	11-15 days	>15 days
Dari	RCP4.5	2.0	1.2	0.3	0.4	1.6	1.2	0.2	0.1
	RCP8.5	1.9	1.3	0.3	0.3	0.8	0.6	0.2	0
Da	RCP4.5	1.9	1.3	0.3	0.2	1.9	1.1	0.6	0.1
Qaidam	RCP8.5	1.9	1.1	0.4	0.3	1.3	0.9	0.3	0.1
Dulan	RCP4.5	2.0	1.4	0.4	0.2	1.8	1.0	0.6	0.1
	RCP8.5	1.5	1.0	0.3	0.1	1.1	0.9	0.2	0
Gangca	RCP4.5	2.1	1.2	0.6	0.4	1.5	1.0	0.4	0.1
	RCP8.5	2.6	2.0	0.3	0.3	1.0	0.7	0.2	0
Golmud	RCP4.5	2.1	1.4	0.3	0.4	2.0	1.3	0.6	0.1
	RCP8.5	2.0	1.4	0.3	0.3	1.3	1.0	0.3	0.1
Lhasa	RCP4.5	1.7	1.0	0.3	0.5	1.3	1.1	0.2	0
	RCP8.5	1.7	1.1	0.4	0.3	0.9	0.7	0.1	0
Lenghu	RCP4.5	1.9	1.0	0.4	0.4	1.4	1.0	0.4	0.1
	RCP8.5	2.2	1.4	0.4	0.3	1.1	1.0	0.1	0
Maduo	RCP4.5	2.4	1.7	0.4	0.3	1.8	1.1	0.5	0.1
	RCP8.5	1.9	1.1	0.4	0.3	1.2	1.0	0.2	0
Qumarleb	RCP4.5	2.1	1.6	0.4	0.1	2.1	1.3	0.6	0.1
	RCP8.5	1.8	1.1	0.4	0.2	1.1	0.9	0.1	0.1
Tuotuohe	RCP4.5	1.9	1.5	0.3	0.1	1.9	0.2	0.5	0.2
	RCP8.5	1.7	1.0	0.5	0.1	1.2	1.0	0.2	0
Xining	RCP4.5	2.4	1.4	0.6	0.3	1.6	1.1	0.4	0.1
	RCP8.5	2.3	1.5	0.6	0.2	1.0	0.8	0.2	0
Yushu	RCP4.5	2.2	1.7	0.4	0.1	1.9	1.4	0.4	0.2

	RCP8.5	2.0	1.5	0.1	0.3	0.9	0.6	0.2	0.1
All TP	RCP4.5	2.1	1.4	0.4	0.3	1.7	1.2	0.4	0.1
	RCP8.5	1.9	1.3	0.4	0.3	1.1	0.8	0.2	0.1

In wintertime, for both simulations, the CSDI events are more than that in summertime (Fig 5.1 (b, d), black circle). For HadGEM3-RA, as shown in Fig 5.1 (b) the CSDI events are from 0 to 1.42 for 6-10 days events, from 0 to 0.83 for 11-15 days events, from 0 to 1.08 for >15 days events, respectively. The average CSDI events in TP in 2024-2050 are 0.7 (6-10 days), 0.3 (11-15 days), and 0.5 (>15 days), respectively (Table 5.2). For RegCM, in wintertime, the CSDI events are from 0 to 2.08 for 6-10 days events, from 0 to 1.08 for 11-15 days events, from 0 to 1.17 for >15days events, respectively (Fig 5.1 (d)). Based on Table 5.3, the average CSDI events in TP for RegCM are 1.3 (6-10 days), 0.4 (11-15 days) and 0.3 (>15 days). The range of average CSDI for all events in all cities are from 1.0 (Maduo) to 2.3 (Tuotuohe) for HadGEM3-RA (Table 5.2) and from 1.5 (Gangca) to 2.6 (Dulan) for RegCM (Table 5.3) in wintertime in 2024-2050.

5.1.1.2 The variation of WSDI temporal analysis

Compared to the CSDI, more WSDI events appear in TP regions in 2024-2050, especially in wintertime (Fig 5.2). Under RCP4.5, in summertime, for HadGEM3-RA, the WSDI events are from 0.33 to 1.83 for 6-10 days events (Fig 5.2 (a), blue), from 0.17 to 1.50 for 11-15 days events (Fig 5.2 (a), pink), from 0.08 to 1.83 for >15 days events (Fig 5.2 (a), green), respectively. Additionally, the average WSDI events in TP in 2024-2050 are 1.1 (6-10 days), 0.7 (11-15 days), and 1.1 (>15 days), respectively (Table 5.4). For RegCM, in summertime, as shown in Fig 5.2 (c), the WSDI events are from 0.25 to 2.0 for 6-10 days events (blue), from 0 to 1.67 for 11-15 days events (pink), from 0.25 to 2.42 for >15days events (green), respectively. Based on Table 5.5, the average WSDI events in TP for RegCM are 0.9 (6-10 days), 0.7 (11-15 days) and 1.2 (>15 days), separately. The range of average WSDI for all events in all of cities are from 2.0 (Lhasa) to 3.3 (Dulan) for HadGEM3-RA (Table 5.4) and from 2.2 (Lhasa) to 3.1 (Lenghu) for RegCM (Table 5.5) in summertime in 2024-2050. Lhasa shows the least number of WSDI events by both simulations in summertime under RCP4.5.

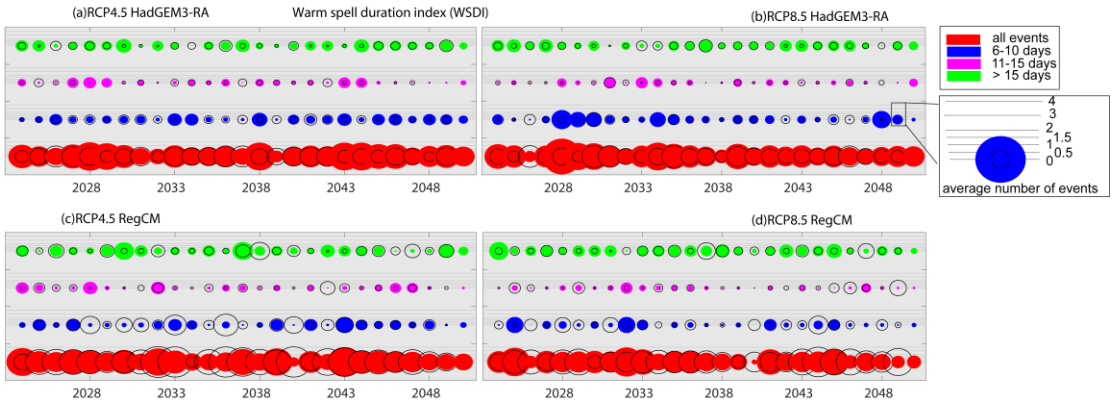

Fig 5.2 As Fig 5.1, just for time series of WSDI in TP regions. The horizontal line includes 4, besides from 0 to 3 the same to Fig 5.1.

In wintertime, RegCM shows more WSDI events than HadGEM3-RA (Fig 5.2 (a, c), black circle). The average events in 27-years in TP are 1.3 (6-10 days), 0.7 (11-15 days), and 1.1 (>15 days) by RegCM and 0.9 (6-10 days), 0.5 (11-15 days) and 0.8 (>15 days) by HadGEM3-RA (Table 5.3, Table 5.5). As shown in Fig 5.2 (c), For RegCM, more WSDI events appears in wintertime, especially for 6-10 days (0~2.92) and 11-15 days (0~1.75). However, the number of >15 days events (0~2.33) decrease than in summertime. For HadGEM3-RA, the numbers of events are less in wintertime for every category. According to Fig 5.2 (a), the WSDI events are from 0 to 1.50 (6-10 days), 0 to 1.08 (11-15 days), and 0 to 1.58 (>15 days), respectively. The range of average WSDI for all events in all cities are from 1.2 (Da Qaidam) to 3.1 (Lhasa) for HadGEM3-RA (Table 5.4) and from 2.8 (Lenghu) to 3.3 (Dulan) for RegCM (Table 5.5) in wintertime in 2024-2050. Lhasa shows the most WSDI events as in wintertime and least WSDI events by simulation of HadGEM3-RA, which means the warmer variation in wintertime and cooler in summertime.

Table 5.4 The WSDI average number of the events by the simulation of HadGEM3-RA in TP in 2024-2050 (unit: days)

Warm spell duration index events— HadGEM3-RA									
		Winter				Summer			
		All events	6-10 days	11-15 days	>15 days	All events	6-10 days	11-15 days	>15 days
Dari	RCP4.5	2.8	1.2	0.4	1.0	3.2	1.3	0.7	1.1
	RCP8.5	2.7	1.0	0.6	1.1	3.1	1.3	0.6	1.2

Da	RCP4.5	1.2	0.3	0.6	0.5	2.9	1.0	0.9	1.0
Qaidam	RCP8.5	1.4	0.5	0.3	0.6	2.7	1.0	0.7	1.1
Dulan	RCP4.5	3.0	1.3	0.9	0.7	3.3	1.6	0.6	1.1
	RCP8.5	2.7	0.9	0.6	1.2	3.0	1.3	0.6	1.1
Gangca	RCP4.5	2.5	1.1	0.6	0.7	3.2	1.2	0.9	1.1
	RCP8.5	2.4	0.9	0.5	1.0	3.2	1.5	0.7	0.9
Golmud	RCP4.5	2.5	1.1	0.4	1.0	2.8	1.0	0.7	1.2
	RCP8.5	2.4	1.0	0.4	1.0	3.0	1.3	0.6	1.1
Lhasa	RCP4.5	3.1	1.4	0.7	0.9	2.0	0.7	0.4	0.8
	RCP8.5	2.9	1.4	0.6	0.9	2.0	0.9	0.4	0.7
Lenghu	RCP4.5	1.7	0.6	0.4	0.7	3.1	1.4	0.5	1.3
	RCP8.5	2.0	0.6	0.6	0.8	2.9	1.1	0.6	1.2
Maduo	RCP4.5	1.4	0.5	0.3	0.7	2.7	1.0	0.7	1.0
	RCP8.5	1.6	0.5	0.4	0.7	3.1	1.0	0.6	1.4
Qumarleb	RCP4.5	2.0	0.9	0.4	0.7	3.0	1.0	0.8	1.2
	RCP8.5	2.0	0.6	0.4	0.9	3.1	0.9	0.8	1.3
Tuotuohe	RCP4.5	2.6	1.1	0.6	0.9	2.5	0.8	0.6	1.1
	RCP8.5	2.2	0.9	0.3	1.0	2.7	1.0	0.7	1.0
Xining	RCP4.5	1.2	0.4	0.3	0.5	3.2	1.3	0.6	1.3
	RCP8.5	1.4	0.4	0.3	0.6	2.9	1.3	0.8	0.9
Yushu	RCP4.5	1.7	0.6	0.4	0.7	2.9	1.0	0.7	1.2
	RCP8.5	1.7	0.7	0.4	0.5	3.0	0.9	0.6	1.6
All TP	RCP4.5	2.9	0.9	0.5	0.8	2.1	1.1	0.7	1.1
	RCP8.5	2.9	0.8	0.5	0.9	2.1	1.1	0.6	1.1

Under RCP8.5, more WDSI events appear in both simulations and both seasons (summer and winter), especially for >15 days events (Fig 5.2 (b, d), Table 5.4, and Table 5.5). In summertime, by HadGEM3-RA, the WSDI events are from 0.25 to 2.58 (6-10 days, Fig 5.2 (b), blue), 0.08 to 1.5 (11-15 days, Fig 5.2 (b), pink), and 0.17 to 1.75 (>15 days, Fig 5.2 (b), green). For RegCM, 6-10 days events are from 0 to 2.17 (Fig 5.2 (d), blue); 11-15 days events are from 0 to 1.5 (Fig 5.2 (d), pink) and 0.25 to 2.42 for >15 days (Fig 5.2 (d), green) events. The frequency of >15 days events appear more than other two event categories. The average WSDI events in TP in

2014-2050 were shown in Table 5.2 and Table 5.3. The average WSDI events are 1.1 (6-10 days), 0.6 (11-15 days) and 1.1 (>15 days) for HadGEM3-RA (Table 5.4) and 0.8 (6-10 days), 0.5 (11-15 days) and 1.3 (>15 days) for RegCM (Table 5.5). In all cities, Lhasa shows the least average WSDI events (all events, 2.0) and Gangca shows the most (all events, 2.9) in summer time (Table 5.4) for HadGEM3-RA; for RegCM, the range is from 2.3 (Lhasa) to 3.2 (Tuotuohe) (Table 5.5). Lhasa shows the least WSDI events for both simulations in summer time.

Table 5.5 The WSDI average number of the events by the simulation of RegCM in TP in 2024-2050 (unit: days)

Warm spell duration index events— RegCM									
		Winter				Summer			
		All events	6-10 days	11-15 days	>15 days	All events	6-10 days	11-15 days	>15 days
Dari	RCP4.5	3.1	1.3	0.8	1.1	2.9	0.9	0.7	1.3
	RCP8.5	2.9	1.0	1.0	0.9	2.7	0.7	0.6	1.4
Da	RCP4.5	3.1	1.2	0.9	1.1	2.9	1.1	0.6	1.1
Qaidam	RCP8.5	2.9	0.9	1.0	1.0	2.7	1.0	0.4	1.3
Dulan	RCP4.5	3.3	0.3	0.9	1.1	2.7	0.9	0.6	1.3
	RCP8.5	2.6	0.7	0.8	1.0	2.4	0.6	0.4	1.4
Gangca	RCP4.5	3.0	1.0	0.7	1.3	2.9	1.0	0.8	1.1
	RCP8.5	3.1	1.2	0.9	1.0	2.4	0.7	0.5	1.1
Golmud	RCP4.5	3.1	1.4	0.8	1.0	2.9	1.2	0.7	1.0
	RCP8.5	2.6	1.1	0.6	0.9	2.8	0.7	0.7	1.3
Lhasa	RCP4.5	2.9	1.1	0.5	1.3	2.2	0.7	0.3	1.1
	RCP8.5	2.1	0.8	0.4	0.9	2.3	0.6	0.3	1.4
Lenghu	RCP4.5	2.8	1.2	0.6	1.0	3.1	1.3	0.7	1.1
	RCP8.5	2.9	1.2	0.5	1.2	2.8	1.0	0.7	1.1
Maduo	RCP4.5	3.1	1.7	0.6	0.9	2.6	0.9	0.5	1.3
	RCP8.5	2.9	1.1	0.6	1.3	2.5	0.5	0.7	1.3
Qumarleb	RCP4.5	3.1	1.3	0.7	1.1	3.0	1.0	0.9	1.1
	RCP8.5	3.0	1.3	0.6	1.1	2.7	0.8	0.7	1.3
Tuotuohe	RCP4.5	3.2	1.3	0.6	1.2	2.8	0.8	1.0	1.0

	RCP8.5	2.9	1.2	0.6	1.0	3.2	1.3	0.6	1.3
Xining	RCP4.5	3.2	1.2	0.8	1.1	2.8	1.1	0.6	1.3
	RCP8.5	3.1	1.0	0.9	1.3	2.7	0.7	0.7	1.3
Yushu	RCP4.5	3.1	1.6	0.4	1.1	2.8	0.6	0.6	1.6
	RCP8.5	2.7	1.2	0.4	1.1	2.4	0.8	0.4	1.2
All TP	RCP4.5	3.1	1.3	0.7	1.1	2.8	0.9	0.7	1.2
	RCP8.5	2.8	1.0	0.7	1.1	2.6	0.8	0.5	1.3

In wintertime, for both simulations, the WSDI events are less than in summertime for HadGEM3-RA and more events for RegCM (Fig 5.2 (b, d), black circle). For HadGEM3-RA, as shown in Fig 5.2 (b) the WSDI events are from 0 to 1.92 for 6-10 days events, from 0 to 1.42 for 11-15 days events, from 0 to 1.67 for >15days events, respectively. The average WSDI events in TP in 2024-2050 are 0.8 (6-10 days), 0.5 (11-15 days), and 0.9 (>15 days), respectively (Table 5.4). For RegCM, in wintertime, the WSDI events are from 0 to 2.42 for 6-10 days events, from 0 to 2.08 for 11-15 days events, from 0 to 2.25 for >15 days events, respectively (Fig 5.2 (d)). Based on Table 5.5, the average WSDI events in TP for RegCM are 1.0 (6-10 days), 0.7 (11-15 days) and 1.1 (>15 days). The range of average WSDI for all events in all of cities are from 2.0 (Lhasa) to 3.2 (Gangca) for HadGEM3-RA (Table 5.2) and from 2.1 (Lhasa) to 3.1 (Gangca and Xining) for RegCM (Table 5.3) in wintertime in 2024-2050. Lhasa shows the least events and Gangca appears the most events for both simulations.

5.1.2 Variation of the WSDI and CSDI in different regions in TP

The coefficients of variations (CV) in every city under RCP4.5 and RCP8.5 are shown in Fig 5.3 and Fig 5.4. The coefficient of variation is calculated by the following equation:

$$\mathrm{CV} = \frac{Standard\ deviation}{average} \qquad (5.3)$$

Fig 5.3 shows the CV for WSDI and CSDI in evert city in 2024-2050 under RCP4.5 by the simulation of HadGEM3-RA and RegCM. Compared to RegCM, HadGEM3-RA shows larger CV for CSDI and WSDI in winter time than that of summertime. In wintertime, the larger CV for CSDI and WSDI by the simulation of HadGEM3-RA, show in Maduo (1.36, 0.91), Yushu (1.10, 0.85), Da Qaidam (1.06, 0.81) and Xining (1.00, 0.83). The smallest CV for CSDI and WSDI appear in Dari (0.53, 0.49), Dulan

(0.73， 0.43), Lhasa (0.77, 0.39), and Tuotuohe (0.78, 0.50) (Fig 5.3). The CV for CSDI is larger than WSDI in wintertime. This may due to the cold weather in TP in wintertime and the strong cold stress can dominant the whole TP. Because of the climate warming, the cold spells decrease and changes on the intensity and duration. Even though, the cold weather still has very strong influence on the whole TP and WSDI is less than CSDI in wintertime. As shown in Fig 5.3, the CV for both CSDI and WSDI events in summertime is smaller than in wintertime, which means the more stable weather or less climate variation in summertime by simulation of HadGEM3-RA. The maximum CV shows in Lhasa (WSDI: 0.71, CSDI: 0.97). Other cities show very similar CV, especially for CSDI (0.29-0.45, other 11 cities) and CV for WSDI is from 0.54 to 0.75 which pronounce the small difference between each other (Fig 5.3). The CV of WSDI in wintertime is larger than that in summertime, except for Lhasa.

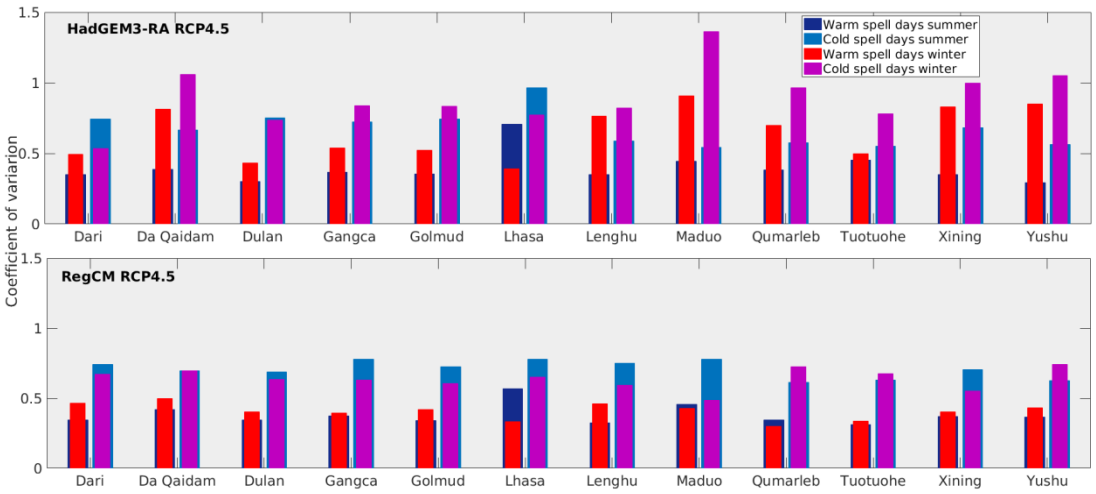

Fig 5.3 The annual variability of cold and warm spells days under RCP4.5

Compared to HadGEM3-RA, RegCM shows smaller CV for both CSDI and WSDI in summertime and wintertime under RCP4.5 (Fig 5.3). The CV of CSDI in summertime and wintertime are very similar in most cities, except for Maduo, Lenghu, Gangca and Xining; the difference between summertime and wintertime is from 0.15 to 0.30. For the CV of WSDI in wintertime is larger than in summertime for most of the cities, except for Lhasa and Qumarleb (Fig 5.3). This trend is more clear in Lhasa and the difference is 0.24 (CSDI difference between summertime and wintertime). Under RCP4.5, WSDI (CSDI) shows larger variation in wintertime (summertime) for both simulations in most cities.

Fig 5.4 indicates the CV for WSDI and CSDI in 2024-2050 under RCP 8.5 by the simulation of HadGEM3-RA and RegCM in 12 cities. By simulation of HadGEM3-

RA, the fluctuation of CV for CSDI and WSDI in each city is larger than by RegCM. The CV of CSDI in wintertime is larger than in summertime for most of city. Except for Lhasa, the CV in summertime (1.7) is larger than in wintertime (0.75). Dulan and Tuotuohe also show the same trend, though the difference is smaller (Fig 5.4). The CV for WSDI in wintertime is larger than in summertime for most cities. Lhasa shows the opposite trend and the CV in summertime is 0.71; in wintertime is just 0.41 (Fig 5.4). This may due to the valley location of Lhasa and warmer than others (most of cities locate around the mountain areas). There will be more CSDI and WSDI in summertime compared to wintertime due to the climate change.

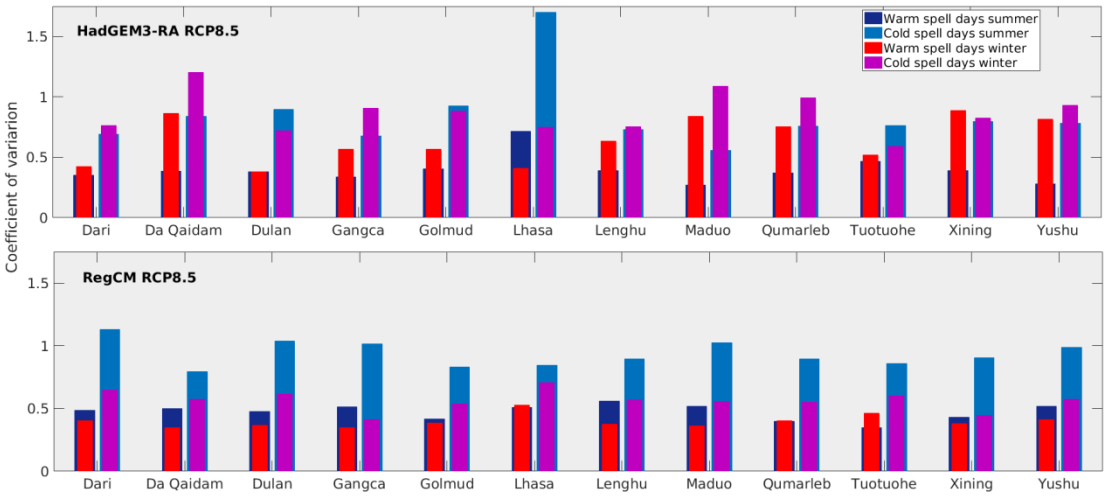

Fig 5.4 The annual variability of cold and warm spells days under RCP8.5

The CV of CSDI and WSDI for RegCM is smaller than that of HadGEM3-RA under RCP8.5 which indicates more stable climate conditions by simulation of RegCM (Fig 5.4). The CV of CSDI in summertime is larger than that of wintertime for all of the cities. For CV of WSDI in summertime is also larger than in wintertime of most of cities. In summertime, there will be more events (both CSDI and WSDI) by the simulation of RegCM.

5.2 The WSDI and CSDI analysis in Lhasa and Xining

Xining and Lhasa are the provincial capital city of Qinghai Province and Tibet Autonomous Region of China, respectively. In addition, Xining and Lhasa are also the starting and terminal stations of Qinghai-Tibet Railway. Besides, both cities are the most popular cities for tourists in TP, according to their distinctive natural scenery, religious culture, etc. It's meaningful to investigate the extreme climate conditions in the future for those two cities to provide scientific evidence of tourism plan, urban

planning, population migration, etc. In order to explore the extreme climate events in those cities, in the following parts the frequency, duration and intensity of WSDI and CSDI events in Xining and Lhasa in 2024-2050 under RCP4.5 and RCP8.5 are evaluated and discussed.

5.2.1 The annual frequency of WSDI and CSDI analysis in Lhasa and Xining

Fig 5.5 shows the WSDI and CSDI events and the duration of every event in Xining and Lhasa in 2024-2050 under RCP4.5 and RCP8.5. **Under RCP4.5**, the WSDI shows more events than the CSDI for both cities and both simulations. For WSDI by HadGEM3-RA, the distribution of events present into increasing trend in both cities, especially for Xining. It shows a very clear increasing in long term events (>15 days) after the year of 2044. For Lhasa, the increasing concentrates in the numbers of events after 2042 (Fig 5.5 (a)). Except those, there are also some very long term WSDI events for both cities. There are eight very long term events which the duration is longer than 40 days in Lhasa and seven in Xining (Fig 5.5 (a)). It indicates that not only the number of WSDI events is large, but also the durations of events are very long in both cities.

The WSDI for RegCM under RCP4.5, two cities show the different trends. For Lhasa, the trend present as a quasi W-shaped over time. There are three valley-time periods for decreasing, 2024-2026, 2035-2036, and 2045-2046; it shows more events in other time. For Xining, it also shows a more clear quasi W-shaped. Except the beginning and ending five years, the period of 2032-2041 appears more events, especially for the long time events (>15 days) than other time (Fig 5.5 (a)). There are also some very long term WSDI events by simulation of RegCM. The very long term WSDI events (duration is longer than 40 days) in Lhasa is ten and six in Xining. There is no big difference between two simulations on the very long term events.

For CSDI under RCP4.5, both simulations show fewer events than WSDI in the same city (Fig 5.5 (a)). Besides, short time events (6-10 days) are more than other events. For RegCM, there are more CSDI events appear than that of HadGEM3-RA in both cities. Xining shows more CSDI events than Lhasa by the same simulation (Fig 5.5 (a)). This may due to the valley terrain of Lhasa and the climate is warmer than Xining; it appears not as many as the CSDI events in Xining. As WSDI events, very long term CSDI events appear in both cities and both simulations. However,

compared with WSDI events, the very long term CSDI events decrease for both cities (Fig 5.5 (a)). There are two very long term CSDI events in Lhasa and four in Xining by HadGEM3-RA; by RegCM only one very long term CSDI event appears in Lhasa and none of them occurs in Xining (Fig 5.5 (a)).

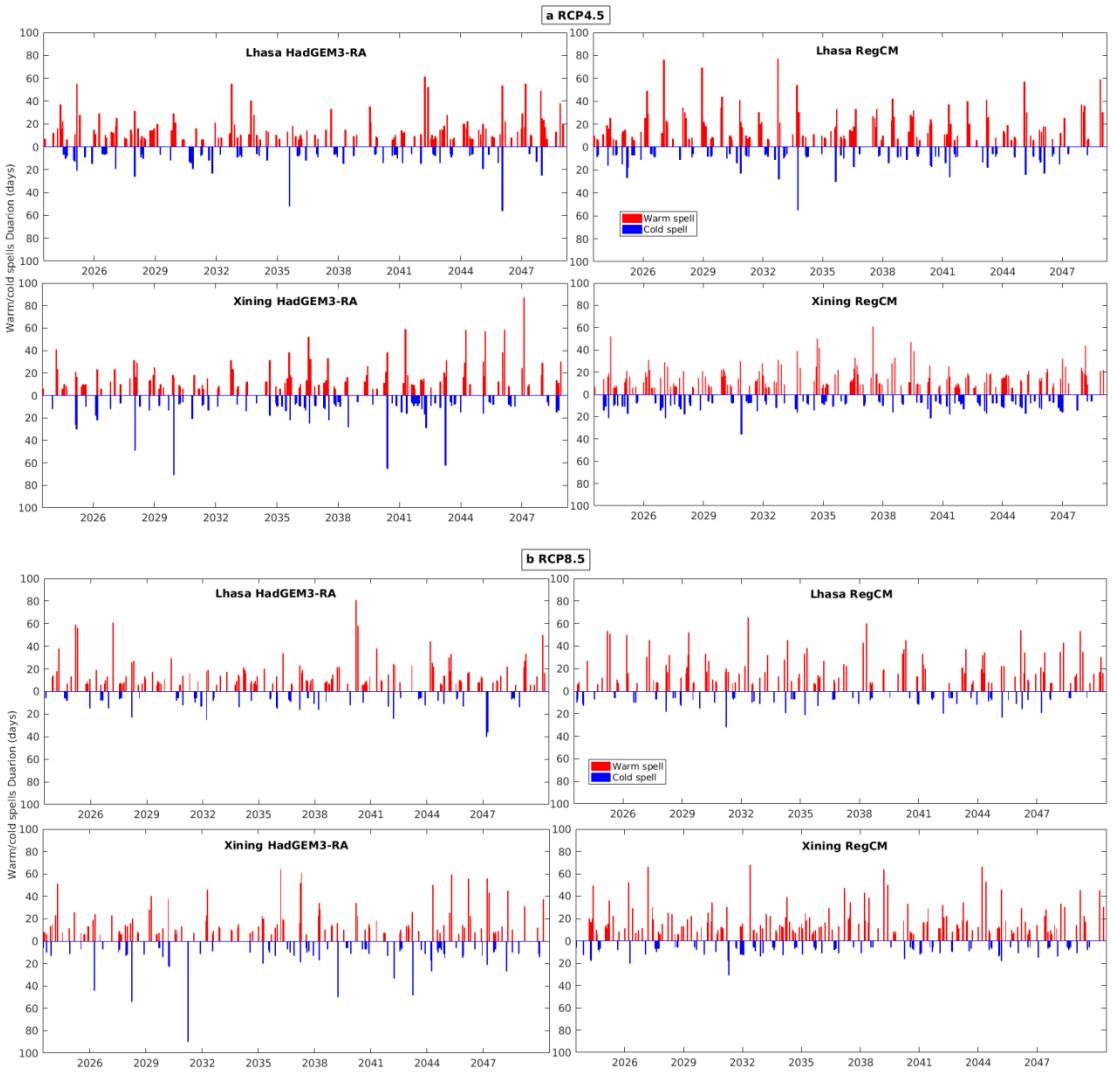

Fig 5.5 The annual CSDI and WSDI events in Lhasa and Xining in 2024-2050 under (a) RCP4.5 and (b) RCP8.5

Under RCP8.5, there are more WSDI events and less CSDI for both cities and both simulations than under RCP4.5 (Fig 5.5 (b)). It also shows more WSDI events than CSDI for both simulation; additionally, more long (>15 days) and medium (11-15 days) WSDI events. It shows more very long term WSDI events by RegCM than by HadGEM3-RA. By HadGEM3-RA, there are seven very long term WSDI events in Lhasa and twelve in Xining. However, both 13 very long term WSDI events (>40 days) appear in Lhasa and Xining by RegCM (Fig 5.5 (b)). It's a very clear increase

compared with RCP4.5 which indicates that the frequency of longer duration WSDI events will increase under RCP8.5.

Furthermore, the number of CSDI events decrease under RCP8.5. Even in some years, no CSDI events appear for both cities (Fig 5.5 (b)). Compared with two cities, Lhasa shows decreasing for CSDI events (less medium (11-15 days) and long term (>15 days) events). The variation of Xining show long term events than RCP4.5 by HadGEM3-RA (Fig 5.5 (b)). Especially for the very long term CSDI events in Xining; there are five very long term CSDI events by HadGEM3-RA in Xining and no one in Lhasa (Fig 5.5 (b)). For both RCP4.5 and RCP8.5, more WSDI and less CSDI show in both cities by both simulations. Compared with two cities, Lhasa shows more WSDI events and less CSDI events than Xining.

5.2.2 The seasonal frequency of CSDI and WSDI analysis in Lhasa and Xining

Fig 5.6 shows the CSDI events distribution in Lhasa and Xining in summer and winter in 2024-2050 under RCP4.5 and RCP8.5. No clear increasing or decreasing trend shows for both cities over time. For both cities, there are more CSDI events in wintertime than in summertime. This may because of the cold and windy weather in wintertime and more stable weather in summertime.

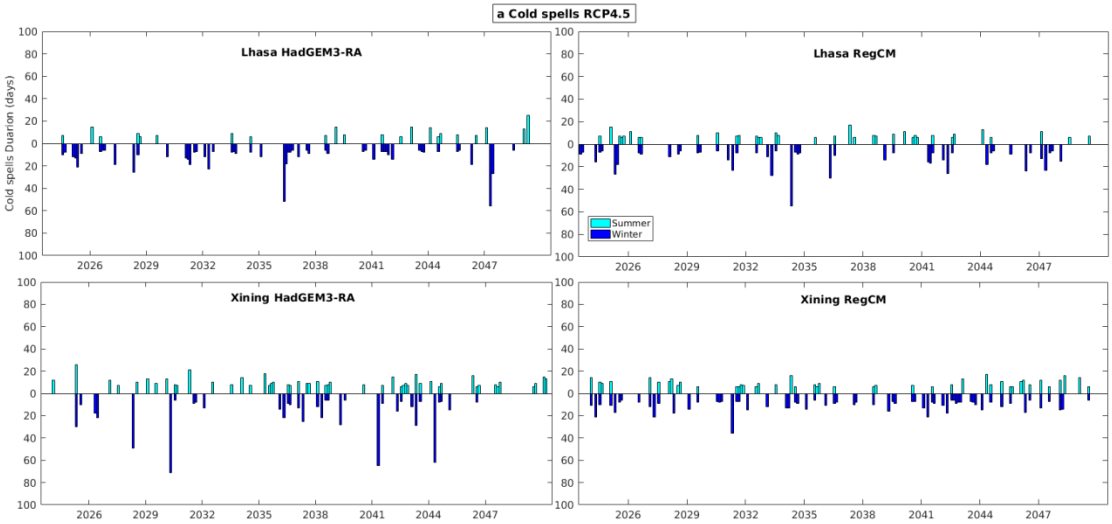

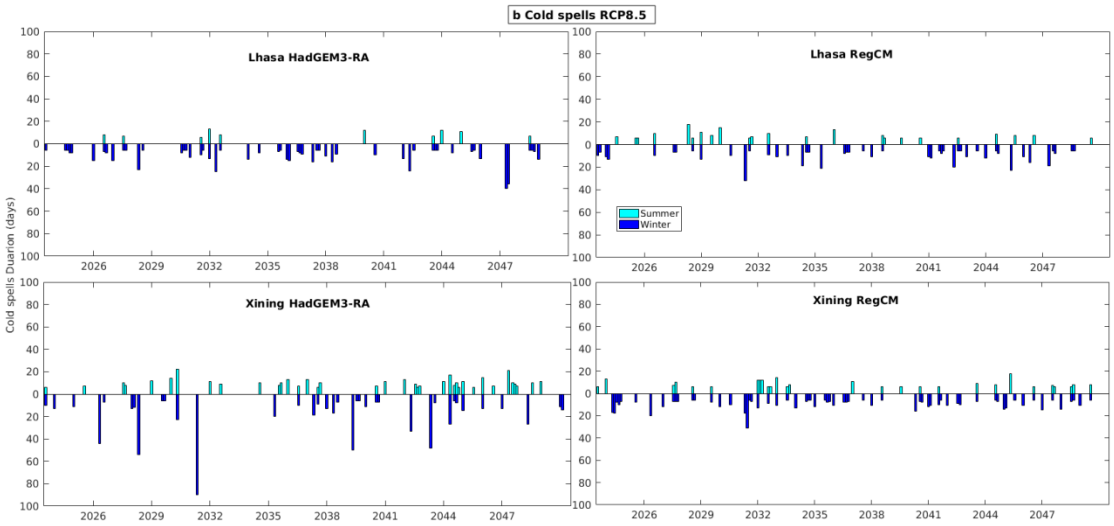

Fig 5.6 The CSDI events in Lhasa and Xining in summer and winter in 2024-2050 under (a) RCP4.5 and (b) RCP8.5

Under RCP4.5, more CSDI events appear in wintertime than in summertime for both cities, especially for Xining; there are some long term events (>15 days) appear by HadGEM3-RA. Lhasa shows less CSDI events in both seasons (Fig 5.6 (a)). RegCM simulates more CSDI events in both cities and both models. However, more long term CSDI events (>15 days) show in both cities by HadGEM3-RA (Fig 5.6(a)). There is no very long term CSDI events appear in summertime in both cities by both simulations. In winter time, compared to RegCM, HadGEM3-RA simulates more very long term CSDI events. There are two very long term CSDI events (>40 days) in Lhasa and four in Xining by HadGEM3-RA. On the contrary, by RegCM the very long term CSDI events (>40 days) only appear in Lhasa and it is just one (Fig 5.6 (a)). Under RCP8.5, less CSDI events appear than under RCP4.5 for both cities and both seasons. Especially for Lhasa in summer time, there are just ten CSDI events and all of them are short term events (6-10 days) by simulation of HadGEM3-RA (Fig 5.6 (b)). However, for Xining, there are still some long term events (>15 days) appear by HadGEM3-RA and short term events (6-10 days) show by RegCM in wintertime. As to RCP4.5, there is no very long term CSDI event in summertime for both cities. The very long term events (>40 days) also just show in Xining in wintertime and it is five which is the same number to RCP4.5 (Fig 5.6(b)).

Fig 5.7 shows the WSDI events distribution in Lhasa and Xining in summer and winter in 2024-2050 under RCP4.5 and RCP8.5. More events appear in both seasons for both cities, compared with CSDI events, especially by the simulation of RegCM.

Under RCP4.5, more WSDI events show in wintertime for Lhasa, especially by HadGEM3-RA. However, more long term events (>15 days) appear in summer time for Lhasa by both simulations (Fig 5.7 (a)). The WSDI events present a quasi V-shaped distribution and show an increasing over time after the valley value in summer time. There is no clear increasing or decreasing trend in wintertime for Lhasa by both simulations (Fig 5.7 (a)). For Xining, a considerable increasing trend in wintertime and decreasing trend in summertime by the simulation of HadGEM3-RA; on the opposite of Lhasa, the WSDI events present a peak increasing in 2034-2041 and then decrease for both seasons by RegCM (Fig 5.7 (a)). In summertime, there are six very long term WSDI events (>40 days) by HadGEM3-RA and 11 by RegCM. For Xining, there are three very long term WSDI events (>40 days) in summertime by both simulations (Fig 5.7 (a)). In wintertime, the very long term WSDI events (>40 days) in Lhasa decrease compared with summertime and there are just two by HadGEM3-RA and one by RegCM. For Xining, the difference between summertime and wintertime is very small. There are 4 very long term WSDI events (>40 days) by HadGEM3-RA and 2 by RegCM (Fig 5.7 (a)).

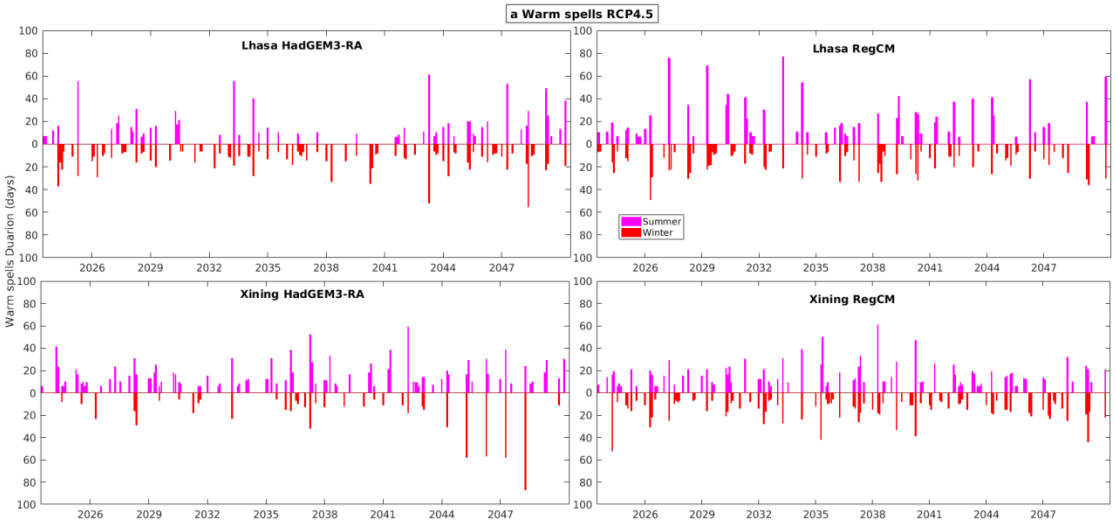

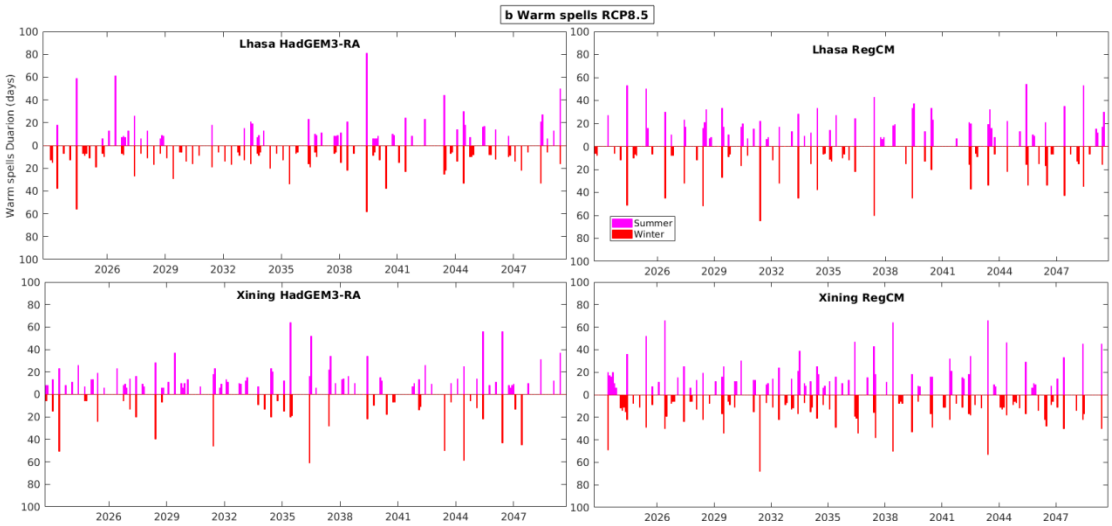

Fig 5.7 The WSDI events in Lhasa and Xining in summer and winter in 2024-2050 under (a) RCP4.5 and (b) RCP8.5

Under RCP8.5, similar to RCP4.5, more WSDI events show than CSDI events for both seasons and cities (Fig 5.7 (b)). There are events in both seasons and cities by the simulation of RegCM than HadGEM3-RA. For HadGEM3-RA, Lhasa show more WSDI events in wintertime Xining more in summertime. Two cities present the different variations over time (Fig 5.7 (b)). For RegCM, less short term events (6-10 days) and medium term events (11-15 days) and more long term events (>15 days) appear in wintertime compared with RCP4.5 for both cities, especially for Lhasa. There are even seven long term events (>15 days) which duration is longer than 40 days (Fig 5.7 (b)). That indicates the clear warming trend in cities in wintertime. Compared to RCP4.5, the very long term WSDI events (>40 days) increase in wintertime for both cities. For Lhasa, there are 2 very long term WSDI events by HadGEM3-RA and 8 by RegCM; For Xining, the increased trend is more visible compared to wintertime under RCP4.5 conditions. There are 7 very long term WSDI events by HadGEM3-RA and 4 by RegCM in Xining (Fig 5.7 (b)). In summertime, the very long term WSDI events decrease for Lhasa (HadGEM3-RA: 4, RegCM: 5), but increase for Xining (HadGEM3-RA: 4, RegCM: 9) under RCP8.5 conditions (Fig 5.7 (b)).

5.2.3 The annual intensity of WSDI and CSDI analysis in Lhasa and Xining

In order to explore the Ta intensity of events, the average maximum Ta and minimum Ta of every event is calculated in Xining and Lhasa in 2024-2050 under RCP4.5 and

RCP8.5. For the WSDI events, the increaseed intensity of events compared to historical data is analyzed; for CSDI, the decreaseed intensity of events is calculated. The equations are as following:

$$Event_{intensity}(yr,n) = \frac{1}{N(yr,n)} \sum_{i=N_{start(yr,n)}}^{N_{end(yr,n)}} Ta_{fut}(i) - Ta_{his}(i) \qquad (5.4)$$

where yr is the year, n is the nth event for this year, $N(yr,n)$ indicates the duration of the nth event, $N_{start(yr,n)}$ and $N_{end(yr,n)}$ represent the first and last calendar day separately. $Ta_{fut}$is the Ta in 2024-2050 (WSDI: Ta maximum, CSDI: Ta minimum) while $Ta_{his}$is the Ta in 1979-2005 (WSDI: Ta maximum, CSDI: Ta minimum).

The changing values are from -12°C to 12°C and according to the increasing or decreasing intensity, it can be divided into 8 classes. Table 5.6 shows the 8 classes of intensity and the related changing values. The order from 1 to 8 is based on the values from small to large. The intensity of variation is from "- - - -" to "+ + + +" (Table 5.6).

Table 5.6 The class of variation intensity

Class	Value (°C)	Intensity of variation description
1	-12.00 ~ -9.01	- - - -
2	-9.00 ~ -6.01	- - -
3	-6.00 ~ -3.01	- -
4	-3.00 ~ -0.01	-
5	0.01 ~ 3.00	+
6	3.01 ~ 6.00	+ +
7	6.01 ~ 9.00	+ + +
8	9.01 ~ 12.00	+ + + +

Fig 5.8 shows the annual Ta event intensity of variation by comparing 2024-2050 with 1979-2005 under RCP4.5 and RCP8.5 in Lhasa and Xining. Under RCP4.5, the dominant intensity are class3 ("- -"), class4 ("-"), class5 ("+"), and class6 ("+ +") and the changing value is -6.00°C ~ 6.00°C. Compared with two cities, all of the "+ + + +" events appear in Lhasa by simulation of HadGEM3-RA and all of the "- - - -" show in Xining which appear by both simulations (Fig 5.8 (a)). Additionally, all the "+ + + +" events are long term WSDI events (>15 days) in Lhasa. By simulation of HadGEM3-RA, there are more "+ + + +" and "+ + +" events compared with RegCM for both

cities. On the contrary, more "- - - -" and "- - -" appear by the simulation of RegCM (Fig 5.8 (a)). Under RCP4.5, Lhasa shows stronger intensity WSDI events and Xining stronger intensity CSDI events. Compared with RegCM, HadGEM3-RA simulates stronger intensity WSDI events and less intense CSDI events (Fig 5.8 (a)).

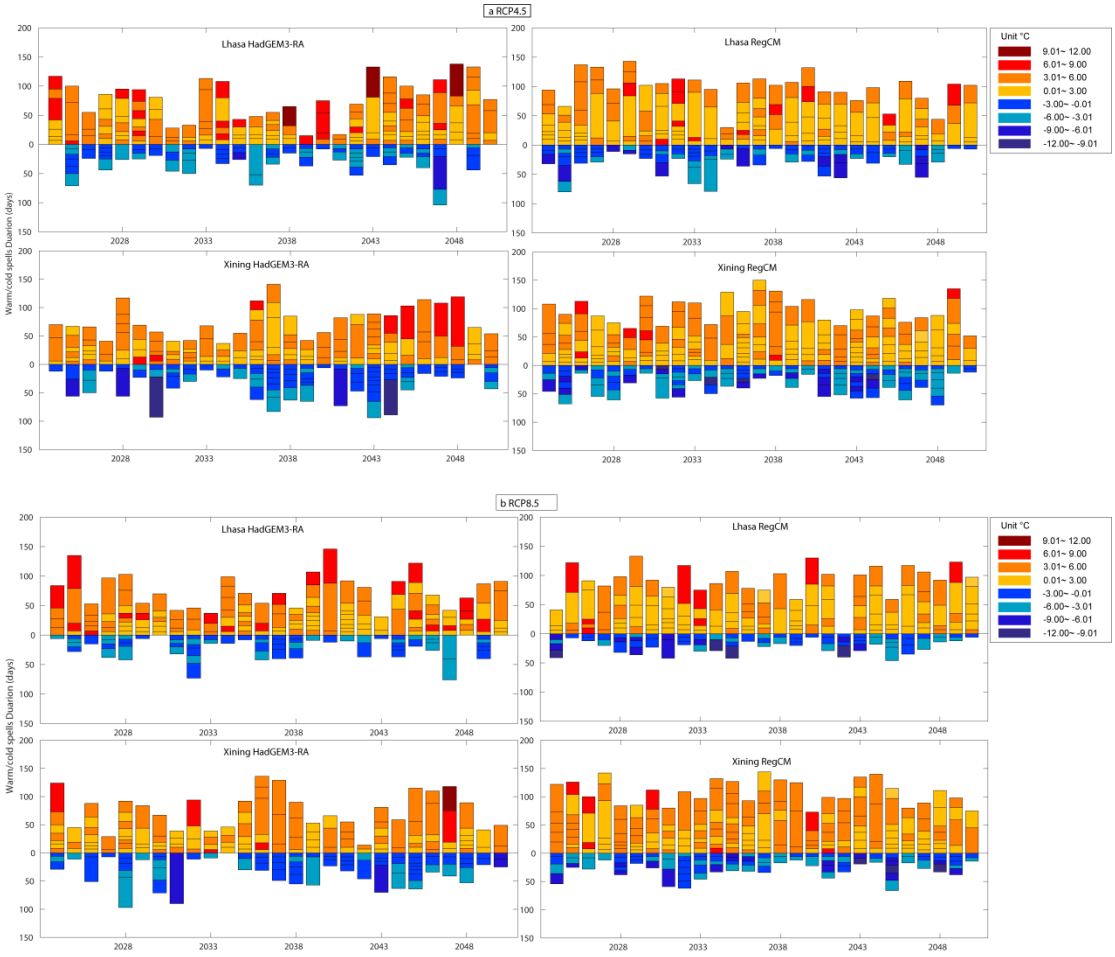

Fig 5.8 The annual event intensity of CSDI and WSDI events in Lhasa and Xining in 2024-2050 under (a) RCP4.5 and (b) RCP8.5

Under RCP8.5, the dominant intensity are also class3 ("- -"), class4 ("-"), class5 ("+") and class6 ("+ +") which is the same to RCP4.5 (Fig 5.8 (b)). Less "+ + + +" events appear under RCP8.5 which is just one time in Xining by HadGEM3-RA. Besides, the "- - - -" events also decrease compared to RCP4.5 for both cities and both simulation. Furthermore, there is no "- - - -" events by the simulation of HadGEM3-RA for both cities (Fig 5.8 (b)). Generally, compared with RegCM, HadGEM3-RA simulates stronger intensity WSDI events and less strong intensity CSDI events (Fig 5.8 (b)). Under RCP4.5, it also indicates that Lhasa shows stronger intensity WSDI events and Xining appears stronger intensity CSDI events.

5.2.4 The analysis of seasonal intensity change of WSDI and CSDI in Lhasa and Xining

In the following parts, the distribution of WSDI and CSDI intensity in summer and winter in 2024-2050 under RCP4.5 and RCP8.5 for Lhasa and Xining are discussed, as shown in Fig 5.9 and Fig 5.10.

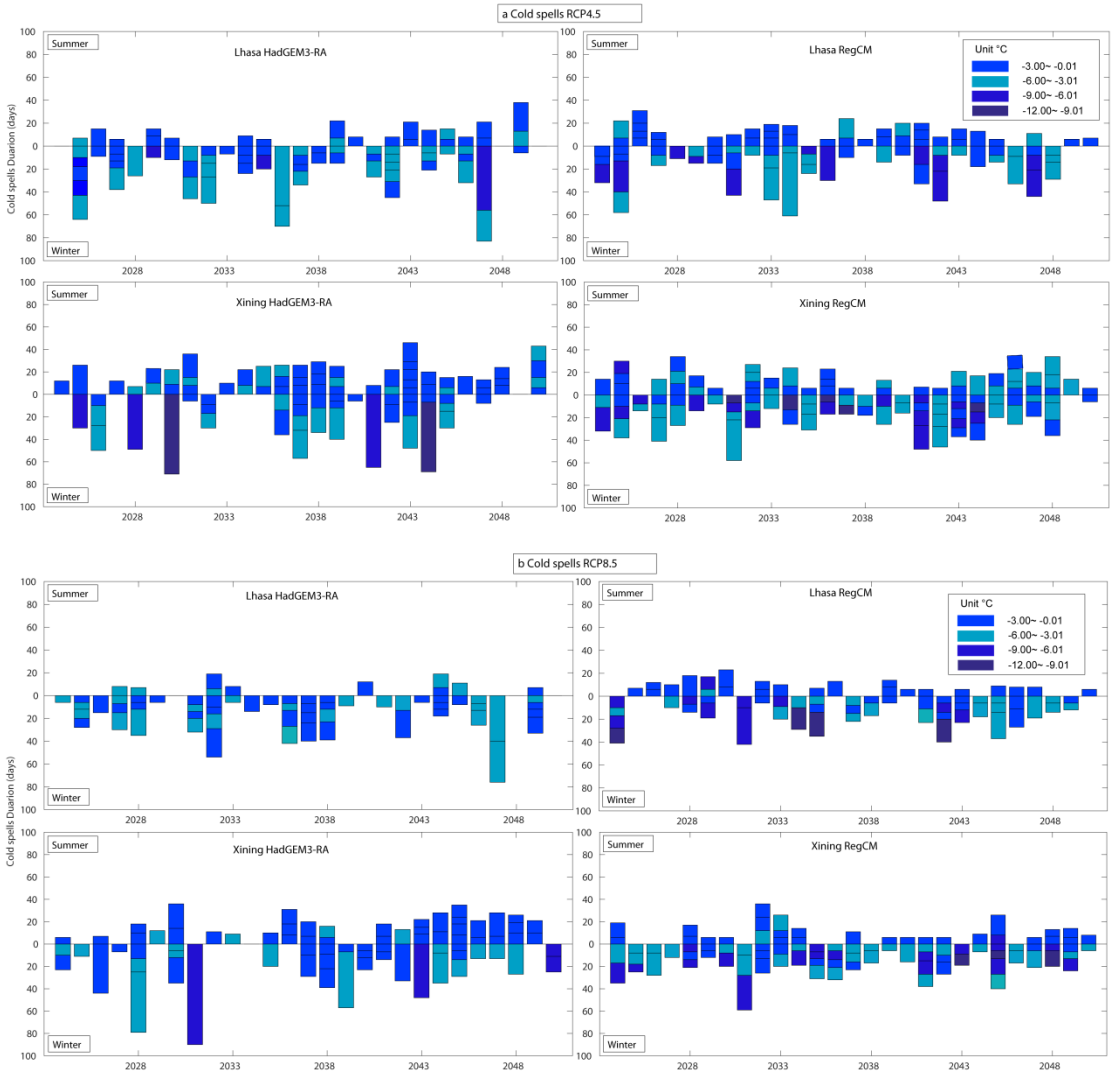

Fig 5.9 The seasonal intensity change of CSDI events in Lhasa and Xining in summer and winter under (a) RCP4.5 and (b) RCP8.5

As shown in Fig 5.9, the intensity of CSDI events is stronger in wintertime than in summertime for both cities and both simulations. Under RCP4.5, the dominant intensity are class3 ("- -") and class4 ("-") for both cities and both simulations. However, all of the "- - - -" events appear in Xining for both simulations. Compared to RegCM, HadGEM3-RA simulates less strong intensity CSDI events for both cities (Fig 5.9(a)). Lhasa shows less strong intensity events than Xining.

Fig 5.10 The seasonal intensity change of WSDI events in Lhasa and Xining in summer and winter under (a) RCP4.5 and (b) RCP8.5

Under RCP8.5, the dominant intensity is also class3 ("- -") and class4 ("-") and the number of strong intensity CSDI events decrease compared to RCP4.5 (Fig 5.9 (b)). By the simulation of HadGEM3-RA, there is no "- - - -" events for both cities. However, it shows more "- - - -" events in Lhasa than under RCP4.5, though the number of CSDI events decrease by RegCM (Fig 5.9 (b)). Xining shows less strong intensity events and the number of events also decrease compared with RCP4.5. For Lhasa, though the number of events decreases by both simulations, strong intensity events increase compared with RCP4.5 by simulation of RegCM (Fig 5.9 (b)). RegCM simulated more strong intensity CSDI events under both scenarios for the same city (Fig 5.9).

Fig 5.10 shows the intensity of WSDI events in summertime and wintertime in 2024-2050 under RCP4.5 and RCP8.5 in Lhasa and Xining. The dominant intensity is

shown by class5 (“+”) and class6 (“+ +”) for both RCP4.5 and RCP8.5. Under RCP4.5, HadGEM3-RA simulates more strong intensity events than by RegCM (Fig 5.10 (a)). All of the “+ + + +” events appear in Lhasa by simulation of HadGEM3-RA. There is no “+ + + +” events appear by RegCM and the number of “+ + +” events are less than by HadGEM3-RA (Fig 5.10 (a)). Lhasa shows more strong intensity events than that of Xining, though more WSDI events appear in Xining (most of them are “+” slight + or “+ +” events). It indicates that there are more strong intensity events, though less number of WSDI events for both cities by simulation of HadGEM3-RA (Fig 5.10 (a)).

Under RCP 8.5, the “+ + +” events and “+ + + +” events decrease compared with RCP4.5 (Fig 5.10 (b)). There is just one “+ + + +” event which appear in Xining by HadGEM3-RA. For Lhasa, more “+ + +” and “+ +” events appear than Xining (Fig 5.10 (b)). The HadGEM3-RA simulates stronger intensity WSDI events than RegCM. RegCM simulates a higher number of WSDI events, though most of them are “+” events (Fig 5.10 (b)).

According to the results, over the whole time we found more WSDI events than CSDI events. This reflects that the warming in the future is accompagnied with less cold related events. However, we found no clear increasing or decreasing trend for both indices in TP over time during 2024-2050. The number of extreme events ranges from 0.4 to 3.3 in all selected cities in TP analysed. Comparing Lhasa with Xining Calculated trends of WSDI shows increase more in summertime and CSDI appears more in wintertime. Comparing Lhasa with Xining, variations are very similar and small among cities, except for Lhasa, which shows more variations in both indices. Comparing Lhasa with Xining, Lhasa shows more clear warming trend, longer duration of long term WSDI events and shorter duration of CSDI events. For the intensity of extreme events, the dominant intensity are “- -”, “-”, “+” and “+ +” for both Xining and Lhasa. Xining shows stronger intensity of CSDI events and Lhasa appears stronger intensity of WSDI events.

Chapter 6

6 Discussion

6.1 Complementarity between different types of cities based on thermal comfort

The present study presents a synopsis of the thermal comfort conditions in all provincial capital cities of mainland China, widening the limited information given in previous studies on the thermal comfort of a single city or a few cities (Wang et al. 2004; Ji et al. 2006; Zhai et al. 2009; Lin and Matzarakis 2011; Lai et al. 2014). One can find complementarities and huge potential for cooperation between different types of cities in terms of the thermal comfort. In winter, there is no thermal stress in low-latitude Type-II cities, *i.e*. Haikou, Guangzhou, Nanning and neighbouring cities, but the cold stress prevail in the cities of all the remaining four types. Type-II cities are winter resorts in mainland China. In summer, the population suffers under heat stress in Type-III and Type-IV cities, but pleasant thermal sensation dominates in Type-I and Type-V cities. Therefore, the latter cities are natural summer resorts for the populations of the other city types, particularly Type-III and Type-IV cities. With the improvement in transportation and accessibility, many cities in West China, such as Lhasa, Xining, Kunming, and Guiyang are becoming popular holiday destinations in summer.

The seasonal variation in the duration of pleasant days in various cities in mainland China has already now significantly influenced on the seasonal rhythm of urban tourist flow (Lu et al. 2002; Sun and Ma 2007; Wu and Ge 2009; Cao et al. 2012) (Fig. 3.6-Fig. 3.20, Fig. 3.14), the largest tourist flow was mainly concentrated in thermally pleasant months, and the smallest tourist flow occurred in the period under cold or heat stress (Fig. 3.6-Fig. 3.20, Fig. 3.14). This is similar to the influence of the thermal comfort on the behaviour of sun and beach tourists in Spain (Gomez-Martin and Martinez-Ibarra 2012).

6.2 Thermal-dependent urban design

The thermal-comfort based classification of cities roughly coincides with China's Standard of Climatic Regionalization for Architecture (MOHURD 1994). Type-I cities, characterizing by severe cold winter, are located in the high altitude/latitude

region, where the average air temperature in January is as low as -5 to -20°C and the minimum air temperature may be below -30°C. Thus, their buildings must meet the requirements of heat preservation, cold-proof, antifreeze, *etc.* and should prevent the dangers from ice and snow in winter. Type-II cities, characterizing by severe heat summer and pleasant winter, are situated in South China，where the average air temperature in January is above 10°C and that in July amounts to 25–29°C (MOHURD 1994). Therefore，their indoor and outdoor facilities should be well shaded and ventilated，and protect against hot weather and heavy rain in summer. Type-III cities, characterizing by cold winter & slightly pleasant summer, are placed in middle-high-latitude region, where the average air temperature in January and July are -10–0°C and 18–28°C respectively. Therefore, their buildings should not only meet the requirements of winter protection, but also have to consider the prevention of overheating in summer. Type-IV cities lie in the subtropical region with hot and humid summers and clammy winter, where the average air temperature in January and July ranges 0–10°C and 25–30°C respectively. Therefore, their buildings must not only satisfy the shading, ventilation, cooling and rain-proofing requirements in summer, but also take into account the cold-proof demand in winter. In Type-V cities with mild climate all the year round, ventilation and rain-proof are the main requirements for buildings. Furthermore, from the view point of energy efficiency, the design of building envelop structure, heating, ventilation and air conditioning system as well, should vary between different thermal comfort type of cities (MOHURD 2005).

Presently, the urban public central heating system is commonly used to regulate the indoor environment in cold stress winter in most Type-I and Type-III cities in northern China, while the independent household air-conditioning is privately adopted to improve the indoor environment in cold/heat stress winter/summer in Type-II and Type-IV cities in South China. With the increase in the ability of energy supply and long distance trans-regional power transmission, the demand for change to install collective public heating network in many Type-IV cities in southern China, such as Hangzhou and Nanchang etc., is growing (Xinhua 2013). Nevertheless, because of the shortage of pipelines and radiators in most urban buildings in these cities, it is of great expensive to reconstruct infrastructure massively to support public heating in built-up

area. Our results provide information of heating/cooling demands for future urban planning in cities in various regions of mainland China.

6.3 Changes in urban thermal comfort and possible influences

With global warming and intensifying UHI, the thermal comfort in the 31 provincial capital cities in mainland China will change, but the extent varies with cities and seasons. The annual cumulative number of cold stress days in most Type-I and Type-III cities in the period of 1981–2010 is reduced, as a result, the monthly cumulative number of pleasant days in late winter and early spring increased (Fig. 3.2, Fig. 3.6, Fig. 3.8 and Fig. 3.12). The annual cumulative number of heat stress days is increased in most of these cities in summer; the increase is larger in the cities in most Type-III and Type-IV cities (Fig. 3.2, Fig. 3.8, Fig. 3.9 and Fig. 3.13), the largest increase occur in Lanzhou, Hangzhou, Hefei, and Wuhan in subtropical South China. The climate of these cities (except for Lanzhou) is dominated by a subtropical anticyclone. In general, the increase in annual cumulative number of pleasant days and reduction in cold stress days in higher latitude/altitude cities will be more widespread than the increase in annual cumulative number of heat stress days in lower latitude/altitude cities. This confirms the simulations by Endler and Matzarakis (2011), Cheung et al. (2014), Petri and Caldeira (2015). They show that under global warming conditions, cold stress might be reduced in high latitude/altitude places such as the northern United States and the highland in the Black Forest in Germany, while heat stress might intensify in low latitude/altitude places like Hong Kong and lowland of the Black Forest region.

In higher latitude/altitude cities such as Lhasa and Changchun, the increase in annual cumulative number of pleasant days will not only improve the living suitability for local residents, but might also attract more tourists and immigrants. In addition, their urban energy consumption might be reduced (Yang et al. 2011). On the contrary, in a number of cities in the middle and lower reaches of the Yangtze River, the increase in annual cumulative number of heat stress days can reduce their activity, and is bound to increase the demand for indoor and outdoor cooling facilities (Yang et al. 2011). All of these effects of the climate change are posing new challenges for urban planning and management.

6.4 The application of the PET and UTCI for the present day climate

The present study shows that both PET and UTCI present similar spatiotemporal thermal comfort pattern across mainland China (Fig. 3.1-Fig. 3.13), a region with large spatial extend, variable topography and diverse climates (Fig. 1.1, Table 1.2). Although the sensitivity of the models to the meteorological input variables differs to some degree, and the present result also confirms that the PET is more closely related to temperature, while the UTCI is more sensitive to wind velocity and vapour pressure (Blazejczyk et al. 2012; Fröhlich and Matzarakis 2016).

The present study adopts the Western/Middle European PET ranges to assess the thermal comfort conditions of all provincial capital cities in mainland China (Table 2.1); this is beneficial to the comparison of the thermal comfort conditions between various regions in terms of the same PET range. Nevertheless, the perception thresholds for thermal comfort to residents varies with places, *e.g.* the neutral PET range found in Tianjin was 11–24°C, lower than the range in Europe (Lai et al. 2014); while it was 26–30°C in Taiwan, higher than the range in Europe (Lin and Matzarakis 2008). Therefore, for studies on the thermal comfort of more specific places, it is better to modify the PET ranges according to local people's adaptive thresholds to various thermal comfort conditions, than to use the European PET scale as a benchmark. The same is true for the UTCI.

6.5 The human bio-meteorological conditions in TP

One of the focusses of the study lies in an assessment of the effect of climate change on human bio-meteorological conditions of the TP, including its spatial and temporal variations during the recent 27 years (1979-2005) and the next 27 years (2024-2050). The UTCI index is calculated from data of simulations of HadGEM3-RA and RegCM regional climate models. The results show that the proportion of no thermal stress will increase and even moderate heat stress will emerge in some cities in the near future. Guo et al. 2016 discussed that whether the TP would be warmer in the future mainly depends on the elevation and showed that the warming would increase to a peak and then decrease slightly. Guo and Wang 2007 estimated that the temperature increased by an average increase of 1.3°C of TP during 1961-2007. However, based on the results of the RegCM model, some cold stress conditions will also increase although the percentage will be small. From the viewpoint of human thermal comfort, the main

trend will be warmer conditions in the future; however, the extreme cold stress will also increase slightly.

Our research focuses on the present human bio-meteorological conditions in the TP; predicts the its change in the near future. The stability of weather conditions or the human thermal comfort continuity in the TP is demonstrated and discussed. We find that in summertime, especially in July, August and September has the most stable conditions during a whole year. The results provides useful guidance for tourism- and human well-being management considering that pleasant climate conditions are one of the most important factors for travelling (Kozak 2002; Matzarakis et al. 2004; Goh 2012).

In this research, the regional model data of HadGEM3-RAand RegCM are used to simulate the input meteorological data for UTCI. Generally, RegCM outputs have a problem of being biased compared to observational data (Piani 2010). Therefore, a correction of the bias has to be performed by pre-processing the data. The corrected data are used to calculate UTCI. We focussed on 12 stations using the same grid as the model data. These stations are situted in urban settlements and can be considered representing large share of the inhabited regions.

6.6 The evaluation of Ta extremes in TP region

We also evaluate the Ta extreme warm spell duration index (WSDI) and cold spell duration index (CSDI) events in the selected 12 cities of TP regions in summertime and wintertime in 2024-2050 under scenario RCP4.5 and RCP8.5 in comparison with data for the years 1979-2005. We find a warming in the future together with more WSDI than CSDI events. Other research groups show significant less cold related extreme events in other regions in China in the past decades. For example, Tao et al. 2014 find significant warming trends and a higher percentage of stations of experiencing an increase of minimum temperature related indices than maximum related indices in the Poyang Lake basin in 1959-2010 by applying various extreme indices. For the source region of Yellow River, a significant warming trend was also observed mainly in 1960-2006 due to the changes of the magnitude and decreasing frequency of minimum temperatures (Hu et al. 2011). Other research also appliess the observation data to investigate the Ta extremes in other regions of China, the Yangtze River Basin (Su et al. 2006), and mainland of China (Zhou and Ren 2011) and also in

Tibetan Plateau (Liu et al. 2006) and all of the research found the positive trend in Ta extremes.

All of the previous work are based on the observation data and explore the Ta extreme in the past decades. Regional climate models (RCMs) are proved to be capable to present the extreme climate conditions as well as the mean climate conditions (Beniston et al. 2007). In our study, we evaluate the Ta extremes in 2024-2050 from data simulated by the HadGEM3-RA and RegCM regional model, which were generated witnin the framework of the CORDEX-East Asia project. We are not able to identity any strong warming trend in the general TP region over time in 2024-2050, but comparing RCP4.5 to RCP8.5 simulations, we find there is less CSDI events for RCP 8.5, especially for Lhasa and Xining. Guo et al. 2016 discussed the warming trend in TP depending on elevations in the future with 6 various downscaling model data sets and found that the peak warming at the elevation of 4400-5200 m.

During the last half century, the significant warming was identified in TP with an average 1.3°C increase during 1961-2007 (Guo and Wang 2012). Even an average of 2.7°C has been simulated for TP in 2081-2100 under RCP4.5 conditions compared to 1986-2005 (Hu et al. 2015; Zhang et al. 2015). In order to find out the change in intensity of the extreme events, we explore the intensity of WSDI and CSDI events in Xining and Lhasa. The dominant intensity are "-" (-3.00~ -0.01°C), "- -" (-6.00~ -3.00°C), "+" (0.00~ 3.00°C) and "+ +" (3.00~ 6.00°C) in 2024-2050 under both RCP4.5 and RCP8.5. There are also several events which intensity classes are "- - - -" (-12.00~ -9.01°C) and "+ + + +" (9.01~ 12.00°C). Compared to the mean climate conditions, the Ta extremes show a more distinct warming in TP. However, there will still cold related CSDI events appear in TP.

Chapter 7

7 Conclusions and outlook

7.1 Conclusions

7.1.1 The human thermal comfort analysis in provincial capital cities of China

Our analysis shows that in the 31 provincial capital cities in mainland China, the thermal comfort conditions during 1981–2010 covers 6–8 PET classes, or 4–8 UTCI classes, depending on the location of the city. We detect no *extreme heat stress* situations in any of these cities. Yang and Matzarakis (2016) described the human thermal comfort (HTC) and air humidity (AH) information by frequencies of PET and frequencies of vapour pressure (VP) in 12 representative Chinese cities of 11 Köppen-Geiger climate classification types in 2000-2012. Instead of the average values, they presented the frequencies to represent the human thermal comfort conditions.

Because of the difference in physical geography, the annual cumulative number of pleasant days varies greatly from city to city. The shortest in terms of the PET (about 120.2 days/year) is in Lhasa in Qinghai-Tibet Plateau, and in terms of the UTCI Tianjin (129.2 days/year) in North China, This city is exposed to both, heat stress in summer and cold stress in winter. The longest spell in terms of both PET and UTCI (more than 200.0 days/year) can be found in Kunming in Yunnan-Guizhou Plateau where the annual cumulative number of pleasant days is 161.0–165.0 days/year, accounting for 44%–45% of the whole year.

The pleasant days are mainly concentrated in the period from April to October, especially in April, May, September, and October. In the winter months of January, February, and December, the monthly cumulative number of pleasant days drops to a minimum.

The thermal comfort values of the 31 provincial capital cities in mainland China based on the PET are quite similar to the ones derived from the UTCI. The annual average PET and UTCI are 13.7°C and 13.2°C respectively. The difference between daily PET and UTCI range from -0.2°C to 1.8°C over the year, being larger in spring and winter, and smaller in summer and autumn. The daily PET values of the 31 capital provincial cities are highly correlated with the daily UTCI. Nevertheless, their

sensitivities to the meteorological variables input in the models differ to some extent; the PET is more closely related to temperature, while the UTCI is more sensitive to wind velocity and vapour pressure.

Generally, in the past three decades, with global warming and intensifying UHI, in higher latitude/altitude cities the cold stress decreases. At the same time, in lower latitude/altitude cities, particularly the cities in the middle and lower reaches of the Yangtze River under the influence of the heat wave of subtropical anti-cyclone, the annual cumulative number of heat stress days increases. In the Yangtze River Valley and South China, the UHI effect enhances the warming trends by about 0.011 ℃/decade in 1951-2001 (Li et al. 2004).

In terms of the seasonal variation in PET and UTCI thermal comfort conditions throughout the year, the 31 provincial capital cities in mainland China can be classified into 5 types. Type-I cities are characterized by pleasant summer and severe cold winter, including many cities in high-latitude northern China, or in high-altitude plateau, like Changchun, Harbin, Shenyang, Hohhot, Yinchuan, Xining, Urumqi, Lhasa. Type-II cities are characterized by pleasant spring, autumn, winter and severe hot summer. They include Haikou, Guangzhou, and Nanning, three tropical and subtropical cities in South China. Type-III cities are characterized by pleasant spring, autumn, slightly pleasant summer, and cold winter. Some middle-high-latitude cities, such as Beijing, Tianjin, Shijiazhuang, Jinan, Shanghai, Nanjing and Zhengzhou fall in this category. Their seasonal thermal comfort features is roughly similar to that of the Type-IV, but the number of pleasant days in summer is more than that in Type-IV cities, while in winter it is much shorter. Type-IV cities are characterized by pleasant spring, autumn, hot stress summer and slightly cold winter. They were “stove cities” under the control of monsoon and subtropical anticyclone, including Wuhan, Changsha, Nanchang, Hangzhou, Chongqing, Chengdu, and Fuzhou. Considering the hot stress summer for this type, some research also explored the hot stress in some city which belonged to this type. Wang et al. 2014 studied the spatial variation of urban human thermal comfort in Hangzhou in summertime in 1991-1999 based on discomfort index and Landsat TM images using meteorological variables of air temperature and relative humidity. Then they discussed the results from the standpoint of urban planning, construction and environmental protection. Type-V cities were characterized by pleasant spring, summer and autumn and cool winter. Kunming, Guiyang, and Hsian belonged to this type.

In the study of Yang and Matzarakis (2016), they found the very similar results, e.g. Beijing shows almost 100% percent of PET ≤ 8°C in coldest months and more than 60% of PET = 8~35°C which is belonged to Type-III (characterized by pleasant spring, autumn, slightly pleasant summer, and cold winter). Additionally, other cities also show the similar classifications to this research, e.g. Kunming, Shanghai, Lhasa, Hohhot and Urumqi (Yang and Matzarakis 2016). The above mentioned results may widen and deepen the understanding of urban thermal comfort conditions of mainland China, and provide sound references for urban planners, residents, tourists, etc.

7.1.2 Human bio-meteorological conditions evaluation in TP regions at present and in the future

The human bio-meteorological conditions of the TP, including its spatial and temporal variations during the past 27 years (1979-2005) and the next 27 years (2024-2050) are assessed from data provided by the simulation of the regional models HadGEM3-RA and RegCM. The human bio-meteorological condition covers 4 UTCI stress categories according to HadGEM3-RA, RegCM and ERA-Interim reanalysis at present day conditions. For the changing trend, Guo and Wang 2007 revealed that an average increase of 1.3°C of TP during 1961-2007. The simulations underestimate the human thermal comfort compared to the observation data. No thermal stress days will increase significantly according to the projections of the HadGEM3-RA and RegCM models under the scenarios of RCP4.5 and RCP8.5. The cold stresses decreases and the TP will become warmer based on both of HadGEM3-RA and RegCM data. However, according to RegCM, *slight cold stress* increases marginally. In general, the main human thermal comfort will still be cold, however, the percentage of *no thermal stress* will increase and the *moderate heat stress* will show in some cities. In general, human bio-meteorological conditions will be more pleasant in the TP. Guo et al. 2016 discussed that whether the TP would be warmer in the future mainly depended on elevation and showed that the warming would increase to a peak and then decrease slightly.

The periods of pleasant (*no thermal stress*) and unpleasant (cold stresses) are comparable between the present and the near future. The whole year can be divided into two parts: the first half warm and the second half cold. The warm days mainly concentrate on the period from the middle of May to the middle of September, especially in June, July and August. In the cold half year, the monthly cumulative

number of no thermal stress days drop to a minimum. The monthly change rate of Ta and UTCI show a similar trend. The lowest rate is from July to October and the highest is was from March to May. Compared to Ta, the UTCI shows higher values for the same model.

Lokys et al. 2015 projected the human thermal comfort conditions in the next century in the temperate region of Luxembourg in Western-Central Europe by using PET and UTCI. Although they used the uncorrected model data, they focused on the change between the reference period and the future period. According to their results, the cold stress will decrease in the near future up to 2050 and heat stress will turn significant in the far future up to 2010. The human thermal comfort will shift to more heat stress, compared to this study (as we found increasing no thermal stress trend). This may because of the climate difference between TP (cold climate) and Luxembourg (temperate climate). Both this study and research of Lokys et al. 2015 project the warmer human biometeorological conditions in both studied regions based on the RCM data.

Because of the differences in the topography, and the annual percentage of no thermal stress and cold stresses, varies greatly from region to region in the simulations of HadGEM3-RA and RegCM under the scenarios of RCP4.5 and RCP8.5. For both models, Tuotuohe, Gangca, Maduo and Lenghu will be the coldest cities compared to others in TP. The coldest region (sum of four cold stresses is 83.4%, HadGEM3-RA; 63.8%, RegCM) will be Tuotuohe in terms of RCP4.5 and 82.1% and 53.9% for HadGEM3-RA and RegCM in terms of RCP8.5. According to the study of Li and Chi 2014, Lhasa, Xining and Yushu are the top three cities among the selected cities in terms of the human thermal favourability in 1961-2010. In this study, the warmest cities will be in Lhasa, Xining and Yushu for both RCP4.5 and RCP8.5. The proportion of warm stresses days for Lhasa is larger than 70% for both models under both RCP4.5 and RCP8.5. Qumarleb, Golmud, Dulan, DaQaidam and Dari experience about average human bio-meteorological conditions within the TP.

All of the simulations show a high level of agreement with the observation data after a bias correction, which is necessary to compensate for the height differences between the model grids and the observation stations. Especially for the ERA-Interim, the correlation coefficient is 0.989. The human bio-meteorological conditions of the TP are quite consistent in the simulations of HadGEM3-RA and RegCM.

Future research should utilize more available data instead of the single stations, for planners, residents, and tourists etc.

7.1.3 Evaluation of Ta extremes in TP regions

The warm spell duration index (WSDI) and cold spell duration index (CSDI) events in TP regions in summer and winter in 2024-2050 under scenario RCP4.5 and scenario RCP8.5 are evaluated by considering 12 cities in TP and compared to the reference time period of 1979-2005.

Overall, we detect more WSDI events than CSDI events for both simulations under both scenarios in TP. It indicates a warming trend in the future. However, there we find no clear increasing or decreasing trend of extreme events over time in 2024-2050. Generally, more extreme events appear in wintertime than in summertime. On average, RegCM simulates more extreme events than HadGEM3-RA. HadGEM3-RA (RegCM) simulates larger coefficient variation of extreme events in wintertime (summertime). Coefficient variation is larger under RCP8.5 than that of RCP4.5 on average. Matthes et al. 2015 applied the same CSDI and WSDI extreme indices to explore the recent changes in Arctic temperature extremes during summer and winter in 1979-2013. Based on their results, the decreasing cold spells trend is significant in both summer and winter. No significant warming trend was found which is similar to this research.

All of the 12 cities show no clear difference with regard to extreme events. The number of CSDI events (all events) ranges from 0.8 to 2.6 in wintertime and from 0.4 to 2.1 in summertime, by considering both simulations and scenarios in all cities. Lenghu and Lhasa have the least CSDI events in wintertime and summertime, respectively. Gangca and Maduo show the most CSDI events in wintertime and summertime. WSDI events (all events) have increased more than CSDI events, not only on average, but also in every city. Lhasa shows the most WSDI events in wintertime (3.1), and the lowest number is 1.2, which appears in DaQaidam and Xining. The smallest number of WSDI in summertime appears in Lhasa (2.0) and Dulan shows the most (3.3). Lhasa shows the warmer trend in wintertime and colder in summertime. However, Lhasa also shows the large coefficient variation in both seasons, especially in wintertime under RCP4.5 and in summertime under RCP8.5.

Analyzing the capital provincial cities of Lhasa and Xining, an increasing trend for extreme events is apparent in both cities in both frequency and intensity, especially for the long term events (>15 days) for both scenarios.

Under RCP4.5, for WSDI events, more extreme events appear in summertime than in wintertime. Xining shows more numbers extreme events and Lhasa appears longer duration of extreme events. The dominant intensity of events are slight + and medium +. In summertime, there are more WSDI events than in wintertime for both cities. Moreover, an apparent increasing trend shows in Xining by HadGEM3-RA in wintertime over time. The intensity of extreme events is stronger in Lhasa than in Xining, especially for the "+ + + +" events. For CSDI events, contrary to the WSDI events, more extreme events appear in wintertime than in summertime. Lhasa shows less number of events than Xining, especially for the long-term events (>15 days). "-" and "- -" are the main intensity for both cities. There is no clear increasing or decreasing trend for CSDI events in both cities over time. Xining shows strong intensity of CSDI events, especially for the very strong - events.

Under RCP8.5, there is no big change for both frequency and intensity of the extreme events in both cities over time. For WSDI events, it shows more in summertime than in wintertime on average. The main intensity are also the "+" and "+ +". However, Lhasa shows more in wintertime than in summertime by HadGEM3-RA. Xining shows more numbers of events and Lhasa shows longer duration of events. Lhasa shows stronger intensity of events than in Xining, though the only one "+ + + +" event appear in Xining by HadGEM3-RA. For CSDI events, there are less numbers of events than under RCP4.5. Xining shows more numbers, longer duration and also stronger intensity of events than in Lhasa.

7.2 Outlook

Different human thermal indices are been applied and compared by using station and model data to comprehensively analyse the human bio-meteorological conditions in mainland China. Further research on this topic should include:

Thermal indices: It has been proven that people from different regions of climate zones have different thermal sensations. In this study, considering comparing our results with other results worldwide or for the general implication, UTCI and PET have been applied to evaluate the human thermal comfort in China. Actually, there are 10 climate zones in mainland China and people from different climate zones may

have different thermal sensations. The Chinese standard human thermal indices should be developed to get more accurate thermal information in different regions of China. Cao et al. 2011 studied that the adaptations of people from different climate zones in summer and winter. According to their research, the Northern and Southern people of China showed the similar adaptability in summer and Southern people present the same adaptability to Northern people in winter after living in the North for at least one year.

Extreme events: In this study, we evaluate the Ta extremes by applying WSDI and CSDI in TP regions. Extreme events are not only referring to Ta extremes, but also droughts, floods, and frost, etc. The frequency and intensity of heat waves and floods are increasing and will intensify in the future based on GCM and RCM (IPCC 2013). China is affected by the East Asia Monsoon changes, which bring floods, droughts, heat waves and frost damages. For TP regions, experiences the severe snowstorms and Ta extreme events. In this study we focus only on human thermal comfort, Ta and the duration of warm and cold spells, but the other extreme events also impact human well being and should be investigated.

Other applications based on human thermal comfort estimates: There are potential topics for the applications of human thermal comfort, i.e. sociological, political, environmental and economical issues, which should be investigated.

References

Alexander L, Zhang X, Peterson T, Caesar J, Gleason B, Klein Tank A, Haylock M, Collins D, Trewin B, Rahimzadeh F, Tagipour A (2006) Global observed changes in daily climate extremes of temperature and precipitation. ***Journal of Geophysical Research: Atmospheres.*** (1984–2012) 111: D05.

Alho CJ, Silva JS (2012) Effects of severe floods and droughts on wildlife of the Pantanal Wetland (Brazil) – a review. ***Animals*** 2: 591–610.

Analitis A, Katsouyanni K, Biggeri A, Baccini M, Forsberg B et al. (2008) Effects of cold weather on mortality: results from 15 European cities within the PHEWE project. ***American Journal of Epidemiology*** 168: 1397-1408.

Anderson GS (1999) Human morphology and temperature regulation. ***International Journal of Biometeorology*** 43(3):99–109.

ASHRAE (1966) Thermal comfort conditions. In: ASHRAE Standards. New York: Association of the Heating, Refrigeration and Air-Conditioning Engineers, pp 55–66

ASHRAE, (2010) ANSI/ASHRAE Standard 55-2010: Thermal Environmental Conditions for Human Occupancy. American Society of Heating, Refrigerating and Air-Conditioning Engineers, Inc., Atlanta.

Auliciems A and Szokolay SV (1997) Thermal comfort. PLEA.

Barrett EC (1974) Climatology from satellites. Methuen, London

Beniston M, Stephenson DB, Christensen OB, Ferro CA, Frei C, Goyette S, Halsnaes K et al. (2007) Future extreme events in European climate: an exploration of regional climate model projections. ***Climate Change*** 81(1):71-95.

Blazejczyk K et al (2012) Comparison of UTCI to selected thermal indices. ***International Journal of Biometeorology*** 56(3):515–535.

Bröde P, Fiala D, Blazejczyk K, Holmér I, Jendritzky G, Kampmann B, Tinz B, Havenith G (2012) Deriving the operational procedure for the Universal Thermal Climate Index (UTCI). ***International Journal of Biometeorology*** 56: 481–494.

Cao WH, H YQ, Li ZS, Wang SX et al. (2012) The correlation analysis of tourist thermal comfort and variation of intra-annual tourist flow in Lijiang. ***Scientia Geographica Sinica*** 32(12): 1459-1464. (in Chinese)

Charalampopoulos I, Tsiros I, Chronopoulou-Sereli A, Matzarakis A (2013) Analysis of thermal bioclimate in various urban configurations in Athens, Greece. ***Urban Ecosystem*** 16(2): 217-233.

Chen L, Ng E (2012) Outdoor thermal comfort and outdoor activities: a review of research in the past decade. ***Cities*** 29(2):118–125.

Chen P, Hoerling MP, Dole RM (2001) The origin of the subtropical anticyclones. ***Journal of the Atmospheric Sciences*** 58(13):1827–1835.

Chen YC and Matzarakis A (2014) Modification of physiologically equivalent temperature. ***Journal of Heat Island Institute International*** 9: 2.

Chen YC, Lin TP, Matzarakis A (2014) Comparison of mean radiant temperature from field experiment and modelling: a case study in Freiburg, Germany. ***Theoretical and Applied Climatology*** 118(3): 535-551.

Cheung CSC, Hart MA (2014) Climate change and thermal comfort in Hong Kong. ***International Journal of Biometeorology*** 58(2):137–148.

China Meteorological Administration National Meteorological Information Center (2013) China surface weather dataset (fixed time). http://cdc.cma.gov.cn/dataSetDetailed.do?changeFlag=detai

Corburn J (2009) Cities, climate change and urban heat island mitigation: localizing global environmental science. ***Urban Study*** 46(2):413–427.

Coumou D, Petoukhov V, Rahmstorf S et al. (2014) Quasi-resonant circulation regimes and hemispheric synchronization of extreme weather in boreal summer. ***Proceedings of the National Academy of Sciences*** 111(34): 12331–12336.

de'Donato, Francesca K et al. (2013) The impact of the February 2012 cold spell on health in Italy using surveillance data. ***PloS one*** 8(4): e61720.

Dodson R and Marks D (1997) Daily air temperature interpolated at high spatial resolution over a large mountainous region. ***Climate Research*** 8(1): 1–20.

Drijfhout S, Bathiany S, Beaulieu C, Brovkin V, Claussen M, Huntingford C et al. (2015) Catalogue of abrupt shifts in Intergovernmental Panel on Climate Change climate models. ***Proceedings of the National Academy of Sciences*** 112(43):E5777-E5786.

Endler C and Matzarakis A (2011) Climate and tourism in the Black Forest during the warm season. ***International Journal of Biometeorology*** 55(2):173–186.

Fanger P (1972) Thermal comfort. McGraw-Hill. New York.

Fanger PO (1970) Thermal comfort. Danish Technical Press, Copenhagen.

Fiala D, Havenith G, Bröde P, Kampmann B, Jendritzky G (2012) UTCI Fiala multi-node model of human heat transfer and temperature regulation. ***International Journal of Biometeorology*** 56(3):429–441.

Fiala D, Havenith G, Broede P, Kampmann B, Jendritzky G (2012) UTCI-Fiala multi-node model of human heat transfer and temperature regulation. ***International Journal of Biometeorology*** 56(3):429–441.

Fiala D, Kevin JL, Martin S (1999) A computer model of human thermoregulation for a wide range of environmental conditions: the passive system. ***Journal of Applied Physiology*** 87(5):1957–1972

Fiala D, Lomas KJ, Stohrer M (2001) Computer prediction of human thermoregulatory and temperature responses to a wide range of environmental conditions. ***International Journal of Biometeorology*** 45:143–159.

Fodor N, Dobi I, Mika J, Szeidl L (2010) MV-WG: a new multi-variable weather generator. ***Meteorology and Atmospheric Physics*** 107: 91–101.

Fouillet A, Rey G, Laurent F, Pavillon G, Bellec S, Guihenneuc-Jouyaux C, Clavel J, Jougla E, Hemon D (2006) Excess mortality related to the August 2003 heat wave in France. ***International Archives of Occupational and Environmental Health*** 80: 16-24.

Fröhlich D, Matzarakis A (2016) Aquantitative sensitivity analysis on the behaviour of common thermal indices under hot and windy conditions in Doha, Qatar. ***Theoretical and Applied Climatology*** 124(1):179–187.

Gagge AP, Forbelets AP, Berglund LG (1986) A standard predictive index of human response to the thermal environment. ASHRAE

Gandemer J, Guyot A (1976) Integration du phenomene vent dans la conception du Milieu Bati: Guide Methodologique et Conseils Pratiques. Premiere Ministre. Groupe Central des Villes Nouvelles,

Gao L, Bernhardt M, Schulz K et al. (2017) Elevation correction of ERA-Interim temperature data in the Tibetan Plateau. ***International Journal of Climatology*** 37(9): 3540-3552.

Gerlitz L, Conrad O, Thomas A, Bohner J (2014) Warming patterns over the Tibetan Plateau and adjacent lowlands derived from elevation- and bias-corrected ERA-Interim data. ***Climate Research*** 58(3): 235–246.

Goh C (2012) Exploring impact of climate on tourism demand. ***Annals of Tourism Research*** 39(4):1859–188.

Gomez-Martin MB, Martinez-Ibarra E (2012) Tourism demand and atmospheric parameters: non-intrusive observation techniques. ***Climate Research*** 51(2):135–145.

Gong P, Liang S, Carlton EJ, Jiang Q, Wu J, Wang L et al (2012) Urbanisation and health in China. ***The Lancet*** 379 (9818): 843-852.

Gray ST, Betancourt JL, Jackson ST, Eddy RG (2006) Role of multidecadal climate variability in a range extension of pinyon pine. ***Ecology*** 87: 1124–1130.

Grigg D (1965) The logic of regional systems. ***Annals of the American Association of Geographers*** 55:465–491

Grigorieva E, Matzarakis A (2011) Physiologically equivalent temperature as a factor for tourism in extreme climate regions in the Russian.

Guo D, Yu E, Wang H (2016) Will the Tibetan Plateau warming depend on elevation in the future? ***Journal of Geophysical Research*** 121(8):3969-3978.

Guo DL and Wang HJ (2012) The significant climate warming in the northern Tibetan Plateau and its possible causes. ***International Journal of Climatology*** 32: 1775–1781.

Havenith G, Fiala D, Blazejczyk K, Richards M, Broede P, Holmer I, Rintamaki H, Benshabat Y, Jendritzky G (2012) The UTCI-clothing model. ***International Journal of Biometeorology*** 56(3):461–470.

Havenith G, Holmér I, den Hartog EA et al. (1999) Clothing evaporative heat resistance-proposal for improved representation in standards and models, ***Annals of Occupational Hygiene*** 43:339-346.

Healy JD (2003) Excess winter mortality in Europe: a cross country analysis identifying key risk factors. ***Journal of Epidemiology and Community Health*** 57: 784-789.

Helbig A, Baumüller J, Kerschgens MJ (1999) Urban climate and air pollution control. 2nd, completely revised and supplemented edition.

Herring SC, Hoerling MP, Peterson TC, Stott PA (2014) Explaining extreme events of 2013 from a climate perspective. ***Bulletin of the American Meteorological Society*** 95(9): S1-S104.

Herrmann J, Andreas Matzarakis (2010) Influence of mean radiant temperature on thermal comfort of humans in idealized urban environments." Berichte des Meteorologischen Instituts der Albert-Ludwigs-Universität Freiburg Pp: 522.

Höppe PR (1993) Heat balance modeling. ***Experientia*** 49(9):741–746

Höppe PR (1999) The physiological equivalent temperature—a universal index for the biometeorological assessment of the thermal environment. ***International Journal of Biometeorology*** 43:71–75.

Horton RM, Mankin JS, Lesk C et al. (2016) A Review of Recent Advances in Research on Extreme Heat Events. ***Current Climate Change Reports*** 2(4):242-259.

Hu Q, Jiang DB, Fan GZ (2015) Climate change projection on the Tibetan Plateau: Results of CMIP5 models. ***Journal of the Atmospheric Sciences*** 39: 260–270. (in Chinese)

Hu YR, Maskey S, Uhlenbrook S (2011) Trends in temperature and rainfall extremes in the Yellow River source region, China. ***Climattic Change*** 110:403–429.

Huang W, Kan H, Kovats S (2010) The impact of the 2003 heat wave on mortality in Shanghai, China. ***Science of the Total Environment*** 408: 2418-2420.

IPCC (2007) Climate Change 2007 Synthesis Report. Cambridge University Press, New York.

Jendritzky G (1990) Methodik zur räumlichen Bewertung der thermischen Komponente im Bioklima des Menschen: fortgeschriebenes Klima-Michel-Modell.

Jendritzky G, deDear R, HavenithG (2012) UTCI—why another thermal index? ***International Journal of Biometeorology*** 56:421–428.

Jendritzky G, Staiger H, Bucher K et al (2000) The perceived temperature: the method of the DeutscherWetterdienst for the assessment of cold stress and heat load for the human body. In: Proceedings of Internet Workshop on Wind Chill, 3–7 April 2000. Environment Canada, Fredericton, New Brunswick

Ji XL, Lou WZ, Dai ZZ (2006) Predicting thermal comfort in Shanghai's non-air-conditioned buildings. ***Building Research and Information*** 34(5):507–514.

Kakon AN, Mishima N, Kojima S (2009) Simulation of the urban thermal comfort in a high density tropical city: analysis of the proposed urban construction rules for Dhaka, Bangladesh. ***Building Simulation*** 2(4):291–305.

Kántor N, Unger J (2011) The most problematic variable in the course of human-biometeorological comfort assessment—the mean radiant temperature. ***Open Geosciences*** 3(1): 90-100.

Kendrick JR (2005) Social statistics: an introduction using SPSS for Windows, 2nd edn. Pearson Custom Publishing, Boston

Kim MK, Kim S (2011) Quantitative estimates of warming by urbanization in South Korea over the past 55 years (1954-2008). ***Atmospheric Environment*** 45(32):5778–5783.

Krüger E, Drach P, Emmanuel R Corbella (2013) Urban heat island and differences in outdoor comfort levels in Glasgow, UK. ***Theoretical and Applied Climatology*** 112(1–2):127–141.

Lai DY, Guo DH, Hou YF, Lin CY, Chen QY (2014) Studies of outdoor thermal comfort in northern China. ***Building Environment*** 77:110–118.

Li Q, Liu X, Zhang H et al (2004) Detecting and adjusting on temporal inhomogeneity in Chinese Mean Surface Air Temperature Dataset. Adv Atmos Sci 21(2) (in press)

Li Q, Zhang H, Liu X, Huang J (2004) Urban heat island effect on annual mean temperature during the last 50 years in China. ***Theoretical and Applied Climatology*** 79:165–174.

Li Q, Zhang H, Liu X, Huang J (2004) Urban heat island effect on annual mean temperature during the last 50 years in China. ***Theoretical and Applied Climatology*** 79(3): 165-174.

Li R, Chi XL (2014) Thermal comfort and tourism climate changes in the Qinghai–Tibet Plateau in the last 50 years. ***Theoretical and Applied Climatology*** 117:613–624.

Lin TP, Matzarakis A (2008) Tourism climate and thermal comfort in Sun Moon Lake, Taiwan. ***International Journal of Biometeorology*** 52(4):281–290.

Lin TP, Matzarakis A (2011) Tourism climate information based on human thermal perception in Taiwan and Eastern China. ***Tourism Manage*** 32(3):492–500.

Lokys HL, Junk J, Krein A. (2015) Future changes in human-biometeorological index classes in three regions of Luxembourg, western-Central Europe. ***Advances in Meteorology***.

Lu L, Xuan G, Zhang JH, Yang XZ, Wang DG (2002) An Approach to Seasonality of Tourist Flows Between Coastland Resorts and Mountain Resorts: Examples of

Sanya, Beiha, Mt. Putuo, Mt. Huangshan and Mt. Jiuhua. ***Acta Geologica Sinica*** 57(6): 731-740. (in Chinese)

Maras I, Schmidt T, Paas B, Ziefle M, Schneider C (2016) The impact of human-biometeorological factors on perceived thermal comfort in urban public places. ***Meteorologische Zeitschrift*** 25(4):407–420.

Masek JG, Lindsay FE, Goward SN (2000) Dynamics of urban growth in the Washington DC metropolitan area, 1973–1996, from Landsat observations. ***International Journal of Remote Sensing*** 21(18): 3473-3486

Matthes H, Rinke A, Dethloff K (2015) Recent changes in Arctic temperature extremes: warm and cold spells during winter and summer. ***Environmental Research Letters*** 10(11): 114020.

Matthes, H., Rinke, A. and Dethloff, K., 2015. Recent changes in Arctic temperature extremes: warm and cold spells during winter and summer. ***Environmental Research Letters*** 10(11), p.114020.

Matzarakis A (2008) Relevance of thermal bioclimate for tourism in Japan. ***Global Environmental Research*** 12:129–136

Matzarakis A and Rutz F (2005) Application of RayMan for tourism and climate investigations. ***Annalen der Meteorologie*** 41(2): 631-636.

Matzarakis A, Amelung B (2008) Physiological equivalent temperature as indicator for impacts of climate change on thermal comfort of humans. In: Seasonal forecasts, climatic change and human health. Springer, Netherlands, pp 161–172

Matzarakis A, de Freitas C, Scott D (2004) Advances in tourismclimatology. Berichte des Meteorologischen Institutes der Universität, Freiburg

Matzarakis A, De Rocco M, Najjar G (2009) Thermal bioclimate in Strasbourg—the 2003 heat wave. ***Theoretical and Applied Climatology*** 98(3–4): 209–220.

Matzarakis A, Mayer H (1997) Heat stress in Greece. ***International Journal of Biometeorology*** 41:34–39.

Matzarakis A, Mayer H, Iziomon MG (1999) Applications of a universal thermal index: physiological equivalent temperature. ***International Journal of Biometeorology*** 43:76–84.

Matzarakis A, Rammelberg J, Junk J (2013) Assessment of thermal bioclimate and tourism climate potential for central Europe—the example of Luxembourg. ***Theoretical and Applied Climatology*** 114(1–2):193–202.

Matzarakis A, Rutz F, Mayer H (2007) Modeling radiation fluxes in simple and complex environments—application of the RayMan model. ***International Journal of Biometeorology*** 51:323–334.

Matzarakis A, Rutz F, Mayer H (2010) Modeling radiation fluxes in simple and complex environments: basics of the RayMan model. ***International Journal of Biometeorology*** 54:131–139.

Matzarakis A. (2001) The thermal componet of the urban climate. Ber. Meteor. Inst. Univ. Freiburg No. 6. (in german)

Mayer H, Holst J, Dostal P, Imbery F, Schindler D (2008) Human thermal comfort in summer within an urban street canyon in Central Europe. ***Theoretical and Applied Climatology*** 17(3):241–250.

Mayer H, Höppe PR (1987) Thermal comfort of man in different urban environments. ***Theoretical and Applied Climatology*** 38(1):43–49.

Mayhew B, Bellezza J, Wheeler T, Taylor C (1999) Lonely Planet Tibet, 4th edn. Lonely Planet Publications, Melbourne

McCarthy MP, Best MJ, Betts RA (2010) Climate change in cities due to global warming and urban effects. ***Geophysical Research Letters*** 37: 9.

McCullough EA, Eckels S, Harms C (2009) Determining temperature ratings for children's cold weather clothing. ***Applied Ergonomics*** 40(5): 870-877.

McMichael A, Haines A, Slooff R et al. (1996) Climate change and human health. WHO, Geneva

Meehl GA, Zwiers F, Evans J et al (2001) Trends in extreme weather and climate events: issues related to modeling extremes in projections of future climate change. ***Bulletin of the American Meteorological Society*** 81:427–436

MOHURD (Ministry of Housing and Urban-Rural Development of the People's Republic of China) (1994) The standard of climatic regionalization for architecture (GB50178-93). China Planning Press, Beijing

MOHURD (Ministry of Housing and Urban-Rural Development of the People's Republic of China) (2005) Design standard for energy efficiency of public buildings (GB50189-2005). China Building Industry Press, Beijing

Molenaar RE, Heusinkveld BG, Steeneveld GJ (2015) Projection of rural and urban human thermal comfort in The Netherlands for 2050. ***International Journal of Climatology***.

Murry Mitchell J Jr (1961) The temperature of cities. ***Weather wise*** 12: 225–229.

NBSC (National Bureau of Statistics of China) (2011) Major figures of the 2010 national population census. http://www.stats.gov.cn/tjgb/rkpcgb/April 28 2011

NBSC (National Bureau of Statistics of China) (2013) Statistical communiqué of the People's Republic of China on the 2012 national economic and social development http://www.stats.gov.cn/english/newsandcomingevents/t20130222_402874607.htm.

NEAC (National Energy Administration of China) (2012) Technical code of meteorological surveying for electrical power engineering (DL/T5158-2012). China Planning Press, Beijing, pp 10–11

Ng E, Cheng V (2012) Urban human thermal comfort in hot and humid Hong Kong. ***Energy and Buildings*** 55:51–65.

Oliver JE (2011) Climate and man's environment: an introduction to applied climatology. John Wiley, New York

O'Loughlin J, Witmer FD, Linke AM, Laing A, Gettelman A, Dudhia J (2012) Climate variability and conflict risk in East Africa, 1990–2009. ***Proceedings of the National Academy of Sciences of the United States of America***, 109:18344-18349.

Otto FE, van Oldenborgh GJ, Eden J, Stott PA, Karoly DJ, Allen MR (2016) The attribution question. ***Nature Climate Change*** 6: 813–816.

Pachauri RK, Allen MR, VR Barros VR et al. Climate change 2014: synthesis report. Contribution of Working Groups I, II and III to the fifth assessment report of the Intergovernmental Panel on Climate Change.

Pappenberger F, Jendritzky G, Staiger H, Dutra E et al. (2015) Global forecasting of thermal health hazards: the skill of probabilistic predictions of the Universal Thermal Climate Index (UTCI). ***International Journal of Biometeorology*** 59(3): 311-323.

Pappenberger F, Jendritzky G, Staiger Het al (2015) Global forecasting of thermal health hazards: the skill of probabilistic predictions of the Universal Thermal Climate Index (UTCI). ***International Journal of Biometeorology*** 59:311–323.

Park S, Tuller SE, Jo M (2014) Application of Universal Thermal Climate Index (UTCI) for microclimatic analysis in urban thermal environments. ***Landscape and Urban Plan*** 125(SI):146–155.

Parsons KC (2003) Human thermal environments: the effects of hot, moderate and cold environments on human health, comfort and performance. Taylor and Francis, New York.

Patz JA, Campbell-Lendrum D, Holloway T, Foley JA (2005) Impact of regional climate change on human health. ***Nature*** 438: 310-317.

Patz JA, Khaliq M (2002) Global climate change and health: challenges for future practitioners. ***Journal of the American Medical Association*** 287:2283–2284.

Peterson TC (2003) Assessment of urban versus rural in situ surface temperature in the contiguous United States: No difference found. ***Journal of Climate*** 16: 2941–2959.

Peterson TC, Zhang X, Brunet-India M, Vázquez-Aguirre JL (2008) Changes in North American extremes derived from daily weather data. ***Journal of Geophysical Research*** 113(D7).

Petri Y, Caldeira K (2015) Impacts of global warming on residential heating and cooling degree-days in the United States. Sci Rep 5:12427.

Provencal S, Bergeron O, Leduc R, Barrette N (2016) Thermal comfort in Quebec City, Canada: sensitivity analysis of the UTCI and other popular thermal comfort indices in a mid-latitude continental city. ***International Journal of Biometeorology*** 60(4):591–603.

Rodwell MJ, Hoskins BJ (2001) Subtropical anticyclones and summer monsoons. ***Journal of Climate*** 14(15):3192–3211.

Roth M (2007) Review of urban climate research in (sub) tropical regions. ***International Journal of Climatology*** 27(14):1859–1873.

Salata F, Golasi I, Vollaro RD, Vollaro AD (2016) Outdoor thermal comfort in the Mediterranean area: a transversal study in Rome, Italy. ***Building Environment*** 96(2):46–61.

Secretariat General, Ministere de la Qualite de la Vie, France, Pp 139.

Shimoda Y (2003) Adaptation measures for climate change and the urban heat island in Japan's built environment. ***Building Research and Information*** 31(3–4):222–230.

Shiue I, Matzarakis A (2011) Estimation of the tourism climate in the Hunter Region, Australia, in the early twenty-first century. ***International Journal of Biometeorology*** 55(4):565–574.

Smith TT, Zaitchik BF, Gohlke JM (2013) Heat waves in the United States: definitions, patterns and trends. ***Climatic Change*** 118: 811–825.

Stahl K, Moore RD, Floyer JA, Asplin MG, McKendry IG (2006) Comparison of approaches for spatial interpolation of daily air temperature in a large region with complex topography and highly variable station density. ***Agricultural and Forest Meteorology*** 139(3-4): 224–236.

Staiger H, Laschewski G, Gratz A (2012) The perceived temperature—a versatile index for the assessment of the human thermal environment. Part a: scientific basics. ***International Journal of Biometeorology*** 56:165–176.

Stanton NA, Hedge A, Brookhuis et al. (2004) Handbook of Human Factors and Ergonomics Methods, CRC Press, Boca Raton, FL.

Steadman RG (1984) A universal scale of apparent temperature. ***Journal of Climatology & Applied Meteorology*** 23:1674–1687

Steadman RG (1994) Norms of apparent temperature in Australia. ***Australian Meteorological Magazine*** 43:1–16

Stocker TF, Qin D, Plattner G-K, Tignor M, Allen SK, Boschung J, Nauels A, Xia Y, Bex V, Midgley PM: IPCC, 2013: climate change 2013: the physical science basis: contribution of working group I to the fifth assessment report of the intergovernmental panel on climate change. 2013, Cambridge, United Kingdom and New York, NY, USA: Cambridge University Press.

Su BD, Jiang T, Jin WB (2006) Recent trends in observed temperature and precipitation extremes in the Yangtze River basin, China. ***Theoretical and Applied Climatology*** 83(1-4): 139-151.

Sun GN and M LJ (2007) The correlation analysis of tourist thermal comfort and variation of intra-annual tourist flow in Hsian. ***Tourism Tribune*** 22(7): 34-39. (in Chinese)

Taffé P (1997) A qualitative response model of thermal comfort. ***Building Environment*** 32:115–121.

Tebaldi C, Hayhoe K, Arblaster JM, Meehl GA (2006) Going to the extremes. ***Climatic Change*** 79: 185–211.

Terjung WH (1966) Physiologic climates of the conterminous United States: a bioclimatic classification based on man. ***Annals of the American Association of Geographers*** 56(1):141–179

Tromp SW (1963) Medical biometeorology. Elsevier, Amsterdam

United Nations. Department of Economic and Social Affairs, Population Division. World urbanization prospects: The 2014 revision, New York: NY, United Nations (2014) 2014.

VDI (2008) Richtlinie 3633 Blatt 1, Simulation von Logistik-, Materialfluss- und Produktionssystemen". Berlin: Beuth.

VDI-Kommission Reinhaltung der Luft (1988) Stadtklima und Luftreinhaltung. Tech. rep., Berlin

Wang WC, Zeng ZM, Karl TR (1990) Urban Heat Islands in China. ***Geophysical Research Letters*** 17: 2377–2380.

Wang WW, Zhu LZ, Wang RC (2004) An analysis on spatial variation of urban human thermal comfort in Hangzhou, China. ***Journal of Environmental Sciences*** 16(2):332–338.

Whitman S, Good G, Donoghue ER, Benbow N, Shou W, Mou S (1997) Mortality in Chicago attributed to the July 1995 heat wave. ***American Public Health Association*** 87: 1515-1518.

Wu P and Ge QS (2009) The correlation analysis of variation of intra-annual tourist flow and climate change. ***Geographical Research*** 28(4):1078-1084. (in Chinese)

Xie ZQ, Du Y, Zeng Y, Yan ML, Zhu CY (2010) Accelerated human activities affecting the spatial pattern of temperature in the Yangtze River Delta. ***Quaternary International*** 226(1–2):112–121.

Xinhua (China Daily) (2013) Debate gets hot on issue of heating South China. China Daily, August 1, 2013. Pp 4.

Yang SQ, Matzarakis A (2016) Implementation of human thermal comfort information in Koppen-Geiger climate classification-the example of China. ***International Journal of Biometeorology*** 60:1801–1805.

Yang W, Wong NH, Jusuf SK (2013) Thermal comfort in outdoor urban spaces in Singapore. ***Building Environment*** 59:426–435.

Yang XB, Sun DF, Zhou XJ et al (2011) Indoor thermal comfort and its effect on building energy consumption. ***Applied Mechanics and Materials*** 71-78: 3516–3519.

Zhai YC, Jin L, Meng QL (2009) A field study of thermal comfort in outdoor environment in Guangzhou, China. 6th International Symposium on Heating, Ventilating and Air Conditioning VOLSI-III, PROCEEDINGS. Pp 796–803.

Zhang KX, Wang R, Shen CC, Da LJ (2010) Temporal and spatial characteristics of the urban heat island during rapid urbanization in Shanghai, China. ***Environmental Monitoring and Assessment*** 169(1):101–112.

Zhang RH, Su FG, Jiang ZH, Gao XJ, Guo DL, Ni J et al. (2015) An overview of projected climate and environmental changes across the Tibetan Plateau in the 21st century. ***Chinese Science Bulletin*** 60: 3036–3047. (in Chinese)

Zhang X, Zwiers FW, Hegerl G (2009) The influences of data precision on the calculation of temperature percentile indices. ***International Journal of Climatology*** 29: 321–327.

Zhang XL, Yan XD (2014) Temporal change of climate zones in China in the context of climate warming. ***Theoretical and Applied Climatology*** 115(1-2): 167-175.

Zhao SQ (1994) Geography of China: environment, resources, population, and development. Wiley, New York

Zheng JR, Huang YM (2013) Hainan sets price controls on rooms in Haikou. China Daily http://www.chinadaily.com.cn/china/2013-01/04/content_16078674.htm

Zhou MG, Wang LJ, Liu T, Zhang YH, Lin HL, Luo Y et al. (2014) Health impact of the 2008 cold spell on mortality in subtropical China: the climate and health impact national assessment study (CHINAs)." ***Environmental Health*** 13(1): 60.

Zhou Y and Ren G (2011) Change in extreme temperature event frequency over mainland China, 1961− 2008. ***Climate Research*** 50(2-3): 125-139.

Abbreviations

AT	Apparent Temperature
CORDEX	Coordinated Regional climate Downscaling Experiment
CSDI	Cold Spell Duration Index
ETCCDI	Expert Team on Climate Change Detection and Indices
GCM	General Circulation Model
GHG	Green House Gas
HadGEM3-RA	Hadley Centre Global Environment Model
HTC	Human Thermal Comfort
IPCC	Intergovernmental Panel for Climate Change Fourth Assessment Reports
PET	Physiologically Equivalent Temperature
PMV	Predicted Mean Vote
PT	Perceived Temperature
RCM	Regional Climate Model
RCP	Representative Concentration Pathway
RegCM4	Regional Climate Model Version 4
SET	Standard Effective Temperature
Tmrt	Mean Radiant Temperature
TP	Tibetan Plateau
UHI	Urban Heat Island
UTCI	Universal Thermal Climate Index
WSDI	Warm Spell Duration Index

Acknowledgements

The three year study life in Berlin is and will be the most unforgettable time in my whole life. I learn to listen, speak out, cooperate, explore. I grow up to be an independent woman. I get lots of support and help and I appreciate all of you.

I would like to express my sincere gratitude to my supervisor Prof. Dr. Ulrich Cubasch for giving me the opportunity to have this wonderful period and support on my study. Special thanks to another supervisor Prof. Dr. Sahar Sodoudi. I appreciate her encouragement for the whole time and also the constructive suggestions on my study and life. I appreciate both of them, for their unconditional help, time, patience, and immense knowledge. Their powerful guidance supports me to guide me throughout the whole three years to write this thesis.

My sincere thanks to China Scholarship Council (CSC) for providing me the financial support. Even I stay in the forge in country; I can still feel the warm from my motherland.

I would like to thank all of my colleagues and friends of Klimod and StadtKlimod. Our groups are the very warm, friendly and positive teams and I enjoy the whole time we stay together. Particularly, Thomas Bergmann, Dr. Bijan Fallah, Ines Höschel, Dr. Ingo Kirchner, Dr. Kerstin Prömmel, Dr. Ines Langer, Bo Huang, Zhihong Zhuo, Matthias Straka, Patricia Margerison.

I appreciate Prof. Dr. Andreas Matzarakis for his comments, guidance and support on my study.

My sincere gratitude goes to my mother and my father, for their love, support and encouragement as always. Their love accompanied me for the whole time.

In the end, I would express my heartfelt appreciate to my husband Mr. Honglei Shen, for his unconditional love, understanding, encouragement and trust. His love and support is the energy to encourage me to keep moving. Without his support, I could not have finished this thesis.